UNIVERSITÄT ZU KÖLN

FULL STOKES POLARIMETRY WITH THE EFFELSBERG 100-M RADIO TELESCOPE

Inaugural – Dissertation
zur
Erlangung des Doktorgrades
der Mathematisch – Naturalwissenschaftlichen Fakultät
der Universität zu Köln
vorgelegt von

Elena Cenacchi
aus Bologna (Italien)

Köln, 2009

Berichterstatter: Prof. Dr. Andreas Eckart
Prof. Dr. Anton Zensus

Betreuer: Dr. Alexander Kraus
Dr. Karl-Heinz Mack

Tag der mündlichen Prüfung:

27. November 2009

The Effelsberg radio telescope, picture from Norbert Tacken.

This research was supported by the EU Framework 6 Marie Curie Early Stage Training programme under contract number MEST-CT-2005-19669 “ESTRELA”

"...it's rather curious, you know, this sort of life! I do wonder what *can* have happened to me! When I used to read fairy tales, I fancied that kind of thing never happened, and now here I am in the middle of one! There ought to be a book written about me, that there ought! And when I grow up, I'll write one."

Lewis Carroll, *Alice's Adventures in Wonderland*

I dedi- cate this thesis to those who make me live in Wonder- land every day of my life: Roberto, Marina, Isabella, Angel- ica, Andreas

♡

"...dobbiamo rinunciare all'idea che vi siano leggi valide per tutti; piuttosto, ciascuno deve far di sé stesso la materia per la propria arte..."

Sinesio di Cirene, *I Sogni*

Abstract

All that we know about celestial bodies, from planets to galaxies, comes, in large part, from the study of the electromagnetic radiation that they emit. We use the telescopes to observe the radiation and we study its properties to acquire information about its origin. In this thesis we focus on the polarized radiation at radio wavelengths.

The Stokes parameters, I, Q, U and V, describe the state of polarization of the electromagnetic radiation, which depends on the direction of the electric vector of the observed waves (we do not treat the magnetic vector as it is always oriented perpendicular to that of the electric one). Recognizing a single direction within a wave beam can be very challenging or even impossible: if the waves are emitted at different wavelengths, at different moments and in all directions (e.g. light from the Sun, or from a common light bulb), the vectorial sum of the electric vectors will give a different result at each time and the resulting beam will appear unpolarized. If, on the contrary, the examined beam is composed of monochromatic, coherent and collimated waves only (e.g. emitted by a laser pointer), the radiation will be 100% polarized and the direction of the measured electric vector will be definite and constant.

Commonly, within a beam, a polarized component is superimposed onto an unpolarized one. We have linear polarization when the direction of the electric vector is constant along a line (e.g. a single electromagnetic wave, for definition, is always 100% linearly polarized) and elliptical or circular polarization when the direction changes constantly along an elliptical or circular trace (e.g. cyclotron emission from a single electron spiraling along a magnetic field whose vector is parallel to the line of sight).

The presence of a polarized component in the observed radiation is always related to a certain degree of order in the emission process. The four Stokes parameters measure the intensity of the incoming radiation (I), the characteristic of a possible linearly polarized component (Q e U) and of a circularly polarized one (V). Their definition is a combination of amplitudes and phases of the received waves.

The percentage and kind of polarization that we observe from a source is linked to the radiative process involved. In particular, in radio astronomy an important mechanism of emission is the synchrotron radiation, which is intrinsically characterized by high percentages of linear and circular polarization.

Nevertheless, the fractional polarization observed from radio sources, especially if extra-galactic (AGN, Active Galactic Nuclei), is lower than that theoretically estimated for the process itself, because of depolarization mechanisms that act inside the source and along the path towards the observer. The most important of these are the Faraday rotation (that implies depolarization at low frequencies and a typical rotation of the polarization angle with the square of the wavelength) and the Faraday conversion (that implies conversion between linear and circular polarization and vice versa). When observed, the first effect supplies information about the medium crossed by the radiation and the component of the magnetic field along the line of sight, the second effect adds information about the component of the magnetic field perpendicular to the line of sight.

The idea of measuring all the four Stokes parameters from an AGN, at different frequencies, becomes then extremely attractive, aiming at deriving the geometry of the magnetic field inside the source and the description of

the medium crossed by the radiation (density and energy of the electrons). This approach encounters several technical difficulties, mainly due to the high sensitivity and accuracy required for this kind of measurements. Hence, the systematic study of the linear polarization has become possible with the realization of extremely accurate radioastronomical receivers, and the proper measurement of circular polarization is still carried out by very few telescopes.

In this thesis we have faced the technical difficulties of the polarimetric measurements carried out by single-dish radio telescopes. We have developed and successfully applied a new calibration procedure, based on the analysis of the signal propagation within a typical radioastronomical receiver, which allows the contemporary measurement of all four Stokes parameters. The success of this study is largely due to the excellent performance of the Effelsberg radio telescope, that, with its 100-m diameter, can be now defined the best single-dish radio telescope in the world for measuring linear and circular polarization.

We have used this new capability to carry out a polarimetric survey at 5 GHz, targeted on the Northern Kühr catalog. The project has been carried out by the Effelsberg antenna and the Westerbork interferometer and has produced the first statistically complete catalog containing linear and circular polarization measurements. The values for all the Stokes parameters have been measured for 257 sources, at 5 GHz.

Following the very good results obtained at 5 GHz, we have extended the new calibration procedure to the frequencies of 2.7, 8.5 and 10.5 GHz, obtaining the first full Stokes spectra measured at Effelsberg. In order to correlate the spectral features to the physical parameters of the sources, we have used a numerical code that simulated the propagation of the polarized radiation through a simple source model and we have compared the observed spectra with the theoretical simulated ones. One of the most important results of this thesis, which opens interesting perspectives for future applications, is the good consistency of the observed data from 0056-00 with those obtained simulating a radio source with a helical magnetic field spreading along the jet.

To conclude, we have enhanced the capabilities of the Effelsberg radio telescope, by developing a new method of data analysis that allows full Stokes polarimetric measurements. In the next future we plan to enlarge the available frequency range, particularly applying our procedure to the recently installed 32 GHz multi-beam receiver, increasing the quality of the observed polarimetric spectra. We believe that this new technique, coupled with a dedicated simulation code, could become a powerful instrument to carry out detailed studies of the radio source characteristics, such as composition and geometry of the magnetic field.

Kurzzusammenfassung

Unser gesamtes Wissen über Himmelskörper, von Planeten bis zu Galaxien, kommt zu einem großen Teil vom Studium der elektromagnetischen Strahlung die sie aussenden. Wir benutzen Teleskope, um diese Strahlung zu beobachten, und studieren ihre Eigenschaften, um Information über ihren Ursprung zu gewinnen. In dieser Arbeit konzentrieren wir uns auf die polarisierte Strahlung bei Radiowellenlängen. Die Stokes-Parameter I, Q, U und V beschreiben die Polarisation der elektromagnetischen Strahlung, die abhängt von der Richtung des elektrischen Vektors der beobachteten Wellen. (Der magnetische Vektor wird hier nicht behandelt, da er immer senkrecht zum elektrischen Vektor steht.) Die Identifikation einer einzelnen Richtung innerhalb eines Wellenpakets kann sehr schwierig, wenn nicht unmoeglich sein: wenn die Wellen in verschiedenen Wellenlängen ausgestrahlt werden, zu verschiedenen Zeiten und in alle Richtungen (e.g. Sonnenlicht oder das Licht einer Glühbirne), haben die elektrischen Vektoren zu verschiedenen Zeiten verschiedene Werte und werden in der Summe den Lichtstrahl unpolarisiert erscheinen lassen. Auf der anderen Seite, wenn der untersuchte Strahl nur aus monochromatischen, kohärenten und fokussierten Wellen besteht (z.B. ausgesendet von einem Laser), ist er 100% polarisiert, und die Richtung des gemessenen elektrischen Vektors ist definiert und konstant. Innerhalb eines Strahls ist die polarisierte Komponente einer unpolarisierten überlagert. Das Vorhandensein einer polarisierten Komponente in der beobachteten Strahlung ist immer verbunden mit einem gewissen Ordnungsgrad im Emissionsprozess. Die vier Stokes-Parameter messen die Intensität der einfallenden Strahlung (I), die Eigenschaften einer möglicherweise linear polarisierten Komponente (Q und U) und einer weiteren zirkular polarisierten (V). Ihre Definition ist eine Kombination von Amplitude und Phase der empfangenen Wellen.

Der Bruchteil und die Art der Polarisation, die wir von einer Quelle beobachten, haengt vom jeweiligen Strahlungsprozess ab. Im Radioband ist ein wichtiger Emissonsmechanismus die Synchrotronstrahlung, die duch hohe Polarisationsgrade von linearer und zirkularer Polarisation charakterisiert ist.

Nichtsdestotrotz ist der beobachtete Polarisationsgrad von Radioquellen, insbesondere von extragalaktischen (AGN, Aktive Galaxienkerne), niedriger als der theoretisch fuer den Synchrotronprozess erwartet. Dies wird verursacht durch Depolarisationsmechanismen innerhalb der Quelle und entlang der Sichtlinie zum Beobachter. Der wichtigste solche Prozess ist die Faradayrotation (diese verursacht Depolarisation bei niedrigen Frequenzen und eine typische Rotation des Polarisationswinkels als Funktion des Quadrats der Wellenlänge) und die Faradaykonversion (die die Umwandlung von linearer und zirkularer Polarisation und umgekehrt bewirkt). Der erste Effekt liefert Informationen über das Medium, das die Strahlung durchläuft, und die Magnetfeldkomponente entlang der Sichtlinie, der zweite Effekt fügt Informationen über die Magnetfeldkomponente senkrecht zur Sichtlinie hinzu. Die Idee, alle vier Stokes-Parameter eines AGN bei verschiedenen Frequenzen zu messen, ist daher ausserordentlich attraktiv, mit dem Ziel, die Magnetfeldgeometrie innerhalb der Quelle und im von der Strahlung durchlaufenden Medium (Dichte und Energie der Elektronen) zu beschreiben. Dieser Ansatz beinhaltet mehrere technische Schwierigkeiten, hauptsächlich wegen der hohen Empfindlichkeit und Genauigkeit, die für diese Art Messungen benötigt werden. Aus diesem Grund konnten systematische Studien der linearer Polarisation erst in den

letzten Jahren dank extrem empfindlicher radioastronomischer Empfänger durchgeführt werden. Präzise Messungen der zirkularen Polarisation werden noch immer von nur sehr wenigen Teleskopen ausgeführt.

In dieser Arbeit haben wir die technischen Schwierigkeiten der polarimetrischen Messungen durch Einzelteleskope behandelt. Wir haben eine neue Kalibrationsprozedur entwickelt und erfolgreich angewendet, basierend auf der Analyse des Signalverlaufs innerhalb eines typischen radioastronomischen Empfängers, welche die simultane Messung aller vier Stokes-Parameter erlaubt. Der Erfolg dieses Projekts basiert weitgehend auf der exzellenten Eigenschaften des Effelsberger Radioteleskops, das mit seinen 100 Metern Durchmesser nunmehr als das beste Einzelradioteleskop in der Welt für die Beobachtung linearer und zirkularer Polarisation definiert werden. Wir haben diee neue Möglichkeit für eine polarimetrische Durchmusterung des nördlichen Kühr-Katalogs bei 5 GHz genutzt. Dieses Projekt nutzte die Effelsberger Antenne und das Westerbork Interferometer und hat den ersten statistisch kompletten Katalog mit linear und zirkular polarisierten Messungen geliefert. Die Werte aller Stokes-Parameter wurden für 257 Quellen bei 5 GHz gemessen.

Nach den sehr guten Ergebnissen bei 5 GHz haben wir die neue Kalibrationsprozedur auf 2.7, 8.5 und 10.5 GHz ausgedehnt und so die ersten kompletten mit Effelsberg gemessenen Stokes-Spektren erhalten. Um diese spektralen Eigenschaften mit den physikalischen Parametern der Quellen zu korrelieren, haben wir einen numerischen Code verwendet, der die Fortpflanzung der polarisierten Strahlung durch ein einfaches Quellenmodell simuliert. Die beobachteten Spektren wurden entsprechend mit theoretisch erzeugten verglichen. Eins der wichtigsten Resultate dieser Arbeit, das interessante Perspektiven für zukünftige Anwendungen bietet, ist die gute Übereinstimmung der Beobachtungsdaen von 0056-00 mit den für eine Radioquelle mi helikalem Jetmagnetfeld simulierten Daten. Zusammenfassend lässt sich sagen, dass wir die Beobachtungsmöglichkeiten des Effelsberg-Teleskops durch die Entwicklung einer neuen Methode der Datenanalyse erweitert haben, die polarimetrische Messungen von allen Stokes-Parametern ermöglicht. In der nahen Zukunft planen wir diese Methode in andere Frequenzbereiche auszudehnen, inbesondere auf den kürzlich installierten 32-GHz Mehrhornempfänger, was die Qualität der beobachteten polarimetrischen Spektren verbessern wird. Wir glauben, dass diese neue Technik, zusammen mit einem entsprechenden Simulationsalgorithmus, ein wichtiges Instrument darstellt für detaillierte Studien der Eigenschaften von Radioquellen, insbesondere ihrer Beschaffenheit und der Geometrie des Magnetfelds.

Compendio della Tesi

Ció che sappiamo dei corpi celesti, dai pianeti alle galassie, si basa in gran parte sullo studio della radiazione elettromagnetica che questi emettono. Utilizziamo i telescopi per osservare la radiazione e ne studiamo le proprietá per risalire alle caratteristiche della sua sorgente. In questa tesi ci siamo occupati di emissione di radiazione polarizzata alle lunghezze d'onda radio.

I parametri di Stokes, I, Q, U e V, descrivono lo stato di polarizzazione della radiazione elettromagnetica, il quale, a sua volta, dipende alla direzione assunta dal vettore elettrico (e di quello magnetico di conseguenza, essendo questo sempre perpendicolare al primo) delle onde osservate. Non sempre é possibile riconoscere una direzione ben definita all'interno di un fascio di onde, se queste infatti sono emesse a diversa lunghezza d'onda, in diversi momenti e in tutte le direzioni (radiazione luminosa emessa dal Sole, o da una comune lampadina a filamento), la somma vettoriale dei vettori elettrici corrispondenti dará risultati diversi a ogni istante, e il fascio in oggetto sará non polarizzato. Se, al contrario, il fascio in esame é composto da onde monocromatiche, coerenti e molto collimate (emesse ad esempio da un puntatore laser), la radiazione sará polarizzata al 100% e si misurerá un'unica e costante direzione del vettore elettrico. Comunemente, all'interno di un fascio, si ha la sovrapposizione di una componente polarizzata e di una componente non polarizzata. Si parla di polarizzazione lineare quando la direzione del vettore elettrico si mantiene costante lungo una retta (una singola onda elettromagnetica é sempre polarizzata linearmente al 100% per sua stessa definizione) e di polarizzazione ellittica o circolare quando la direzione cambia in ogni istante lungo una traccia ellittica o circolare (radiazione di ciclotrone, emessa da un singolo elettrone spiraleggiante in un campo magnetico il cui vettore é parallelo alla linea di vista). Quando, all'interno del fascio esaminato, é possibile riconoscere una componente polarizzata, questa é sempre correlata a un certo grado di ordine nell'emissione elettromagnica. I quattro parametri di Stokes misurano l'intensitá della radiazione incidente (I), le caratteristiche di un'eventuale componente polarizzata linearmente (Q e U) e di una polarizzata circolarmente (V). La loro definizione coinvolge ampiezza e fase delle onde ricevute.

In natura la percentuale e il tipo di polarizzazione che si misurano da una data sorgente é legata al processo radiativo coinvolto. In particolare, in radioastronomia il principale meccanismo di emissione é la radiazione di sincrotrone, che é intrinsecamente caratterizzata da percentuali di polarizzazione lineare e circolare anche piuttosto alte.

Tuttavia, la polarizzazione che si osserva tipicamente da una sorgente radioastronomica, particolarmente se extra-galattica (AGN, Active Galactic Nuclei), é inferiore a quella prevista dalla teoria del processo, per via di meccanismi di depolarizzazione che avvengono all'interno della sorgente e lungo il percorso verso l'osservatore. Tra questi i piú importanti sono la rotazione di Faraday (che implica depolarizzazione lineare alle basse frequenze e una tipica variazione dell'angolo di polarizzazione a seconda della frequenza osservata) e la conversione di Faraday (che implica conversione tra polarizzazione lineare e circolare). Il verificarsi del primo di questi processi fornisce informazioni sulla composizione del mezzo attraversato dalla radiazione e sulla componente del campo magnetico lungo la linea di vista, il verificarsi del secondo fornisce in aggiunta informazioni sulla componente del campo magnetico perpendicolare

alla linea di vista.

Appare dunque estremamente attraente l'idea di poter misurare contemporaneamente tutti i parametri di Stokes di un AGN a diverse frequenze, cosí da poter derivare il modello geometrico del campo magnetico interno alla sorgente e la descrizione del mezzo attraversato dalla radiazione (densitá e caratteristiche energetiche degli elettroni). Questo tipo di approccio si scontra con diverse difficoltá tecniche, incentrate sull'alta sensibilitá e precisione richiesta per questo tipo di misure, cosicché lo studio sistematico dei parametri Q e U si é affermato solo negli ultimi anni, con la realizzazione di ricevitori radioastronomici sempre piú accurati, e la misura di V é ancora appannaggio di un numero limitatissimo di strumenti

In questa Tesi abbiamo affrontato le problematiche connesse alle misure polarimetriche con radiotelescopi single-dish e abbiamo sviluppato e applicato con successo un nuovo metodo di calibrazione, basato sull'analisi della propagazione del segnale polarizzato all'interno di un tipico ricevitore radioastronomico, che permette la contemporanea misura di tutti e quattro i parametri di Stokes. Gran parte del successo di questo studio é dovuto all'eccellente performance del radiotelescopio di Effelsberg, che, con i suoi 100-m di diametro, in tutto il panorama internazionale puó ora definirsi il miglior radiotelescopio single-dish in grado di misurare polarizzazione lineare e circolare.

Abbiamo utilizzato questa nuova potenzialitá per effettuare una survey polarimetrica che ha avuto come oggetto la parte Nord del catalogo di Kühr. Il progetto ha coinvolto l'antenna di Effelsberg e l'interferometro di Westerbork e ha prodotto il primo catalogo statisticamente completo contenente misure di polarizzazione lineare e circolare. In totale, 257 sorgenti sono state esaminate in tutti i parametri di Stokes, alla frequenza di 5 GHz.

Forti degli ottimi risultati ottenuti a 5 GHz, abbiamo esteso il nuovo metodo di calibrazione ad altre tre frequenze (2.7, 8.5, 10.5 GHz) ottenendo i primi spettri "full Stokes" misurati a Effelsberg. Per poter correlare gli andamenti degli spettri osservati ai parametri fisici delle sorgenti, abbiamo utilizzato un codice numerico che simulasse la propagazione della radiazione polarizzata attraverso un modello semplifcato della sorgente e abbiamo confrontato gli spettri osservati con quelli teorici simulati. Uno dei risultati piú importanti di questa Tesi, che apre interessanti prospettive per il futuro, é stato l'ottima corrispondenza dei dati osservati per la sorgente 0056-00 con quelli ottenuti simulando una radiosorgente caratterizzata da un getto con campo magnetico a geometria elicoidale.

In conclusione, abbiamo arricchito le potenzialitá del radiotelescopio di Effelsberg, sviluppando un nuovo metodo di analisi dei dati che permette di effettuare misure polarimetriche nei quattro parametri di Stokes. In futuro contiamo di aumentare le frequenze utilizzabili, in particolare applicando il nostro metodo di calibrazione al nuovo ricevitore a 32 GHz installato recentemente, migliorando cosí ulteriormente la qualitá degli spettri osservati. Riteniamo che questa nuova tecnica osservativa, unita all'utilizzo di un appropriato codice di simulazione, possa diventare un potente strumento per condurre studi approfonditi sulle caratteristiche delle radiosorgenti, quali la composizione e la geometria del campo magnetico.

Contents

List of Figures

List of Tables

1 Introduction

This thesis is composed of two main parts.

The first part is dedicated to the development of a new calibration procedure that allows full Stokes measurements with the Effelsberg antenna. After introducing some basic concepts and definitions of polarimetry (Ch. 2), we have studied in detail the instrumental noise that a single-dish radio telescope adds to the polarimetric signal once this has been received (Ch. 3), analysing each part of the receiving chain. Focusing on the aberration introduced by the most common radioastronomical receiver, we have derived the degradation in its mathematical formalism, computing the instrumental Müller matrix of the telescope, in order to derive the corrections to be applied to recover the original information carried out by the signal, along with the treatment of the errors during the process (Ch. 4).

The theoretical study of the full Stokes calibration has been followed by a 1-year test phase, carried out with the 5 GHz receiver (one of the most accurate available at Effelsberg). The results of the test phase, along with the comparison of our results with those obtained by the 26-m telescope of the University of Michigan (the only one single-dish telescope that carried out circular polarization measurements, before this PhD work) are presented in Ch. 5.

The second part is dedicated to the full polarimetric survey carried out by the Effelsberg and Westerbork telescopes at 5 GHz. The technical characteristics of the survey are presented in Ch. 6. Once we have completed the data calibration for all the measurements (the complete results are listed in Appendix A), we have carried out some statistical tests, aimed to describe the behaviour of circular polarization according to the main source properties (optical classification, redshift, linear polarization, two-point spectral index, see Ch. 7).

Finally, we have extended the calibration procedure to more frequencies, acquiring, for the first time at Effelsberg, the full Stokes spectra of a sample of sources, that appeared circularly polarized from the 5 GHz survey. The spectra are included in Appendix B for future reference. Ch. 8 contains the first results obtained from the comparison of the observed spectra with the theoretical ones, giving an outlook of the possible scientific results achievable with this new technique.

Part I

Calibration method and test phase

2 | Basics of polarimetry

Contents

2.1 Polarized waves

The nature of light, as a transverse electromagnetic wave ($\vec{E} \perp \vec{B} \perp \vec{c}$, where $\vec{E}$ is the electric field, $\vec{B}$ is the magnetic field and $\vec{c}$ is the speed of light), can be recognized directly from the Maxwell equations, which unify the electric, magnetic and optical phenomena.

A wave can be considered, at a large distance from its source, a plane wave to a good approximation; in this regime its direction of propagation is well defined. The wave can then be represented by a function $f\left(t, \vec{r}\right)$ of the kind $X = f(\vec{k}\vec{r} - ct)$ where X is a quantity like electric field strength, $\vec{r}$ is the position vector of the point at which X is measured and $\vec{k}$ is the propagation constant. In this case, the wave travels in the direction $\vec{k}$ with speed c, $\vec{k}$ is defined such that $|\vec{k}| = 2\pi/\lambda$.

If the wave is monochromatic (sinusoidal oscillations of fixed frequency and amplitude), and travels along the z-axis of our reference system, then the function $f(t, \vec{r})$ takes the form

$$\begin{aligned} E(z,t) &= E_0 \begin{pmatrix} \sin \\ \cos \end{pmatrix} \left[2\pi\left(\frac{z}{\lambda} \pm \frac{t}{T}\right) + \delta_0\right] \\ &= E_0 \begin{pmatrix} \sin \\ \cos \end{pmatrix} (kz \pm \omega t + \delta_0)\,. \end{aligned} \tag{2.1}$$

Representation of a monochromatic wave

The signs $-$ and $+$ stand, respectively, for a progressive and a regressive wave (in the following, this case will not be considered anymore as nature does not display this behaviour), E_0 is the amplitude of the wave and $\begin{pmatrix} \sin \\ \cos \end{pmatrix}$ means that both the functions can be used

Eq. (2.1) is commonly expressed as $E(z,t) = E_0 e^{i(kz-\omega t+\delta_0)}$ without specifying whether the real part of the exponential ("cos" function) or the imaginary one ("sin" function) is taken into consideration.

In the following we will for simplicity focus on the electric field only, the magnetic field can always be derived from $\overrightarrow{E} = -\overrightarrow{c} \times \overrightarrow{B}$. A wave that is travelling along the z-axis with complex amplitude $\widetilde{E}_0$ can always be decomposed into two components, one along the x-axis and one along the y-axis, as follows

$$\begin{aligned}\overrightarrow{E} &= \hat{\imath} E_x e^{i(kz-\omega t+\delta_x)} + \hat{\jmath} E_y e^{i(kz-\omega t+\delta_y)} \\ &= \left[\hat{\imath} E_x e^{i\delta_x} + \hat{\jmath} E_y e^{i\delta_y}\right] e^{i(kz-\omega t)} \\ &= \widetilde{E}_0 e^{i(kz-\omega t)}\end{aligned} \tag{2.2}$$

where $\hat{\imath}$ and $\hat{\jmath}$ are unit vectors in the x and y direction.

Definition of polarization state

Polarization is a phenomenon which can occur in transversal waves and it is described by the "trace" left by a wave passing through a plane perpendicular to the propagation direction. A well defined polarization state (linear, circular, elliptical, also called "mode") can be recognized in all the cases where a constant relation between E_x, E_y and δ_x, δ_y exists and reflects the existence of a defined ordered motion of the electric vector.

Any polarized wave can be considered as composed by two linearly polarized waves, as shown in Eq. (2.2), but any pair of orthogonally polarized waves (e.g. left circular/right circular, left elliptical/right elliptical with axis at 90°, etc.) can be used as a basis for description of a polarization state. The most convenient choice is typically the polarizations to which the telescope outputs respond.

The polychromatic case

If we abandon the monochromatic case for a more realistic polychromatic one we must consider that the quantities $E_x, E_y, \delta_x, \delta_y$ are not constant with time [Tinbergen, 1996]. The faster they vary, the broader the bandwidth of the wave train and the result is not anymore a 100% polarized signal. A polychromatic signal can be treated as the sum of many different monochromatic waves with different phases and amplitudes. The resulting degree of polarization can be significantly low, or even be totally canceled.

2.2 Jones and Stokes vectors, Müller matrix

The polarization properties of the radiation can be described using different vectors. The Jones vector describes the information related to amplitude and phase of the observed signal components, thus it is the preferred one to describe mathematically the receiver internal devices. The Stokes vector reflects the relation between the signal components and defines the overall polarization of the signal, thus it is the preferred one to describe the source physical characteristics.

The Jones and Stokes vectors carry the same information and are linked by a set of transformation equations. As a rule of thumb, the basis for the transformation should be chosen according to the polarization of the outputs delivered by the telescope under examination. The following equations are related to the circular LR frame, which we adopted in this paper following Kraus [1986] and Heiles [2002].

The Jones vector, $\overrightarrow{J}$, and the Stokes vector, $\overrightarrow{S}$, are defined as follows

$$\overrightarrow{J} = \begin{bmatrix} \widetilde{E}_L \\ \widetilde{E}_R \end{bmatrix} = \begin{bmatrix} E_L e^{-i\delta_L} \\ E_R e^{-i\delta_R} \end{bmatrix} \tag{2.3}$$

$$\overrightarrow{S} = \begin{bmatrix} I \\ Q \\ U \\ V \end{bmatrix} \tag{2.4}$$

The Müller matrix relates the polarimetric properties of the source, i.e. the Stokes parameters, of the source with the measurements from the polarimeter at the telescope. Hence it describes the instrument polarization characteristics. An ideal instrument that measures Stokes parameters perfectly, would be characterized by a unitary Müller matrix $\overrightarrow{S}_m = \mathbf{M}\overrightarrow{S}_s$. In a general case

$$\mathbf{M} = \begin{pmatrix} m_{11} & m_{12} & m_{13} & m_{14} \\ m_{21} & m_{22} & m_{23} & m_{24} \\ m_{31} & m_{32} & m_{33} & m_{34} \\ m_{41} & m_{42} & m_{43} & m_{44} \end{pmatrix} \tag{2.5}$$

Relation between the source polarization and the observed one

$$I_m = m_{11}I_s + m_{12}Q_s + m_{13}U_s + m_{14}V_s \tag{2.6a}$$
$$Q_m = m_{21}I_s + m_{22}Q_s + m_{23}U_s + m_{24}V_s \tag{2.6b}$$
$$U_m = m_{31}I_s + m_{32}Q_s + m_{33}U_s + m_{34}V_s \tag{2.6c}$$
$$V_m = m_{41}I_s + m_{42}Q_s + m_{43}U_s + m_{44}V_s \tag{2.6d}$$

where I_m, Q_m, U_m and V_m are the measured Stokes parameters and I_s, Q_s, U_s and V_s are the true Stokes parameters describing the source polarization.

Correction for the parallactic angle rotation

When handling linear polarization, the polarization angle is measured with respect to some instrumental zero point, usually related to a reference direction on the celestial sphere. During the source tracking, the reference system of an alt-azimuth mounted telescope rotates with respect to the source, that is, the parallactic angle of the sources (and consequently its polarization angle) rotates during the observation. Following Turlo et al. [1985] the time-dependent rotation component **B** of the Müller matrix can be extracted and applied separately from the instrumental component of the Müller matrix **T**, which is assumed to be constant with time. The overall Müller matrix can be then expressed as $\mathbf{M} = \mathbf{TB}$, where **B** is the rotation matrix of a linear rotating system (rotation of ϑ)

$$\mathbf{B} = \begin{pmatrix} 1 & 0 & 0 & 0 \\ 0 & \cos 2\vartheta & -\sin 2\vartheta & 0 \\ 0 & \sin 2\vartheta & \cos 2\vartheta & 0 \\ 0 & 0 & 0 & 1 \end{pmatrix}, \quad \mathbf{B^{-1}} = \begin{pmatrix} 1 & 0 & 0 & 0 \\ 0 & \cos 2\vartheta & \sin 2\vartheta & 0 \\ 0 & -\sin 2\vartheta & \cos 2\vartheta & 0 \\ 0 & 0 & 0 & 1 \end{pmatrix}. \tag{2.7}$$

2.3 Stokes and Jones formalism in the LR frame

The Stokes parameters relate the energy carried by the electromagnetic wave and its polarization state [Born and Wolf, 1980], the most widely used definitions are the following

$$I = I_{un} + I_p = I_{un} + I_{lp} + I_{cp} \tag{2.8a}$$
$$I_p = \sqrt{Q^2 + U^2 + V^2} \tag{2.8b}$$

where:
I_{un}=unpolarized radiation
I_p=polarized radiation
I_{lp}=linearly polarized radiation
I_{cp}=circularly polarized radiation

- The Stokes parameters in a linear frame are

Stokes parameters in a linear frame xy

$$I = \langle E_x^2 \rangle + \langle E_y^2 \rangle \tag{2.9a}$$
$$Q = \langle E_x^2 \rangle - \langle E_y^2 \rangle = I_{lp} \cos 2\varepsilon \cos 2\tau \tag{2.9b}$$
$$U = 2 \langle E_x E_y \cos \Delta \rangle = I_{lp} \cos 2\varepsilon \sin 2\tau \tag{2.9c}$$
$$V = 2 \langle E_x E_y \sin \Delta \rangle = I_{cp} \sin 2\varepsilon \tag{2.9d}$$
$$\frac{U}{Q} = \tan 2\tau \tag{2.9e}$$

where:
$\Delta = \delta_y - \delta_x$
$\varepsilon = \arctan \frac{OA}{OB}$ (axial ratio, see Fig. 2.4)
τ =polarization angle
$\langle E_x^2 \rangle = \frac{1}{T} \int_0^T [E_x(t)]^2 \, dt$, represents the output of a typical total power detector.

Choosing a circular frame, LR or RL

When converting the equations to a circular frame the problem arises on which handedness must be chosen to represent the analogue of the x and y axis: left and right vs. right and left. The physical content of the LR and RL frame is the same [Hamaker and Bregman, 1996], despite the opposite sign in the Stokes V definition. Anyhow, the LR frame and the RL frame must not be mixed. Once a frame is chosen, it is important to keep it in all the definitions of the Stokes parameters.

- The Stokes parameters in a circular frame LR are

Stokes parameters in a circular frame LR

$$I = \langle E_L^2 \rangle + \langle E_R^2 \rangle \tag{2.10a}$$
$$Q = 2 \langle E_L E_R \cos \Delta \rangle = I_{lp} \cos 2\varepsilon \cos 2\tau \tag{2.10b}$$
$$U = 2 \langle E_L E_R \sin \Delta \rangle = I_{lp} \cos 2\varepsilon \sin 2\tau \tag{2.10c}$$
$$V = \langle E_L^2 \rangle - \langle E_R^2 \rangle = I_{cp} \sin 2\varepsilon \tag{2.10d}$$
$$\frac{U}{Q} = \tan 2\tau = \tan \Delta \tag{2.10e}$$

where:
$\Delta = \delta_R - \delta_L$.

Figure 2.1: Representation of the field in a 100% linearly polarized wave, with an arbitrary polarization angle τ, decomposed in a linear frame

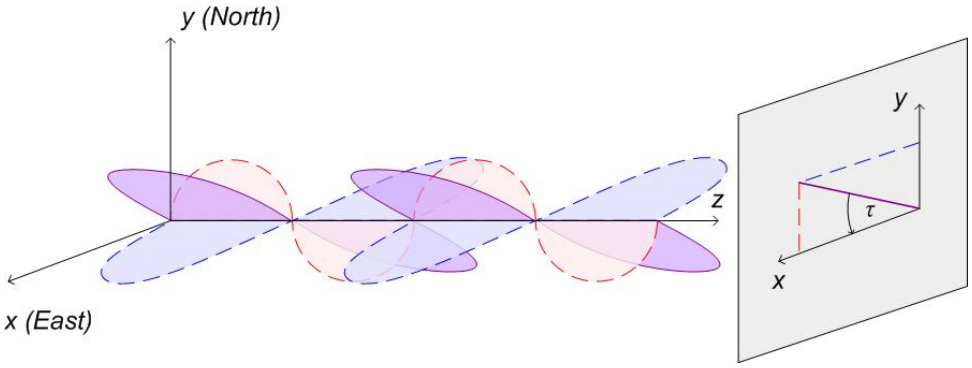

Figure 2.2: Representation of the field in a 100% linearly polarized wave, with an arbitrary polarization angle τ, decomposed in a circular frame

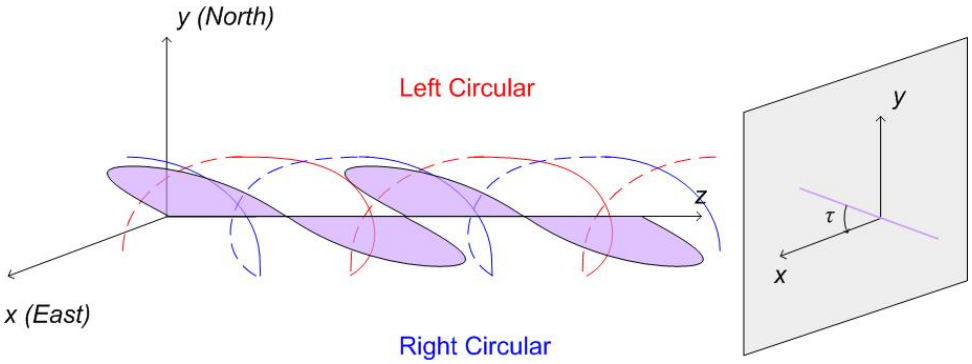

Figure 2.3: Representation of the field in a 100% circularly polarized wave, decomposed in a linear frame

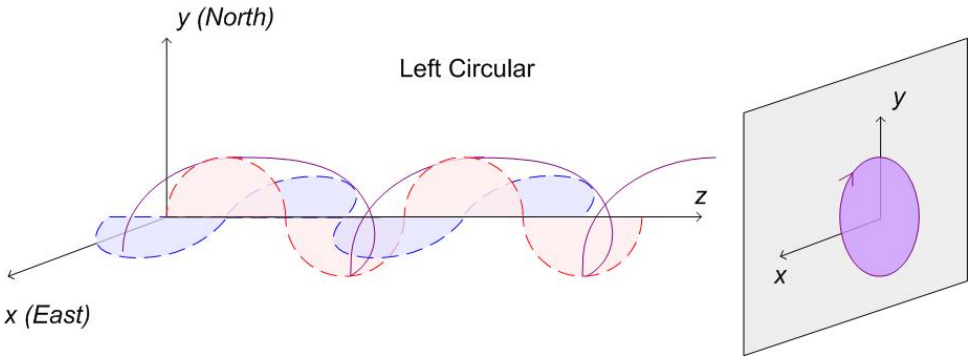

Note the relation between the phase difference and the polarization angle, when the Stokes parameters are expressed in circular components

$$\mathbf{P} = Q + iU = I_{lp} e^{i2\tau} = I_{lp} e^{i\Delta} = I_{lp} \cos\Delta + iI_{lp} \sin\Delta \tag{2.11a}$$
$$\Delta = 0^\circ \rightarrow Q = I_{lp}, U = 0 \rightarrow \tau = 0^\circ \tag{2.11b}$$
$$\Delta = 90^\circ \rightarrow Q = 0, U = I_{lp} \rightarrow \tau = 45^\circ \tag{2.11c}$$
$$\Delta = 180^\circ \rightarrow Q = -I_{lp}, U = 0 \rightarrow \tau = 90^\circ. \tag{2.11d}$$

- The Wolf (or "coherency") matrix and vector are

$$\mathbf{C} = \left\langle \begin{bmatrix} \widetilde{E}_L^* \widetilde{E}_L & \widetilde{E}_L \widetilde{E}_R^* \\ \widetilde{E}_R \widetilde{E}_L^* & \widetilde{E}_R^* \widetilde{E}_R \end{bmatrix} \right\rangle = \left\langle \begin{bmatrix} E_L^2 & E_L E_R e^{i\Delta} \\ E_L E_R e^{-i\Delta} & E_R^2 \end{bmatrix} \right\rangle \tag{2.12}$$
$$= \frac{1}{2} \begin{pmatrix} I + V & Q + iU \\ Q - iU & I - V \end{pmatrix}$$

How the Stokes parameters are related to the complex amplitudes

$$\overrightarrow{C} = \left\langle \begin{bmatrix} \widetilde{E}_L^* \widetilde{E}_L \\ \widetilde{E}_L \widetilde{E}_R^* \\ \widetilde{E}_R \widetilde{E}_L^* \\ \widetilde{E}_R^* \widetilde{E}_R \end{bmatrix} \right\rangle = \frac{1}{2} \begin{pmatrix} I + V \\ Q + iU \\ Q - iU \\ I - V \end{pmatrix}. \tag{2.13}$$

The coherency vector relates the Jones and the Stokes vector, as follows

$$\overrightarrow{J} \otimes \overrightarrow{J}^* = \overrightarrow{C} \tag{2.14a}$$
$$\mathbf{P} \cdot \overrightarrow{C} = \overrightarrow{S} \tag{2.14b}$$

Figure 2.4: Left: the polarization ellipse, the direction of propagation is into the page, from the source point of view. Right: the Q and U reference system superimposed to the North-East one.

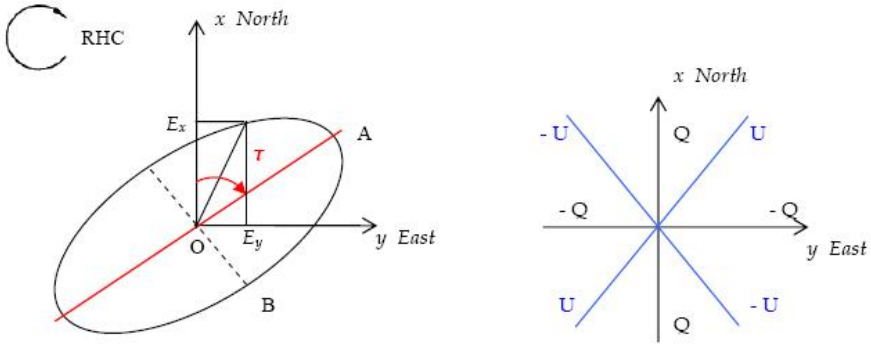

where

$$\mathbf{P} = \begin{pmatrix} 1 & 0 & 0 & 1 \\ 0 & 1 & 1 & 0 \\ 0 & -i & i & 0 \\ 1 & 0 & 0 & -1 \end{pmatrix}, \quad \mathbf{P}^{-1} = \frac{1}{2} \begin{pmatrix} 1 & 0 & 0 & 1 \\ 0 & 1 & i & 0 \\ 0 & 1 & -i & 0 \\ 1 & 0 & 0 & -1 \end{pmatrix}. \tag{2.15}$$

By developing the definition of the Wolf vector, one obtains the final relation between the Stokes parameters and the complex amplitudes of the wave components:

Final relation between the Stokes parameters and the complex amplitudes of the wave components

$$I = \langle E_L^2 \rangle + \langle E_R^2 \rangle = \widetilde{E}_L^* \widetilde{E}_L + \widetilde{E}_R^* \widetilde{E}_R \tag{2.16a}$$

$$Q = 2 \langle E_L E_R \cos \Delta \rangle = \widetilde{E}_L \widetilde{E}_R^* + \widetilde{E}_R \widetilde{E}_L^* \tag{2.16b}$$

$$U = 2 \langle E_L E_R \sin \Delta \rangle = i \left(\widetilde{E}_R \widetilde{E}_L^* - \widetilde{E}_L \widetilde{E}_R^* \right) \tag{2.16c}$$

$$V = \langle E_L^2 \rangle - \langle E_R^2 \rangle = \widetilde{E}_L^* \widetilde{E}_L - \widetilde{E}_R^* \widetilde{E}_R \tag{2.16d}$$

where the asterisk stands for complex conjugate.

3 | Single-dish observations

Contents

McKinnon [1992] and Hamaker et al. [1996] published major works on how to manage polarimetry with a radio interferometer and Johnston [2002] adapted their study to single-dish antennas equipped with linear dipoles. Nowadays telescopes are commonly equipped with scalar feeds and hybrid or wave-guide elements that supply circularly polarized outputs. In the following we describe, step by step, how this instrumentation can affect, in terms of instrumental polarization, the measurement of the incoming radiation. A typical receiving chain is sketched in Fig. 3.1. In Table 3.1 we summarize our notation.

3.1 The antenna

An ideal rotationally symmetric telescope does not change the state of polarization of the incident radiation (though circular polarization changes its state every time it is reflected, due to changing direction of propagation) see McGuire and Chipman [1994].

The first deviation from the ideal case is due to the blockage by the sub-reflector and its supporting structure. The radiation scattering causes a cross-polarization effect, both in amplitude and phase, which can be widely reduced by the usage of an appropriate structure design. Coupling the antenna with corrugated horns or dual mode horns with circularly symmetric patterns offers cross-polarization efficiencies closer to 1.

Presence of the sub-reflector and gravitational deformations

The parabolic shape is usually optimized at a well defined elevation, typically around 45°. When the antenna observes far from this value, its shape deviates from the original parabola (and the symmetry could be broken), unless it is equipped with some correction mechanism that compensates the gravitational deformations (active surfaces or homology). As an example of the deformation involved, Table 3.2 lists the deviation from the best-fit parabola for a typical dish without compensating techniques.

Table 3.1: Here the notation adopted to refer to different quantities is summarized. All complex quantities are expressed in the form $\widetilde{A} = Ae^{ip}$, where A is the amplitude and p is the phase. P is the phase difference between the two channels.

	A	p	P
Incoming radiation $\widetilde{E}$	E_R, E_L	δ_R, δ_L	$\Delta = \delta_R - \delta_L$
Cross term $\widetilde{D}$	D_R, D_L	φ_R, φ_L	$\Phi = \varphi_L - \varphi_R$
Receiver gain $\widetilde{G}$	G_R, G_L	ψ_R, ψ_L	$\Psi = \psi_L - \psi_R$
Backend gain: Total Power g	g_1, g_2	$-$	$-$
Backend gain: Polarimeter $\widetilde{g}$	g_Q, g_U	γ_Q, γ_U	$-$
Outgoing signal $\widetilde{V}$	V_R, V_L	$-$	$-$

Table 3.2: Deviation from the best fit parabolic surface, typical values.

Elevation [°]	Deviation [rms mm]	Deviation [% @ 6 cm]
30 to 60	0.5	0.8
20 to 75	0.8	1.3

Figure 3.1: Receiver sketch. The block diagram shows the main parts of a typical radioastronomical receiver: the scalar feed, sensitive to all the polarization states; the directional coupler, that couples the linearly polarized noise diode signal into the source radiation; the polarizer, that transforms the signal into the circularly polarized representations; the OMT, that splits the orthogonally polarized signals (polarizer and OMT are sometime realized as a single device); the low noise amplifiers (LNA); the down-conversion parts, here represented in a single block (labeled "conversions"; the total power detectors (TP); the two multipliers, here shown as a single device, that take as input the LHC and RHC channels to give out Stokes Q, and the LHC and the 90° phase shifted RHC to give out U. The picture also shows equations giving the electric field strength, or voltage in the parts where propagation is as current on a wire, how those depend on the gain and the D-terms factors and how they are combined during each propagation step, see Ch. 4.1 and Ch. 4.2 for a complete derivation.

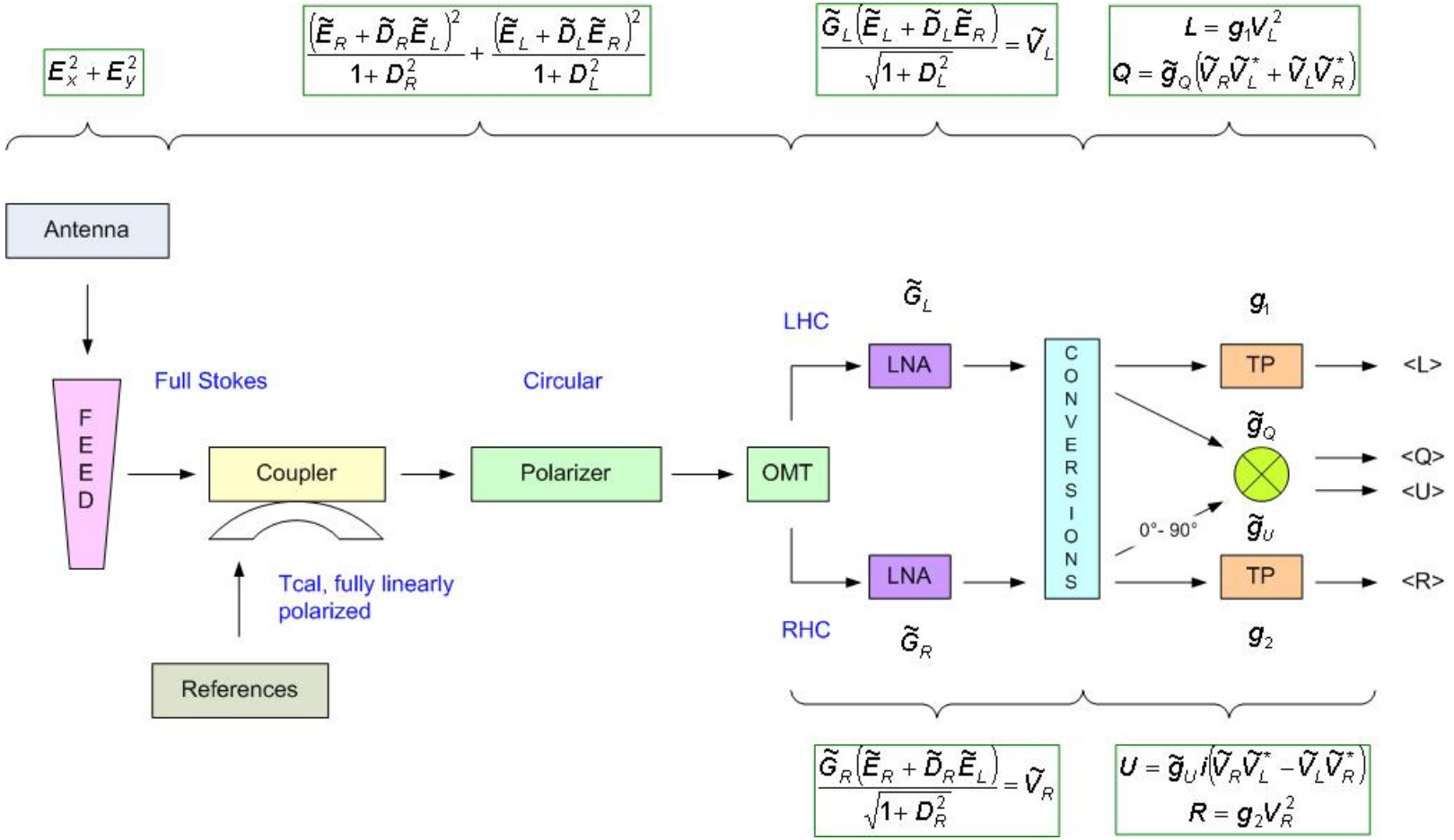

3.2 The feed

The feed is used to obtain a Gaussian beam pattern and converts the electromagnetic field from propagating in free space to propagating in waveguide. The most common type, coupled to Cassegrain and Gregorian antennas, is a conical corrugated horn (often called "scalar feed"), as it provides a Gaussian beam profile and is characterized by negligible cross-polarization. Unlike linear dipoles or helical antennas, the scalar feed usually does not have a single defined polarization mode, as it can support linear, circular and dual polarization, depending on its design and on the electronic devices that are coupled to it. A typical scalar feed provides a single output: some additional devices are needed to split it in the polarized components.

Feed circular symmetry and axial installation

A lack of symmetry in the feed conical shape could lead to some degree of polarization aberrations. As an example of deviation from the ideal feed shape, the typical mechanical accuracy is 0.02 mm to 0.03 mm. This would lead, at 6 cm (nearly 600 mm of diameter, in the secondary focus of the 100-m telescope) to a possible non-circularity of 0.003% to 0.005%.

For off-axis feeds (multibeam receivers or focal plane that permanently hosts several different feeds) the rotational symmetry is broken. As a result, a certain amount of instrumental polarization enters and increases the polarized signal I_p and the antenna patterns for the two orthogonal polarization channels of the receiver are different (beam squint). The result is a constant pointing offset between the two opposite beams which depends on the distance of the feed from the optical axis [Fiebig et al., 1991].

3.3 The directional coupler for calibration

Any radioastronomical receiver suffers from a certain amount of gain instability, due to electronic noise added by each component, thus two measurements of an identical power source could yield slightly different voltage values. To stabilize this fluctuation an internal noise of known temperature (noise Tcal) is added to the astronomical signal using a directional coupler. This calibration signal is linearly polarized and injected into the receiver with a known polarization angle. The noise Tcal is also used to convert the measured voltage into Kelvin.

The value of the noise Tcal is usually known with an accuracy of 3% to 5% over a wide bandwidth (e.g. 500 MHz for the 6-cm receiver at the Effelsberg telescope).

Accuracy and stability with time of the calibration noise diode

A typical value of the stability is 0.01 dB/K, this number must be interpreted as a noise Tcal variation of 0.2% per each 1 K variation in the receiver room temperature (which is usually kept constant). Assuming a noise Tcal nominal value of 2 K and a thermal excursion inside the room of $\pm$ 5 K a value of (2.00$\pm$0.02)K is obtained.

3.4 The polarizer and the ortho-mode transducer (OMT)

The polarizer and the OMT split the signal in two orthogonal circular polarized components. This process is not perfect and some fraction of one component

can affect the other component. This effect is known as "cross-talk" and is quantified by the so called "D-terms" (values $< 1\%$ are usually considered very good).

The ensemble of feed, polarizer and OMT is completely analogous to a pair of circularly polarized feeds, although the instrumental effects on the polarization measurements are different.

At this point in the receiving chain the following can be expected:

- Antenna: the non-perfect rotational symmetry can cause diattenuation and birefringent effects (that is, some instrumental polarization and some conversion among Q, U, V). For circular polarization, a change in sign must be expected at each reflection. These effects are usually canceled by appropriate technical equipment (active surface, appropriate cabling to compensate the change in sign) and by a calibration that compensates possible residual components (e.g. antenna gain curve as function of elevation).

Summary of the introduced polarimetric aberrations (instrumental polarization)

- Feed: small mechanical imperfections cause additional diattenuation and birefringent effects, but at low frequencies this should be a negligible contribution, as, e.g. at 6 cm, the imperfections are typically of the order of 0.01%.

- Directional coupler: the phase of the transmitted signal is not constant over the bandwidth, this typically causes an additional cross-polarization.

- Polarizer and OMT: a small part of the left circularly polarized signal could enter the right circularly polarized signal, and vice versa. This could heavily affect the V measurement while the effect on I, Q, U should be negligible.

- LNA: small fraction of the received radiation is reflected back to the previous components due to inevitable impedance mismatches, an effect called non-zero return loss. Once this spurious signal passes through the polarizer it faces the directional coupler and is reflected back again. The two reflections added to a passage through the polarizer transform the circular polarization into its orthogonal polarization. This leads to a spurious exchange of radiation between the left and right-hand channels.

3.5 The down-conversion

After the OMT, the two circularly polarized signals are amplified and down-converted. The "conversion box" can be considered linear (some deviation appears for very strong sources) but could introduce some polarization aberration: some small difference in the signal path length could alter the phase difference between the two components, and the amplitude could also be slightly modified. The signal, after the front-end according to Conway and Kronberg [1969] and McKinnon [1992], is then (see Table 3.1 for the adopted

notation)

$$\widetilde{V}_R = \frac{\widetilde{G}_R \left(\widetilde{E}_R + \widetilde{D}_R \widetilde{E}_L \right)}{\sqrt{1 + D_R^2}} \tag{3.1a}$$

$$\widetilde{V}_L = \frac{\widetilde{G}_L \left(\widetilde{E}_L + \widetilde{D}_L \widetilde{E}_R \right)}{\sqrt{1 + D_L^2}} \tag{3.1b}$$

where $\widetilde{G}_R = G_R e^{-i\psi_R}$ and $\widetilde{G}_L = G_L e^{-i\psi_L}$ are the gain of the right and left channels and $\widetilde{D}_R = D_R e^{-i\varphi_R}$ and $\widetilde{D}_L = D_L e^{-i\varphi_L}$ are the cross-talk factor.

4 Complete derivation of the measured Stokes parameters

Contents

After the down-conversion, the signals are sent to the devices that perform the measurements by implementing Eqs. (2.16). Typical devices are square law detectors (to obtain the flux densities from the left and right channels) and multiplying polarimeters (which supply Q and U, through a 90° shift of V_L or V_R). In the following treatment the average symbol $<>$ is omitted, subscript s stands for source, and subscript c for calibration noise diode.

4.1 Total power detectors

To measure total power in the R and L polarizations, the measurements $\widetilde{V}_R\widetilde{V}_R^* = V_R^2$ and $\widetilde{V}_L\widetilde{V}_L^* = V_L^2$ are made. According to Eqs. (3.1), introducing the square law detector gain (the scalar quantity g) and recalling that

$$\left(\widetilde{A}\widetilde{B}\right)^* = \widetilde{A}^*\widetilde{B}^*$$
$$\left(\widetilde{A}+\widetilde{B}\right)^* = \widetilde{A}^*+\widetilde{B}^*$$

one obtains

Equations 3.1a and 3.1b, squared

$$\widetilde{V}_R\widetilde{V}_R^* = \frac{g_2 G_R^2}{1+D_R^2}\left[E_R^2 + D_R^2 E_L^2 + \widetilde{E}_R\widetilde{E}_L^*\widetilde{D}_R^* + \widetilde{E}_L\widetilde{E}_R^*\widetilde{D}_R\right] \tag{4.1a}$$

$$\widetilde{V}_L\widetilde{V}_L^* = \frac{g_1 G_L^2}{1+D_L^2}\left[E_L^2 + D_L^2 E_R^2 + \widetilde{E}_L\widetilde{E}_R^*\widetilde{D}_L^* + \widetilde{E}_R\widetilde{E}_L^*\widetilde{D}_L\right] \tag{4.1b}$$

where the asterisk stands for complex conjugate. Eq. (4.1) can be expressed

in terms of the Stokes parameters

$$V_R^2 = \frac{g_2 G_R^2}{1+D_R^2}\left[\frac{I_s}{2}(1+D_R^2)+\frac{V_s}{2}(D_R^2-1)+\widetilde{D}_R\left(\frac{Q_s}{2}+\frac{iU_s}{2}\right)+\widetilde{D}_R^*\left(\frac{Q_s}{2}-\frac{iU_s}{2}\right)\right] \tag{4.2a}$$

$$V_L^2 = \frac{g_1 G_L^2}{1+D_L^2}\left[\frac{I_s}{2}(1+D_L^2)+\frac{V_s}{2}(1-D_L^2)+\widetilde{D}_L\left(\frac{Q_s}{2}-\frac{iU_s}{2}\right)+\widetilde{D}_L^*\left(\frac{Q_s}{2}+\frac{iU_s}{2}\right)\right]. \tag{4.2b}$$

Or, alternatively

Explicit use of Stokes Q and U

$$V_R^2 = \frac{g_2 G_R^2}{1+D_R^2}\left[\frac{I_s}{2}(1+D_R^2)+\frac{V_s}{2}(D_R^2-1)+\frac{Q_s}{2}(\widetilde{D}_R+\widetilde{D}_R^*)+\frac{iU_s}{2}(\widetilde{D}_R-\widetilde{D}_R^*)\right] \tag{4.3a}$$

$$V_L^2 = \frac{g_1 G_L^2}{1+D_L^2}\left[\frac{I_s}{2}(1+D_L^2)+\frac{V_s}{2}(1-D_L^2)+\frac{Q_s}{2}(\widetilde{D}_L+\widetilde{D}_L^*)+\frac{iU_s}{2}(\widetilde{D}_L^*-\widetilde{D}_L)\right]. \tag{4.3b}$$

In terms of source linearly polarized flux density I_{lps} and phase differences

Q and U expressed in terms of linearly polarized flux density and phase differences

$$V_R^2 = \frac{g_2 G_R^2}{1+D_R^2}\left[\frac{I_s}{2}(1+D_R^2)+\frac{V_s}{2}(D_R^2-1)+D_R I_{lps}\cos(\varphi_R-\Delta)\right] \tag{4.4a}$$

$$V_L^2 = \frac{g_1 G_L^2}{1+D_L^2}\left[\frac{I_s}{2}(1+D_L^2)+\frac{V_s}{2}(1-D_L^2)+D_L I_{lps}\cos(\varphi_L+\Delta)\right]. \tag{4.4b}$$

When the noise Tcal calibration is applied, a common post-processing procedure allows one to transform the voltage at the output of the total power devices (TP) into Kelvin, as follows

$$TP_R = \frac{V_{Rs}^2}{V_{Rc}^2}\frac{I_c}{2} \tag{4.5a}$$

$$TP_L = \frac{V_{Ls}^2}{V_{Lc}^2}\frac{I_c}{2} \tag{4.5b}$$

where I_c is the noise Tcal value, TP_R is total power in the R channel and TP_L is total power in the L channel, in Kelvin.

The ratio between this value and the corresponding measured voltage represents the conversion factor K/V applied to the subsequent on-source measurement. By inserting Eqs. (4.4) into Eqs. (4.5), the following results are obtained (to facilitate readibility, the denominators are written separately and

labeled with DN)

$$TP_R = \frac{I_c}{2}\frac{1}{DN_{R1}}\left[\frac{I_s}{2}(1+D_R^2)+\frac{V_s}{2}(D_R^2-1)+\frac{Q_s}{2}(\widetilde{D}_R+\widetilde{D}_R^*)+\frac{iU_s}{2}(\widetilde{D}_R-\widetilde{D}_R^*)\right] \tag{4.6a}$$

$$TP_L = \frac{I_c}{2}\frac{1}{DN_{L1}}\left[\frac{I_s}{2}(1+D_L^2)+\frac{V_s}{2}(1-D_L^2)+\frac{Q_s}{2}(\widetilde{D}_L+\widetilde{D}_L^*)+\frac{iU_s}{2}(\widetilde{D}_L^*-\widetilde{D}_L)\right] \tag{4.6b}$$

where

$$DN_{R1} = \frac{I_c}{2}(1+D_R^2)+\frac{V_c}{2}(D_R^2-1)+D_R I_{lpc}\cos(\varphi_R-\Delta_c)$$
$$DN_{L1} = \frac{I_c}{2}(1+D_L^2)+\frac{V_c}{2}(1-D_L^2)+D_L I_{lpc}\cos(\varphi_L+\Delta_c).$$

The noise Tcal is usually fully linearly polarized and it is characterized by $V_c = 0K$. Thus, after the calibration, Eqs. (4.6) are simplified as follows

$$TP_R = \frac{1}{DN_{R2}}\left[\frac{I_s}{2}(1+D_R^2)+\frac{V_s}{2}(D_R^2-1)+\frac{Q_s}{2}(\widetilde{D}_R+\widetilde{D}_R^*)+\frac{iU_s}{2}(\widetilde{D}_R-\widetilde{D}_R^*)\right] \tag{4.7a}$$

Application of the noise-diode calibration: the gain terms and their fluctuations are removed

$$TP_L = \frac{1}{DN_{L2}}\left[\frac{I_s}{2}(1+D_L^2)+\frac{V_s}{2}(1-D_L^2)+\frac{Q_s}{2}(\widetilde{D}_L+\widetilde{D}_L^*)+\frac{iU_s}{2}(\widetilde{D}_L^*-\widetilde{D}_L)\right] \tag{4.7b}$$

where

$$DN_{R2} = 1+D_R^2+2D_R\cos(\varphi_R-\Delta_c)$$
$$DN_{L2} = 1+D_L^2+2D_L\cos(\varphi_L+\Delta_c).$$

The comparison of Eqs. (4.7) and (4.4) show the principle of the calibration with the noise Tcal: by comparing the measured signal with that of the noise diode, the receiver gain fluctuations, represented by the factors outside the parentheses in Eqs. (4.4) are removed. In addition, the noise Tcal calibration procedure calibrates the source strength measurements in terms of antenna temperatures, in Kelvin.
Recalling the identities

$$\widetilde{A}+\widetilde{A}^* = 2A\cos p$$
$$\widetilde{A}-\widetilde{A}^* = -2iA\sin p$$

and applying those to Eqs. (4.7), one obtains

$$TP_R = \frac{1}{DN_{R2}}\left[\frac{I_s}{2}(1+D_R^2)+\frac{V_s}{2}(D_R^2-1)+Q_s(D_R\cos\varphi_R) + U_s(D_R\sin\varphi_R)\right] \tag{4.8a}$$

$$TP_L = \frac{1}{DN_{L2}}\left[\frac{I_s}{2}(1+D_L^2)+\frac{V_s}{2}(1-D_L^2)+Q_s(D_L\cos\varphi_L) + U_s(-D_L\sin\varphi_L)\right]. \tag{4.8b}$$

Now, Stokes I and V are the sum and difference of the Eqs. (4.8), discarding the terms of order $\geqslant 3$, resulting in

Measured Stokes I_m and V_m

$$\begin{aligned} I_m = \frac{1}{DN_{IV}}\{&I_s[1+D_R^2+D_L^2+D_L\cos(\varphi_L+\Delta_c) \\ &+D_R\cos(\varphi_R-\Delta_c)] \\ &+Q_S[D_R\cos\varphi_R+D_L\cos\varphi_L+2D_RD_L\cos\varphi_R\cos(\varphi_L+\Delta_c) \\ &+2D_RD_L\cos\varphi_L\cos(\varphi_R-\Delta_c)] \\ &+U_S[D_R\sin\varphi_R+2D_RD_L\sin\varphi_R\cos(\varphi_L+\Delta_c)-D_L\sin\varphi_L \\ &-2D_RD_L\sin\varphi_L\cos(\varphi_R-\Delta_c)] \\ &+V_s[D_R^2-D_L^2-D_L\cos(\varphi_L+\Delta_c)+D_R\cos(\varphi_R-\Delta_c)]\} \end{aligned} \tag{4.9a}$$

$$\begin{aligned} V_m = \frac{1}{DN_{IV}}\{&I_s[D_R\cos(\varphi_R-\Delta_c)-D_L\cos(\varphi_L+\Delta_c)] \\ &+Q_S[D_L\cos\varphi_L+2D_RD_L\cos\varphi_L\cos(\varphi_R-\Delta_c)-D_R\cos\varphi_R \\ &-2D_RD_L\cos\varphi_R\cos(\varphi_L+\Delta_c)] \\ &+U_S[-D_L\sin\varphi_L-2D_RD_L\sin\varphi_L\cos(\varphi_R-\Delta_c)-D_R\sin\varphi_R \\ &-2D_RD_L\sin\varphi_R\cos(\varphi_L+\Delta_c)] \\ &+V_s[1+D_R\cos(\varphi_R-\Delta_c)+D_L\cos(\varphi_L+\Delta_c)]\} \end{aligned} \tag{4.9b}$$

where

$$\begin{aligned} DN_{IV} = &1+D_R^2+D_L^2+2D_R\cos(\varphi_R-\Delta_c)+2D_L\cos(\varphi_L+\Delta_c) \\ &+4D_RD_L\cos(\varphi_R-\Delta_c)\cos(\varphi_L+\Delta_c). \end{aligned}$$

These two equations show how the measured I_m and V_m are contaminated by I_s, Q_s, U_s and V_s depending on the values of the D-terms.

4.2 Multiplying polarimeter

To measure the linear polarization components, Q_m and U_m, the measurements $\widetilde{V}_R\widetilde{V}_L^* + \widetilde{V}_L\widetilde{V}_R^*$ and $i\left(\widetilde{V}_R\widetilde{V}_L^* - \widetilde{V}_L\widetilde{V}_R^*\right)$ are made using a multiplying polarimeter. The outputs of the multipliers in the polarimeter are related to the incoming electric fields by

Equations 3.1a and 3.1b, complex product

$$\widetilde{V}_R\widetilde{V}_L^* = \frac{\widetilde{G}_R\widetilde{G}_L^*}{DN_{MP}}\left[\widetilde{E}_R\widetilde{E}_L^* + \widetilde{D}_RE_L^2 + \widetilde{D}_L^*E_R^2 + \widetilde{D}_R\widetilde{D}_L^*\widetilde{E}_L\widetilde{E}_R^*\right] \tag{4.10a}$$

$$\widetilde{V}_L\widetilde{V}_R^* = \frac{\widetilde{G}_L\widetilde{G}_R^*}{DN_{MP}}\left[\widetilde{E}_L\widetilde{E}_R^* + \widetilde{D}_R^*E_L^2 + \widetilde{D}_LE_R^2 + \widetilde{D}_R^*\widetilde{D}_L\widetilde{E}_L^*\widetilde{E}_R\right] \tag{4.10b}$$

where

$$DN_{MP} = \sqrt{1 + D_R^2 + D_L^2 + D_R^2 D_L^2}.$$

The Eqs. (4.10) can be expressed in terms of Stokes parameters

$$\begin{aligned}\widetilde{V}_R\widetilde{V}_L^* =& \frac{\widetilde{G}_R\widetilde{G}_L^*}{DN_{MP}}\left[\frac{Q_s}{2}\left(1+\widetilde{D}_R\widetilde{D}_L^*\right) - \frac{iU_s}{2}\left(1-\widetilde{D}_R\widetilde{D}_L^*\right) + \frac{I_s}{2}\left(\widetilde{D}_L^* + \widetilde{D}_R\right)\right.\\ &\left. + \frac{V_s}{2}\left(\widetilde{D}_R - \widetilde{D}_L^*\right)\right] \qquad (4.11a)\\ \widetilde{V}_L\widetilde{V}_R^* =& \frac{\widetilde{G}_L\widetilde{G}_R^*}{DN_{MP}}\left[\frac{Q_s}{2}\left(1+\widetilde{D}_R^*\widetilde{D}_L\right) + \frac{iU_s}{2}\left(1-\widetilde{D}_R^*\widetilde{D}_L\right) + \frac{I_s}{2}\left(\widetilde{D}_L + \widetilde{D}_R^*\right)\right.\\ &\left. + \frac{V_s}{2}\left(\widetilde{D}_R^* - \widetilde{D}_L\right)\right]. \qquad (4.11b)\end{aligned}$$

Or, alternatively

$$\begin{aligned}\widetilde{V}_R\widetilde{V}_L^* =& \frac{\widetilde{G}_R\widetilde{G}_L^*}{DN_{MP}}\left[\left(\frac{Q_s}{2} - \frac{iU_s}{2}\right) + \widetilde{D}_R\widetilde{D}_L^*\left(\frac{Q_s}{2} + \frac{iU_s}{2}\right) + \frac{I_s}{2}\left(\widetilde{D}_L^* + \widetilde{D}_R\right)\right.\\ &\left. + \frac{V_s}{2}\left(\widetilde{D}_R - \widetilde{D}_L^*\right)\right] \qquad (4.12a)\\ \widetilde{V}_L\widetilde{V}_R^* =& \frac{\widetilde{G}_L\widetilde{G}_R^*}{DN_{MP}}\left[\left(\frac{Q_s}{2} + \frac{iU_s}{2}\right) + \widetilde{D}_R^*\widetilde{D}_L\left(\frac{Q_s}{2} - \frac{iU_s}{2}\right) + \frac{I_s}{2}\left(\widetilde{D}_L + \widetilde{D}_R^*\right)\right.\\ &\left. + \frac{V_s}{2}\left(\widetilde{D}_R^* - \widetilde{D}_L\right)\right]. \qquad (4.12b)\end{aligned}$$

Explicit use of Stokes Q and U

In terms of linearly polarized flux density

$$\begin{aligned}\widetilde{V}_R\widetilde{V}_L^* =& \frac{\widetilde{G}_R\widetilde{G}_L^*}{DN_{MP}}\left[\frac{I_{lps}}{2}\left(e^{-i\Delta} + D_R D_L e^{i(\Phi+\Delta)}\right) + \frac{I_s}{2}\left(\widetilde{D}_L^* + \widetilde{D}_R\right)\right.\\ &\left. + \frac{V_s}{2}\left(\widetilde{D}_R - \widetilde{D}_L^*\right)\right] \qquad (4.13a)\\ \widetilde{V}_L\widetilde{V}_R^* =& \frac{\widetilde{G}_L\widetilde{G}_R^*}{DN_{MP}}\left[\frac{I_{lps}}{2}\left(e^{i\Delta} + D_R D_L e^{-i(\Phi+\Delta)}\right) + \frac{I_s}{2}\left(\widetilde{D}_L + \widetilde{D}_R^*\right)\right.\\ &\left. + \frac{V_s}{2}\left(\widetilde{D}_R^* - \widetilde{D}_L\right)\right] \qquad (4.13b)\end{aligned}$$

Q and U expressed in terms of linearly polarized flux and phase differences

To obtain Q and U one must form respectively $\widetilde{V}_R\widetilde{V}_L^* + \widetilde{V}_L\widetilde{V}_R^*$ and $i\left(\widetilde{V}_R\widetilde{V}_L^* - \widetilde{V}_L\widetilde{V}_R^*\right)$.

Taking the real part of the polarimeter complex gains, one obtains

$$\begin{aligned} Q_m = &\frac{g_Q G_R G_L \cos\gamma_Q}{DN_{MP}} \{I_s [D_L \cos(\Psi + \varphi_L) + D_R \cos(\Psi - \varphi_R)] \\ &+ Q_s [\cos\Psi + D_R D_L \cos(\Psi + \Phi)] \\ &+ U_s [\sin\Psi - D_R D_L \sin(\Psi + \Phi)] \\ &+ V_s [D_R \cos(\Psi - \varphi_R) - D_L \cos(\Psi + \varphi_L)]\} \end{aligned} \tag{4.14a}$$

$$\begin{aligned} U_m = &\frac{g_U G_R G_L \cos\gamma_U}{DN_{MP}} \{I_s [-D_L \sin(\Psi + \varphi_L) - D_R \sin(\Psi - \varphi_R)] \\ &+ Q_s [-\sin\Psi - D_R D_L \sin(\Psi + \Phi)] \\ &+ U_s [\cos\Psi - D_R D_L \cos(\Psi + \Phi)] \\ &+ V_s [-D_R \sin(\Psi - \varphi_R) + D_L \sin(\Psi + \varphi_L)]\}. \end{aligned} \tag{4.14b}$$

Or, alternatively

$$\begin{aligned} Q_m = &\frac{g_Q G_R G_L \cos\gamma_Q}{DN_{MP}} \{I_s [D_L \cos(\Psi + \varphi_L) + D_R \cos(\Psi - \varphi_R)] \\ &+ V_s [D_R \cos(\Psi - \varphi_R) - D_L \cos(\Psi + \varphi_L)] \\ &+ I_{lps} [\cos(\Psi - \Delta) + D_R D_L \cos(\Psi + \Phi + \Delta)]\} \end{aligned} \tag{4.15a}$$

Raw output from the polarimeters, before the noise diode calibration

$$\begin{aligned} U_m = &\frac{g_U G_R G_L \cos\gamma_U}{DN_{MP}} \{I_s [-D_L \sin(\Psi + \varphi_L) - D_R \sin(\Psi - \varphi_R)] \\ &+ V_s [-D_R \sin(\Psi - \varphi_R) + D_L \sin(\Psi + \varphi_L)] \\ &+ I_{lps} [-\sin(\Psi - \Delta) - D_R D_L \sin(\Psi + \Phi + \Delta)]\}. \end{aligned} \tag{4.15b}$$

By assuming that the polarimeters gain amplitude and phase are $g_Q = g_U$ and $\gamma_Q = \gamma_U$ (standard procedure at Effelsberg), it is possible to apply to both the Q and the U channels the same calibration factor, according to

$$I_{lpc} = \sqrt{{Q_c}^2 + {U_c}^2} \tag{4.16}$$

where Q_c and U_c are the noise Tcal signals coming through the Q and U channels and measured at the end of the backend.

Eqs. (4.15) can be used to estimate Q_c and U_c as the calibration signal follows the same path of the source signal. Then the noise Tcal is applied analogously to Eqs. (4.5). The ratio between the I_{lpc} value and the corresponding measured voltage gives the conversion factor K/V to be applied to the on-source Q and U measurements

$$Q_m = \frac{Q_s}{\sqrt{{Q_c}^2 + {U_c}^2}} \cdot I_{lpc} \tag{4.17a}$$

$$U_m = \frac{U_s}{\sqrt{{Q_c}^2 + {U_c}^2}} \cdot I_{lpc} \tag{4.17b}$$

Discarding the terms of order $\geqslant 3$ the following is obtained

$$\begin{aligned} Q_m =& I_{lpc} \frac{1}{DN_3} \{ I_s \left[D_L \cos(\Psi + \varphi_L) + D_R \cos(\Psi - \varphi_R) \right] \\ &+ Q_s \left[\cos\Psi + D_R D_L \cos(\Psi + \Phi) \right] \\ &+ U_s \left[\sin\Psi - D_R D_L \sin(\Psi + \Phi) \right] \\ &+ V_s \left[D_R \cos(\Psi - \varphi_R) - D_L \cos(\Psi + \varphi_L) \right] \} \end{aligned} \tag{4.18a}$$

Application of the noise-diode calibration: the gain terms and their fluctuations are removed

$$\begin{aligned} U_m =& I_{lpc} \frac{1}{DN_3} \{ I_s \left[-D_L \sin(\Psi + \varphi_L) - D_R \sin(\Psi - \varphi_R) \right] \\ &+ Q_s \left[-\sin\Psi - D_R D_L \sin(\Psi + \Phi) \right] \\ &+ U_s \left[\cos\Psi - D_R D_L \cos(\Psi + \Phi) \right] \\ &+ V_s \left[-D_R \sin(\Psi - \varphi_R) + D_L \sin(\Psi + \varphi_L) \right] \} \end{aligned} \tag{4.18b}$$

where

$$\begin{aligned} DN_3 =& I_{lpc} \left[1 + D_L^2 + D_R^2 + 2 D_L D_R \cos(\Phi + \Delta) \cos\Delta \right. \\ &\left. + 2 D_L \cos(\varphi_L + \Delta) + 2 D_R \cos(\Delta - \varphi_R) \right]^{\frac{1}{2}} . \end{aligned}$$

Then, the relation between the measured Stokes Q_m and U_m and the true source Stokes parameters can be derived

$$\begin{aligned} Q_m =& \frac{1}{DN_{QU}} \{ I_s \left[D_L \cos(\Psi + \varphi_L) + D_R \cos(\Psi - \varphi_R) \right] \\ &+ Q_s \left[\cos\Psi + D_R D_L \cos(\Psi + \Phi) \right] \\ &+ U_s \left[\sin\Psi - D_R D_L \sin(\Psi + \Phi) \right] \\ &+ V_s \left[D_R \cos(\Psi - \varphi_R) - D_L \cos(\Psi + \varphi_L) \right] \} \end{aligned} \tag{4.19a}$$

Measured Stokes Q_m and U_m

$$\begin{aligned} U_m =& \frac{1}{DN_{QU}} \{ I_s \left[-D_L \sin(\Psi + \varphi_L) - D_R \sin(\Psi - \varphi_R) \right] \\ &+ Q_s \left(-\sin\Psi - D_R D_L \sin(\Psi + \Phi) \right] \\ &+ U_s \left(\cos\Psi - D_R D_L \cos(\Psi + \Phi) \right] \\ &+ V_s \left(-D_R \sin(\Psi - \varphi_R) + D_L \sin(\Psi + \varphi_L) \right] \} \end{aligned} \tag{4.19b}$$

where

$$\begin{aligned} DN_{QU} =& \left[1 + D_L^2 + D_R^2 + 2 D_L D_R \cos(\Phi + \Delta) \cos\Delta \right. \\ &\left. + 2 D_L \cos(\varphi_L + \Delta) + 2 D_R \cos(\Delta - \varphi_R) \right]^{\frac{1}{2}} . \end{aligned}$$

The channels Q and U could also be calibrated separately. In this case the Eqs. (4.15) should be used to estimate the expressions of the calibration signals, and in Eqs. (4.19) two different denominators, one for each channel, would be present.

With Eqs. (4.9) and (4.19) we have all 16 elements of the Müller matrix in terms of D-terms, required to relate measured and true Stokes parameters.

4.3 Effects on the measurements

The instrumental Müller matrix elements contain information about the amount of contamination among the four Stokes parameters, due to spurious, unwanted, conversions arisen inside the receiver. The conversion of Q, U and V into I is typically negligible, the conversion of I and V into Q and U represents a small but still significant corruption, the conversion of I, Q and U into V can completely overwhelm the result of the measurement, leading to the impossibility of disentangling the instrumental contribution from the intrinsic V value. This clearly appears when dealing with completely unpolarized (thermal) sources.

Raw polarimetry of unpolarized source

As an example, Table 4.1 lists the Stokes values measured in November 2007 during a test observation with the Effelsberg 100-m telescope at 6 cm of two planetary nebulae. Being thermal sources they are expected to be unpolarized. The sources were observed with five beam cross-scans centered on the source. The Q and U values came directly from the multiplying polarimeter. The V value has been estimated as the difference between the left and right channels, after those were separately corrected for pointing (to compensate for the beam squint) and gain curve. The cross-scan technique intrinsically removes possible differences between the internal channel noise (≈ 1 K for the Effelsberg telescope at 6 cm).

The measured Q, U and V values, from unpolarized sources, are believed to be due to a contamination from Stokes I, that is, from a small net exchange in amplitude and phase between the left and right channels that, despite the multiplication and the correction for pointing and gain, still produces a spurious significant LP and CP detection.

4.4 Definition of the matrix elements

From Eqs. (4.9), (4.19) and recalling the definition (2.5), the coefficients of the instrumental Müller matrix $\mathbf{T}$ can be summarized as follows:

- Propagation of I_s into I_m

$$t_{11} = \frac{1}{DN_{IV}} \left[1 + D_R^2 + D_L^2 + D_L \cos(\varphi_L + \Delta_c) + D_R \cos(\varphi_R - \Delta_c)\right] \quad (4.20a)$$

- Propagation of Q_s into I_m

$$\begin{aligned} t_{12} = &\frac{1}{DN_{IV}} [D_R \cos\varphi_R + D_L \cos\varphi_L + 2D_R D_L \cos\varphi_R \cos(\varphi_L + \Delta_c) \\ &+2D_R D_L \cos\varphi_L \cos(\varphi_R - \Delta_c)] \end{aligned} \quad (4.20b)$$

- Propagation of U_s into I_m

$$\begin{aligned} t_{13} = &\frac{1}{DN_{IV}} [D_R \sin\varphi_R + 2D_R D_L \sin\varphi_R \cos(\varphi_L + \Delta_c) - D_L \sin\varphi_L \\ &-2D_R D_L \sin\varphi_L \cos(\varphi_R - \Delta_c)] \end{aligned} \quad (4.20c)$$

Definition of each Müller matrix element

- Propagation of V_s into I_m

$$t_{14} = \frac{1}{DN_{IV}} \left[D_R^2 - D_L^2 - D_L \cos(\varphi_L + \Delta_c) + D_R \cos(\varphi_R - \Delta_c)\right] \quad (4.20d)$$

Table 4.1: Examples of raw measurements of all Stokes parameters for unpolarized sources at Effelsberg at 6 cm. Measurements were calibrated using a noise diode of known strength, but D-terms correction was not applied.

Source	I_m [K]	σ_Δ	Q_m [K]	σ_Δ	U_m [K]	σ_Δ	V_m [K]	σ_Δ	LP [%]	σ_Δ	CP [%]	σ_Δ
NGC 6572	3.861	0.008	-0.016	0.002	0.006	0.013	-0.016	0.004	0.43	0.12	-0.42	0.11
NGC 7027	17.100	0.300	-0.076	0.011	-0.014	0.015	-0.087	0.022	0.45	0.07	-0.51	0.13

• Propagation of I_s into Q_m

$$t_{21} = \frac{1}{DN_{QU}} [D_L \cos(\Psi + \varphi_L) + D_R \cos(\Psi - \varphi_R)] \tag{4.20e}$$

• Propagation of Q_s into Q_m

$$t_{22} = \frac{1}{DN_{QU}} [\cos\Psi + D_R D_L \cos(\Psi + \Phi)] \tag{4.20f}$$

• Propagation of U_s into Q_m

$$t_{23} = \frac{1}{DN_{QU}} [\sin\Psi - D_R D_L \sin(\Psi + \Phi)] \tag{4.20g}$$

• Propagation of V_s into Q_m

$$t_{24} = \frac{1}{DN_{QU}} [D_R \cos(\Psi - \varphi_R) - D_L \cos(\Psi + \varphi_L)] \tag{4.20h}$$

• Propagation of I_s into U_m

$$t_{31} = \frac{1}{DN_{QU}} [-D_L \sin(\Psi + \varphi_L) - D_R \sin(\Psi - \varphi_R)] \tag{4.20i}$$

• Propagation of Q_s into U_m

$$t_{32} = \frac{1}{DN_{QU}} [-\sin\Psi - D_R D_L \sin(\Psi + \Phi)] \tag{4.20j}$$

• Propagation of U_s into U_m

$$t_{33} = \frac{1}{DN_{QU}} [\cos\Psi - D_R D_L \cos(\Psi + \Phi)] \tag{4.20k}$$

• Propagation of V_s into U_m

$$t_{34} = \frac{1}{DN_{QU}} [-D_R \sin(\Psi - \varphi_R) + D_L \sin(\Psi + \varphi_L)] \tag{4.20l}$$

• Propagation of I_s into V_m

$$t_{41} = \frac{1}{DN_{IV}} [D_R \cos(\varphi_R - \Delta_c) - D_L \cos(\varphi_L + \Delta_c)] \tag{4.20m}$$

• Propagation of Q_s into V_m

$$\begin{aligned} t_{42} = & \frac{1}{DN_{IV}} [D_L \cos\varphi_L + 2D_R D_L \cos\varphi_L \cos(\varphi_R - \Delta_c) - D_R \cos\varphi_R \\ & -2D_R D_L \cos\varphi_R \cos(\varphi_L + \Delta_c)] \end{aligned} \tag{4.20n}$$

• Propagation of U_s into V_m

$$\begin{aligned} t_{43} = & \frac{1}{DN_{IV}} [-D_L \sin\varphi_L - 2D_R D_L \sin\varphi_L \cos(\varphi_R - \Delta_c) - D_R \sin\varphi_R \\ & -2D_R D_L \sin\varphi_R \cos(\varphi_L + \Delta_c)] \end{aligned} \tag{4.20o}$$

• Propagation of V_s into V_m

$$t_{44} = \frac{1}{DN_{IV}} [1 + D_R \cos(\varphi_R - \Delta_c) + D_L \cos(\varphi_L + \Delta_c)] \tag{4.20p}$$

4.5 How to apply the calibration of the D-terms

4.5.1 Derivation of the Müller matrix

Instructions to apply the calibration

The proposed calibration scheme is completely based on the observation of astronomical calibration sources. One must always observe a fully unpolarized source ($Q = U = V = 0$) and a highly linearly polarized source (for which one does not require $V = 0$K). The left and right channels must be corrected separately for pointing and gain curve. The raw V value can then be estimated as the difference of the measured antenna temperatures. R and L opacity correction can be applied to the channels and the raw I can be derived as the sum of the R and L temperatures. The raw Q and U come directly from the multiplying polarimeter.

By observing one or more unpolarized sources whose flux density is known, Eq. (2.6) is simplified as follows

$$I_m = t_{11} I_s \tag{4.21a}$$
$$Q_m = t_{21} I_s \tag{4.21b}$$
$$U_m = t_{31} I_s \tag{4.21c}$$
$$V_m = t_{41} I_s \tag{4.21d}$$

where t_{11}, t_{21}, t_{31} and t_{41} are given in Eqs. (4.20). These four matrix elements involve the parameters $D_L, D_R, \varphi_L, \varphi_R, \Delta_c$ and Ψ, all of which must be known for the calibration to be applied.

The polarization angle of the internal noise signal, Δ_c is known (either from technical specifications or from previous measurements) and the remaining five quantities can be solved from six measurements on the calibrators (four measurements of the Stokes parameters of the unpolarized source and, in addition, two measurements of Stokes Q and U of the linearly polarized calibrator).

Once the D-terms, in amplitudes and phases, are determined, all terms of **T** can be calculated, as they depend on only these parameters. By applying this procedure, it is not necessary to make assumptions about the V value from the linearly polarized calibrator.

4.5.2 Treatment of the errors

Let the uncertainties measured on I_m, Q_m, U_m and V_m for the calibrator(s) be $\sigma_I, \sigma_Q, \sigma_U$ and σ_V, then the corresponding uncertainty on the matrix elements are

$$\sigma_{11} = \left| \frac{\sigma_I}{I_s} \right| \tag{4.22a}$$
$$\sigma_{21} = \left| \frac{\sigma_Q}{I_s} \right| \tag{4.22b}$$
$$\sigma_{31} = \left| \frac{\sigma_U}{I_s} \right| \tag{4.22c}$$
$$\sigma_{41} = \left| \frac{\sigma_V}{I_s} \right| \tag{4.22d}$$

An estimate of the Müller matrix elements error

Due to the non-linearity of the equations involved, it is not possible to propagate these errors through the estimate of the cross-terms, to the complete instrumental Müller matrix. It is anyway possible, by comparing the mathematical definitions of the matrix elements, to use the results (4.22) to establish an upper limit for the remaining errors, e.g. it is clear from their definition that the error on m_{11} and m_{14} must be the same. By applying similar qualitative considerations, the complete error matrix can be estimated as

$$\sigma_T = \begin{pmatrix} \sigma_{11} & \sigma_{11} & 3\sigma_{11} & \sigma_{11} \\ \sigma_{21} & \sigma_{21} & \sigma_{21} & \sigma_{21} \\ \sigma_{31} & \sigma_{21} & \sigma_{21} & \sigma_{31} \\ \sigma_{41} & \sigma_{11} & 3\sigma_{11} & \sigma_{41} \end{pmatrix}. \tag{4.23}$$

The intrinsic Stokes vector can be then obtained by inverting $\mathbf{T}$, propagating step by step the errors σ_{nm} during the inversion process and applying the following

$$S_s = \mathbf{B^{-1}T^{-1}}S_m. \tag{4.24}$$

Finally, once S_s is obtained, one or more flux-density calibrators can be used to determine the K/Jy conversion factor for I and V, and a strongly polarized calibrator can be used to determine the K/Jy conversion factor for Q and U.

5 Test phase: observed results

Contents

5.1 Instrumental terms

Test phase at Effelsberg

During the year 2007 several observations were carried out at the 100-m Effelsberg telescope to test the new sub-reflector. Part of this test time has also been used to test the full Stokes polarimetric calibration. A selected sample of 43 sources (39 extragalactic sources, 2 planetary nebulae, 2 planets) have been observed nearly monthly at 6 cm. Subsequently, some observations at 11 cm, 3.6 cm and 2.8 cm were also carried out.

The Stokes parameter measurements listed in Table 5.1 for the planetary nebula NGC 7027 also yielded the following instrumental terms (averages over time, and standard deviations)

$$
\begin{aligned}
D_L &= (0.59 \pm 0.04)\% \\
D_R &= (0.16 \pm 0.08)\% \\
\varphi_L &= (-2.4 \pm 3.8)^\circ \\
\varphi_R &= (-3.7 \pm 8.4)^\circ \\
\Psi &= (-4.1 \pm 2.7)^\circ.
\end{aligned}
$$

These values are in good agreement with the receiver technical specifications. The measured amplitudes are in good agreement also with EVN measurements. Comparing the measured phases with those coming from EVN measurements has not been possible, due to the large uncertainty of the D-term phases obtained with interferometric calibration tools. An example of a measured Müller matrix, as it results from a single onbservation session at 5 GHz, is

$$
\mathbf{M} = \begin{pmatrix}
0.9966 & -0.0039 & -0.0008 & -0.0073 \\
-0.0039 & 0.9927 & -0.0869 & 0.0079 \\
-0.0011 & 0.0869 & 0.9928 & 0.0011 \\
-0.0073 & -0.0079 & -0.0004 & 0.9966
\end{pmatrix}
$$

Table 5.1: Observed Stokes parameters for NGC 7027 at 6 cm. Observations were made in 2007 at Effelsberg. Units are Kelvin

Month	I	σ	Q	σ	U	σ	V	σ
February	17.014	0.143	-0.079	0.004	-0.016	0.006	-0.106	0.018
April	17.438	0.289	-0.070	0.002	-0.015	0.005	-0.133	0.028
May	16.864	0.079	-0.073	0.005	-0.020	0.008	-0.108	0.028
June	16.989	0.061	-0.066	0.004	-0.018	0.008	-0.122	0.019
August	17.179	0.245	-0.066	0.002	-0.015	0.007	-0.124	0.017
November	17.068	0.343	-0.076	0.011	-0.014	0.015	-0.087	0.022
December	17.279	0.265	-0.075	0.010	-0.019	0.015	-0.093	0.025

5.2 Circular polarization

We used our D-term calibration to search for CP in 19 AGNs with improved sensitivity over previous observations at Effelsberg.

Table 5.2 lists a comparison at 6 cm between the raw circular polarization and the values obtained after the calibration, using NGC 7027 as unpolarized calibrator and 3C 286 as strongly polarized calibrator. The data were observed in November 2007.

After the D-term calibration, the second planetary nebula, NGC 6572, appears circularly unpolarized as expected. Significant amounts of CP were detected in the two known CP sources 0743-006 and 1519-273 at levels consistent with published levels (0743-006: $V = (-0.51 \pm 0.08)\%$ from Aller et al. [2003] and $V = (-0.46 \pm 0.05)\%$ from Homan et al. [2001], both adopting the circular RL frame and for 1519-273: $V = (-0.92 \pm 0.17)\%$ from Aller et al. [2003]). In the Effelsberg measurement of 1519-273, the source appeared unpolarized from the raw values, but D-term calibration revealed a level of CP in good agreement with the values reported in the literature. The Effelsberg measurement of the weakly circularly polarized source 3C 279 also shows a level of CP close to that published ($V = (-0.17 \pm 0.01)\%$ from Aller et al. [2003]).

Comparison between the observed CP and previously published values

Time variability in CP and changes of sign are very common [Aller et al., 2003], 1519-273 is the most stable CP source known so far. Table 5.3 shows a sample of CP values that we observed during 2007. Our detections also confirm the stability of the CP level of 1519-273.

Repeatibility of the measurements

5.3 Linear polarization

The proposed calibration scheme maintains the same reliability in the calibration of linear polarization as that reported by Turlo et al. [1985] based on a 3×3 Müller matrix. In addition, our method supplies Stokes V, the D-terms and the complete error treatment.

The polarization calibration is typically applied assuming a Müller matrix unaffected by errors, whereas the scheme that we propose includes the error propagation also during the matrix inversion and its application, hence the

Table 5.2: Observed circular polarization, before and after applying the D-terms calibration.

Source		I_m [K]	σ	V_m [%]	σ	I_s [K]	σ	V_s [%]	σ
0056−00		4.180	0.045	-0.09	0.16	4.193	0.083	0.28	0.12
0134+32	3C 48	17.218	0.183	-0.19	0.10	17.288	0.266	0.24	0.09
0153+74		3.134	0.032	-0.03	0.20	3.147	0.036	0.42	0.04
0316+41	3C 84	46.456	0.478	-0.44	0.11	46.651	0.655	0.00	0.06
0212+73		12.913	0.120	-0.36	0.11	12.967	0.146	0.08	0.04
0607−15		11.352	0.148	-0.16	0.07	11.398	0.201	0.28	0.08
0716+71		2.991	0.028	-0.28	0.16	3.004	0.035	0.18	0.04
0743−00		6.063	0.015	-0.09	0.10	6.089	0.132	0.36	0.08
0835+58		1.867	0.027	-0.21	0.25	1.880	0.031	0.25	0.12
0836+71		6.692	0.069	-0.37	0.15	6.720	0.085	0.09	0.08
0951+69	3C 231	10.320	0.128	-0.20	0.15	10.362	0.117	0.25	0.04
1226+02	3C 273	117.944	1.083	-0.43	0.09	118.458	2.049	0.04	0.09
1253−05	3C 279	36.672	0.223	-0.33	0.11	36.831	0.635	0.11	0.07
1328+30	3C 286	23.331	0.305	-0.28	0.11	23.428	0.307	0.14	0.11
1409+52	3C 295	20.688	0.439	-0.20	0.11	20.763	0.357	0.25	0.07
1519−27		4.700	0.079	0.20	0.21	4.719	0.114	0.62	0.15
1749+09		10.873	0.097	-0.37	0.12	10.919	0.238	0.07	0.10
1800+44		3.830	0.079	-0.49	0.12	3.844	0.044	-0.04	0.05
2134+00		31.723	0.672	-0.45	0.07	31.836	0.551	-0.01	0.07
2145+06		18.925	0.211	-0.39	0.07	19.003	0.284	0.05	0.06
NGC 6572		3.861	0.008	-0.42	0.11	3.878	0.117	0.03	0.12
NGC 7027		17.068	0.343	-0.51	0.13	17.130	0.218	-0.06	0.05
SATURN		1.962	0.028	-0.85	0.19	2.165	0.042	-0.30	0.09

Table 5.3: Repeated observations of circular polarization, in percentage, from a sample of sources, during 2007.

Source		Feb V	σ	Apr V	σ	May V	σ	Jun V	σ	Aug V	σ	Nov V	σ	Dec V	σ
0743−00		0.53	0.04	0.42	0.05	0.24	0.08	0.18	0.06	0.52	0.04	0.36	0.08	0.38	0.06
1253−05	3C 279	0.11	0.05	-0.12	0.08	-0.40	0.09	-0.25	0.06	-0.35	0.10	0.11	0.07	0.29	0.12
1519−27		-	-	0.65	0.14	0.53	0.08	0.61	0.11	-	-	0.62	0.15	-	-
NGC 6572		-	-	-0.33	0.19	-0.06	0.04	-	-	-	-	0.03	0.12	0.19	0.13

resulting error estimates are intrinsically higher than those obtained with the standard procedure. Tables 5.4 and 5.5 show the comparison between the standard and the new calibration schemes, when measuring linear polarization.

Comparison between the observed LP and that obtained with the traditional calibration at Effelsberg

The linear polarization values are consistent with those obtained with the standard method.

5.4 Comparison with the Michigan 26-m telescope

In the last 30 years, the 26-m telescope of the University of Michigan has been the only single-dish radio telescope used to carry out multi-frequency full-Stokes observations of extragalactic radio sources [Aller et al., 2003]. The sample of 43 sources observed at Effelsberg during the test phase contained the QSOs 3C 279 and 2145+06 and the Radiogalaxy 3C 84, all part of the Michigan monitoring program, that in these years have been extensively studied in circular and linear polarization [Homan et al., 2009, Homan and Lister, 2006].

The Michigan 26-m telescope is an equatorial mounted primary focus single dish radiometer. Linear and circular polarizations are obtained by mean of rotating double feed horn systems, equipped with quarter-wave plates (tapered slabs of plastic inserted in the horn). At the vertex of the parabolic mirror a noise diode transmits a signal through a polarizing grid, which is aligned with respect to the North pole. Periodical observations of the transmitted polarized signal guarantee the correct orientation of the wave plates.

Characteristics of the Michigan 26-m telescope

By switching between the two horns (on-off technique) and between the orthogonal modes of the main horn (through the rotation of the system), all four Stokes parameters are obtained.

The instrumental polarization is calibrated by observing galactic HII regions, assumed to be unpolarized. Typical accuracies achieved, after some hours of integration time, are of the order of $0.05 \div 0.2\%$, for strong sources ($I \geqslant 5 Jy$).

Figures 5.1, 5.2 and 5.3 show the values of V observed at 6 cm at Effelsberg and a selection of the V values observed at the same wavelength at the University of Michigan during 2007, for 3C 279, 3C 84 and 2145+06 respectively.

Comparison between the observed CP and that measured at the Michigan telescope

The measurements were carried out independently and typically are not contemporary. Anyhow they have been taken regularly during the year, and the time gap between an Effelsberg observation and a Michigan one ranges from 1 to 20 days.

The plots clearly show a very good agreement between the observed sets of measurements.

Table 5.4: Observed linear polarization, in percentage, from a sample of sources measured at 6 cm at Effelsberg during 2007. Superscripts [1] indicates the results obtained with the new calibration procedure, [2] those obtained with the traditional calibration procedure.

		Feb		Apr		May		Jun		Aug		Nov		Dec	
Source		P	σ	P	σ	P	σ	P	σ	P	σ	P	σ	P	σ
0743−00 [1]		0.81	0.19	0.87	0.12	0.97	0.54	1.28	0.27	1.12	0.17	1.11	0.60	0.84	0.53
0743−00 [2]		0.82	0.13	0.85	0.09	0.97	0.20	1.24	0.06	1.06	0.08	0.98	0.09	0.90	0.13
1253−05 [1]	3C 279	3.25	0.28	1.24	0.21	0.81	0.45	0.96	0.40	1.14	0.36	1.42	0.86	1.11	1.63
1253−05 [2]	3C 279	3.15	0.08	1.17	0.03	0.82	0.03	0.91	0.02	1.11	0.04	1.16	0.04	1.06	0.00
1519−27 [1]		-	-	3.62	0.71	2.96	0.25	5.79	0.58	-	-	4.70	0.62	-	-
1519−27 [2]		-	-	3.50	0.01	3.20	0.16	5.83	0.01	-	-	4.55	0.27	-	-
NGC 6572 [1]		-	-	0.09	0.79	-	-	-	-	-	-	0.21	1.27	0.31	0.77
NGC 6572 [2]		-	-	0.16	0.01	-	-	-	-	-	-	0.24	0.27	0.48	0.59

Table 5.5: Observed polarization angle, in degrees, from a sample of sources measured at 6 cm at Effelsberg during 2007, superscripts [1] indicate the results obtained with the new calibration procedure, [2] those obtained with the traditional calibration procedure.

		Feb		Apr		May		Jun		Aug		Nov		Dec	
Source		PA	σ	PA	σ	PA	σ	PA	σ	PA	σ	PA	σ	PA	σ
0743−00 [1]		29.5	0.4	31.4	0.2	32.2	0.3	28.1	0.4	30.6	0.2	31.0	1.0	26.0	0.6
0743−00 [2]		28.8	1.8	30.6	2.1	31.8	1.4	29.6	1.4	29.8	1.2	34.4	2.3	24.6	7.5
1253−05 [1]	3C 279	-28.9	0.1	-28.7	0.2	-36.5	0.4	-17.7	0.4	-1.3	0.4	12.0	0.5	9.6	0.8
1253−05 [2]	3C 279	-29.9	0.6	-28.8	1.3	-31.6	1.7	-17.9	0.6	-1.9	1.0	13.5	0.5	8.6	0.1
1519−27 [1]		-	-	3.3	0.1	-34.3	0.1	-36.4	0.2	-	-	130.1	0.3	-	-
1519−27 [2]		-	-	2.2	0.3	-28.1	6.6	-36.6	0.1	-	-	129.4	1.8	-	-

Figure 5.1: 3C 279, observations carried out at 6 cm during 2007 at the Effelsberg and University of Michigan telescopes.

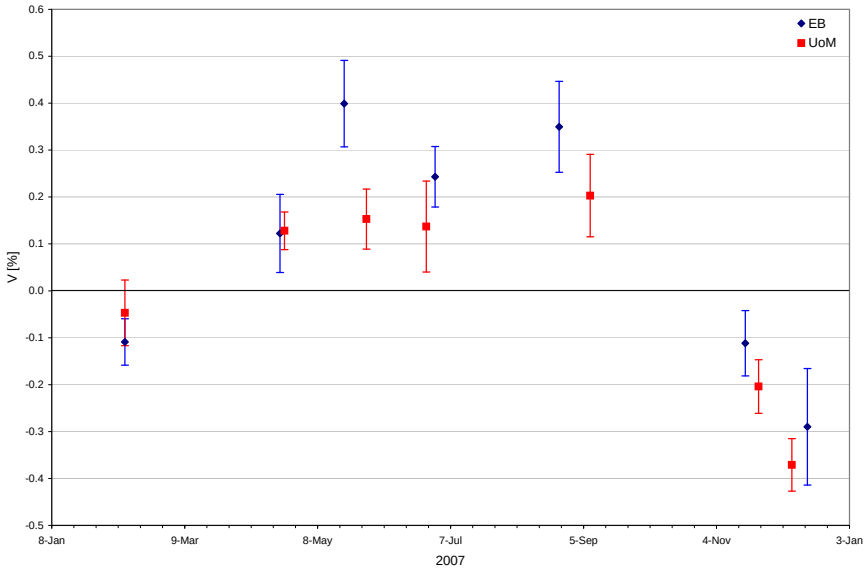

Figure 5.2: 3C 84, observations carried out at 6 cm during 2007 at the Effelsberg and University of Michigan telescopes.

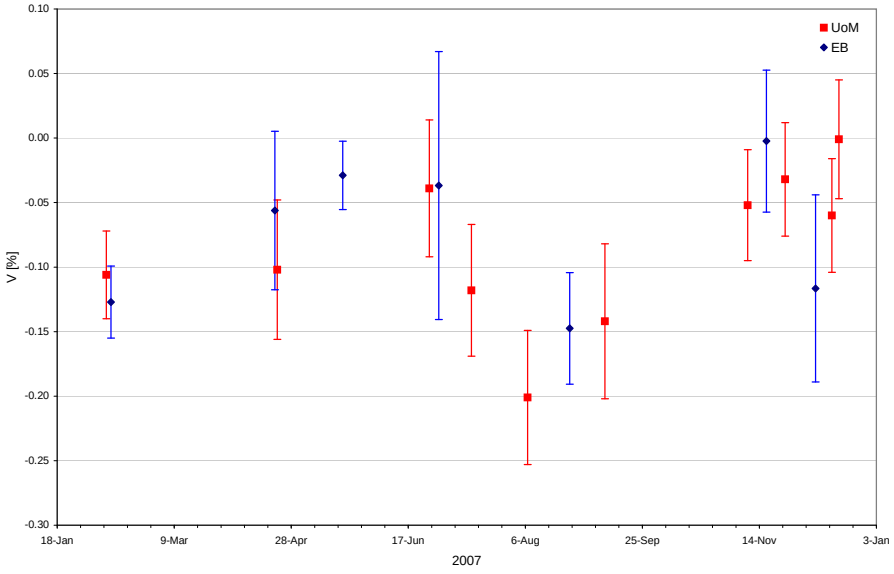

Figure 5.3: 2145+06, observations carried out at 6 cm during 2007 at the Effelsberg and University of Michigan telescopes.

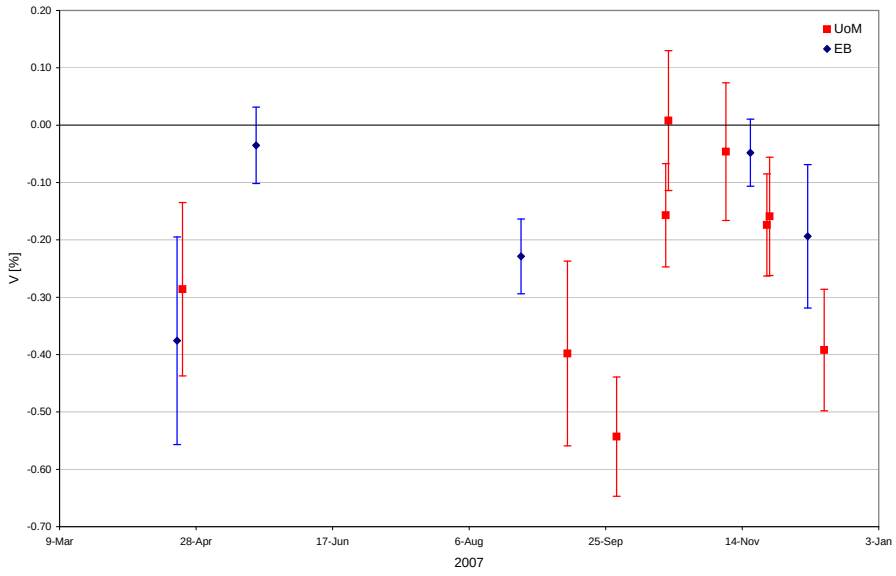

Part II

The northern 1-Jy full polarimetric survey

6 The Effelsberg-WSRT polarimetric survey

Contents

The results obtained during the one year test of the full Stokes calibration were quite encouraging, besides, in November 2007 a cross-check of our results has been performed with the ATCA, during a technical session. Although it has been possible to check 3 sources only, and not at the same time with Effelsberg, the measured values were in good agreement: as an example our observations of 0528+134 gave an average corrected value of V of (0.14±0.06)%, in good agreement with the ATCA that measured (0.192±0.003)%.

Cross-check with ATCA

Whereas on the one hand there was the need of collecting more data, in order to be able to realize some statistical analysis, on the other one a proper cross-check of the observed data was still missing. Hence we planned a full Stokes polarimetric survey that involved both Effelsberg and Westerbork, an interferometer equipped at 5 GHz with native linear feeds. The two telescopes have carried out the survey simultaneously on August 8th to 10th, 2008.

6.1 The need of an updated polarimetric survey

The lack of accurately known CP calibrators and the intrinsically low values involved have often induced the CP measurements to be discarded from the usual radio polarimetric observations. A statistically complete full Stokes catalog was still missing: at present the most complete are Komesaroff et al. [1984] and Weiler and de Pater [1983] with measurements mostly carried out in the 1970s.

At that time, some works were carried out in order to define a few characteristics of CP, e.g. high variability [Komesaroff et al., 1984] and the correlation between high degrees of CP and flat spectrum sources [Weiler and Wilson, 1977].

Rayner et al. [2000] selected a sample of 31 objects belonging to the southern sky and reached the impressive accuracy of 0.01% with the ATCA: their results seem to indicate that BLLac sources and quasars have systematically higher

CP degrees than radio galaxies. Homan and Lister [2006] examined CP of 133 AGN in the MOJAVE sample (VLBA at 15 GHz, typical accuracy around 0.1%) and Homan et al. [2001] examined parsec-scale CP of 40 blazars (VLBA at 5 GHz, typical accuracy around 0.05%). At frequencies higher than 15 GHz and up to 43 GHz, some works have been carried out with the VLBA (typical accuracy around 0.1-0.2%), e.g. Vitrishchak et al. [2008] on a sample of 41 AGN. Implications of high values of CP from IDV sources have been investigated by Jauncey et al. [2003].

We believe that a high-frequency selected complete catalog of bright sources like the 1-Jy sample [Kühr et al., 1981] is the ideal starting point for a complete full Stokes study: with its 518 sources (nearly 300 in the Northern hemisphere) it allows a well-based statistical analysis of the CP sources.

On August 8^{th}-10^{th}, 2008, the northern part of the catalog has been observed at 5 GHz with two different (in concept and location) instruments: the 100-m Effelsberg antenna, equipped with native circular feeds, and the Westerbork interferometer, equipped with native linear feeds. A common sample of sources has been observed by both instruments so that the reliability of the circular polarization calibration methods could be checked.

The whole set of measurements could form the basis of a statistically complete full polarimetric reference catalog.

6.2 The Westerbork Synthesis Radio Telescope

The Westerbork Synthesis Radio Telescope (WSRT) is an interferometer composed of 14 equatorially mounted 25-m dishes that form an East-West array line of 2.7 km length. At 5 GHz it is equipped with circular feeds that offer native linear outputs, consisting in an excellent configuration to measure CP (that in this case is obtained through correlation and not anymore as small difference of two large quantities, see Eqs. 2.9). The accuracy of an interferometer that offers linear outputs when measuring CP represents an ideal reference for a single-dish antenna that instead offers circular outputs. We arranged the survey so that a subset of sources were observed by both instruments nearly contemporary, allowing a direct evaluation of the Effelsberg full Stokes calibration procedure.

Main characteristics of the WSRT

The WSRT is located 266 km north from Effelsberg, providing a large overlap of the portions of sky that the two instruments can access.

At 5 GHz, in continuum mode, the WSRT offers 8 bandwidths of 20 MHz each, to be located in the range $4.770 \div 5.020$ GHz, whereas Effelsberg provides a 500 MHz bandwidth between 4.6 and 5.1 GHz. We do not expect a big influence of the slightly different frequency coverage, anyhow the variation of CP through adjacent frequency channels has still to be properly investigated.

6.3 Source selection and completeness

Our sample has been selected from the 1-Jy catalogue with the following constraints:

1. Sources with $\delta_{2000} < -10^{\circ}$ have been excluded;
2. Sources that, by visual inspection, show an extended structure in the NVSS image [Condon et al., 1998] were excluded. Few additional sources

that, in the Westerbork images, show confusing features beyond a 2-beam radius from the center, were also excluded. A detailed study, focused on extended sources, is planned as integration of the present results.

These selection criteria yield a sample of 270 sources. Bad weather during observations has further reduced the sample to 257 sources.

If we had applied the declination constraint only, the sample would have been composed of 313 sources and would have fully preserved the completeness level of its parent catalogue. By assuming a normal distribution of the CP values across the sample and an occurence of statistically relevant CP values of 15% [Homan and Lister, 2006], our sub-sample can be considered representative of its parent one with a 95% confidence and an error of nearly 1.5%.

Sources with $-10^\circ < \delta_{2000} \leqslant 30^\circ$ were observed with the 100-m Effelsberg single-dish antenna and sources with $\delta_{2000} > 30^\circ$ were observed with the Westerbork interferometer. A sample of 31 sources at $\delta_{2000} > 30^\circ$ have been observed by both instruments in order to cross-check the reliability of the CP calibration techniques.

6.4 Observation and calibration procedures

We have used 3C 286 (1328+301) as common highly linearly polarized main calibrator and added to the source list the planetary nebula NGC 7027 (2105+42, Perley and Butler [2006]). Although the latter is slightly extended for the WSRT, we are currently considering it the only reliable V=0 calibrator.

6.4.1 Effelsberg

The sources were observed with 5-beam wide (i.e. nearly 12′) cross-scans (with 8 to 24 subscans each, depending on general observing conditions) centred on the source position, along the azimuth and elevation directions.

In 2007 we have developed and tested a new calibration procedure that allows full Stokes polarimetry with the Effelsberg antenna in the range 2.7-10.5 GHz, this procedure is described in the first part of this thesis [Cenacchi et al., 2009] and is based on the Müller matrix correction [Turlo et al., 1985]. The elements of the matrix are computed from the observation of a fully unpolarized source and a highly linearly polarized one, allowing the correction for the leakage terms among the four Stokes parameters. As mentioned previously, the Effelsberg telescope offers native circular outputs at 5 GHz, which forces Stokes V to be estimated as difference between the right hand and left hand channel outputs, whereas Stokes Q and U come directly from the polarimeter.

6.4.2 Westerbork

The sources were observed with 3 scans, one during the transit of the source through the meridian and the other two nearly 2-3 hours before and afterwards. The 160-MHz band (split in 64 channels of 312.5 kHz each), was located in the range $4.84 \div 5.00$ GHz. Special care during the scheduling has been applied in order to avoid possible shadowing among the antennas. Under these assumptions, the theoretical reachable rms is around 0.2 mJy. The shortest baseline was 36 m and the longest one 2.7 km.

The data were reduced under AIPS, optimized in the analysis of data obtained with circular feeds, following R. Braun's recipe ("Analysis of WSRT DZB data with classic AIPS", available at the ASTRON web site). Processing linear outputs with AIPS limits the self-calibration procedure to the phase only, besides the Stokes parameters are permuted and changed in sign, so that Q corresponds to $-U$, U corresponds to $-V$ and V corresponds to $-Q$.

WSRT data reduction under AIPS, imaging and estimate of the error

Channels and IF have been averaged in order to obtain a result as similar as possible to the Effelsberg one, a more detailed analysis of possible CP variations over the bandwidth (particularly focused on sources peaked in the examined band) is planned for the next future. Each source has been cleaned and self-calibrated (in phase only) individually. After the corrections, we examined the fluxes obtained for the primary calibrator, and found a variation of 2%, which we took as residual calibration error for all the Stokes parameters.

For each source, we imaged Stokes I (AIPS task TVALL) and we set a rectangular box (TVWIN) around the emission area. We used then the IMSTAT task to read the mean and rms brightness both inside the box (DOINVER -1) and outside (DOINVER 1), this second information was useful to derive the background noise of the image. The IMSTAT task output includes also the beam size and the box area in pixel unit. Without changing the box size, we have run the IMSTAT task on the images of Stokes Q, U and V taking each time two measurements, one inside the box and one outside.

Then, each Stokes integrated value has been derived according to the following:

$$S = [M_1 - M_2] \cdot \frac{Px}{B} \tag{6.1}$$

$$\sigma = \sqrt{(S \cdot \sigma_c)^2 + \left(\frac{\sigma_i}{2}\right)^2 \cdot \frac{Px}{B}} \tag{6.2}$$

Where:
M_1 is the mean value given by the AIPS task IMSTAT inside a box set around the Stokes I image of the source
M_2 is the same value coming from the image area outside the box
Px is the number of pixel contained in the box
B is the beam size
σ_c is the calibration error (0.02)
σ_i is the rms of the image, calculated outside the box

Considerations about the WSRT accuracy

Whereas a new calibration procedure, aimed at increasing the telescope accuracy when observing CP, has been developed at Effelsberg, we have not applied any special calibration to the V values from the WSRT. The accuracy achievable by Effelsberg when measuring CP is now of the order of 0.1%, comparable to that of the "raw" values measured through the correlation of the WSRT linear outputs.

7 Results from the survey

Contents

7.1 Consistency between WSRT and Effelsberg

The sample of sources observed by both instruments is too small to derive a normal distribution of the observed CP values, hence we have performed a Mann-Whitney-Wilcoxon test (MWW hereafter) to check the consistency of the observed Stokes parameters. The MWW test is one of the most commonly used non-parametric method to compare two treatments when the underlying distribution of the outcome variable is not normally distributed. Table 7.1 lists the p-values for each observed Stokes parameter. A good consistency (95% confidence) is assumed for $p>0.05$.

Figs. 7.1 to 7.4 show the observed values, also listed in Table A.1. The measurements of Stokes I and Q exhibit the best agreement. The p-value related to the measurements of Stokes V, despite three divergent points that could be maybe addressed to fast variability, shows that there is a good consistency between the data sets observed by the two instruments, which confirms the reliability of the Effelsberg CP calibration at the 1-mJy error level. The measurements of Stokes U show the worse alignment, although the related p-value still supports the good agreement of the two instruments.

7.2 Complete results and discussion

The survey results are listed in Appendix A, Table A.2. Optical classification and source properties (columns 19÷23) are taken from Stickel et al. [1994].

7.2.1 Distribution of CP within the whole sample

Figure 7.9 shows the distribution of the observed CP values. We have performed an Anderson-Darling test (AD test), to assess the normal distribution

Figure 7.1: Comparison Effelsberg/WSRT, observed Stokes I.

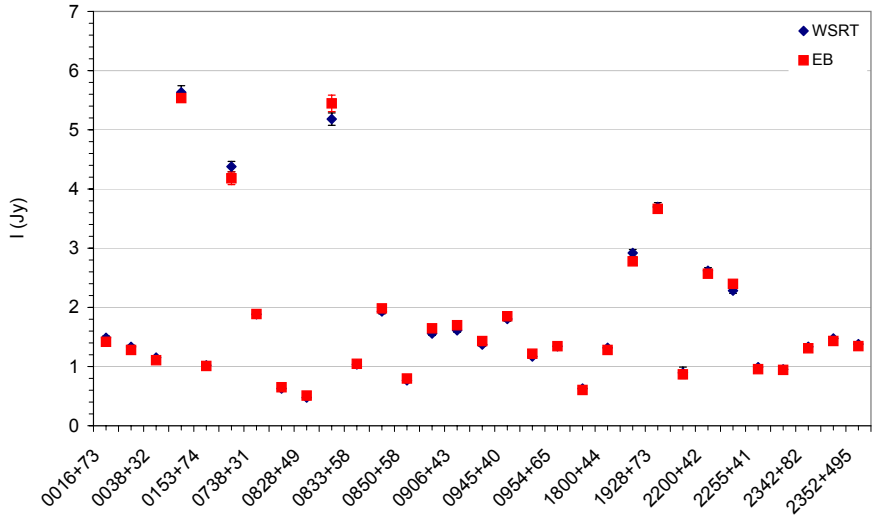

Figure 7.2: Comparison Effelsberg/WSRT, observed Stokes Q.

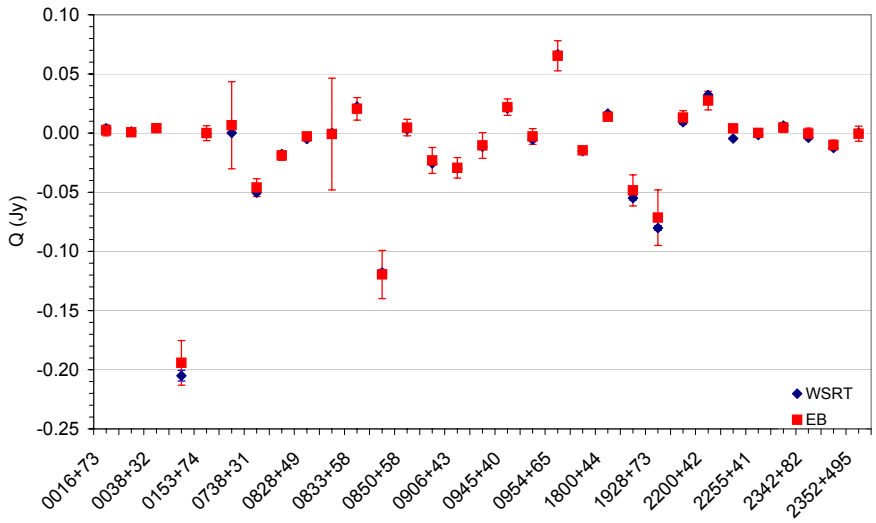

Figure 7.3: Comparison Effelsberg/WSRT, observed Stokes U.

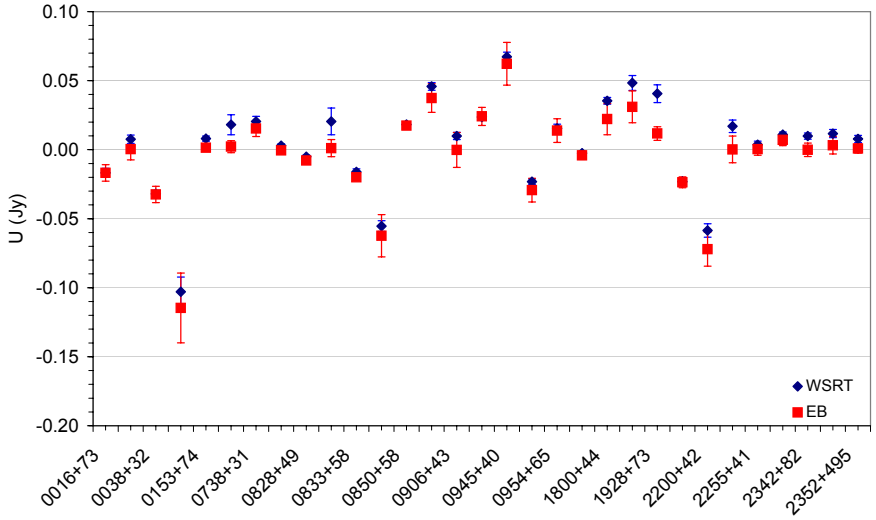

Figure 7.4: Comparison Effelsberg/WSRT, observed Stokes V.

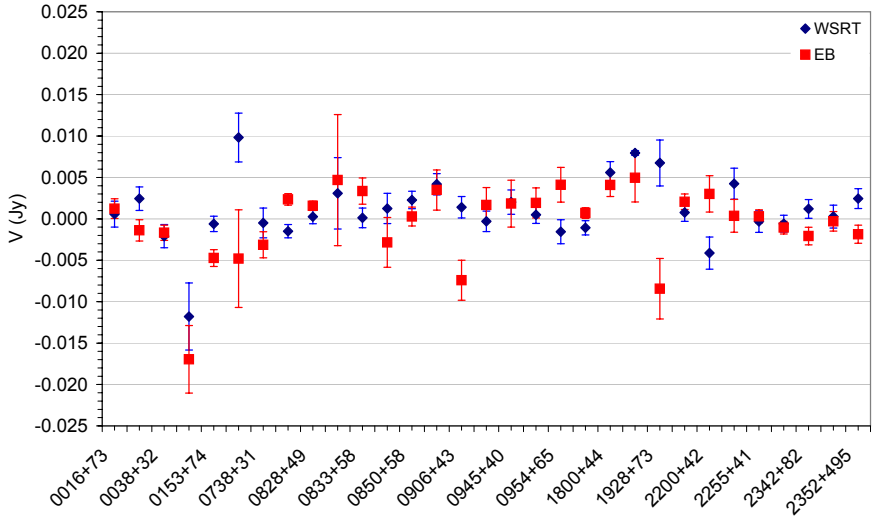

Table 7.1: Comparison Effelsberg/WSRT: p-values from the MWW test. Consistency is verified for p>0.05.

Stokes	p
I	0.9551
Q	0.7461
U	0.1393
V	0.3676

of the observed sample. The AD test, in general, assesses whether a sample comes from a specified distribution, and, in its most common application, is used to find possible departures from normality. Resulting p-values > 0.05 support the assumption of normality and, in this case, we obtained a p-value of 0.404 (Fig. 7.5 shows the related probability plot). No preferred sign for CP can be derived from our measurements.

Nearly 10% of the sample exhibit a CP level above 0.3% at a significance level greater than 3σ.

7.2.2 Optical classification

Referring to Stickel et al. [1994] the optical classification that we adopted can be summarized as follows:

- QSO: presence of a strong bright core on optical images
- galaxies: lack of a dominating bright core
- BL Lac: lack of emission lines. These sources are divided into BL/Gal or BL/QSO depending on the absence/presence of a bright core (we use BL for the entire class of BL Lac objects)

The sample contains 151 QSO, 73 galaxies and 29 BL (plus unclassified sources). Firstly an AD test has been performed on each individual sample, to test the normality of the distributions. As shown in Table 7.2, all three sub-samples satisfy the condition of normality (p>0.05). Figures 7.10 to 7.14 show the distribution of CP for each optical type separately.

26 sources out of 257 exhibit CP above 0.3% with a significance larger than 3σ: 13 are QSO, 10 are galaxies and 3 are BL/QSO.

Following these results the one-tailed Kolmogorov-Smirnov (KS) test has been performed on each couple of classes to investigate possible similarities from the point of view of CP production. As the MWW test, the KS is a non-parametric test used to compare two independent samples and assesses if they are drawn from the same population (see Conover [1998] for a more detailed description of both tests). The KS is less affected by tied values (possible equal CP values) and its output, the distance between the cumulative fractions of the samples, can be easily plotted. The test takes into account the sign of CP

and similarity is assessed for a resulting $p>0.05$. Table 7.3 shows the values that we obtained.

Our results do not show any similar behaviour of CP emission among the classes. Particularly we do not observe a similarity between QSO and BL objects against galaxies, as previously observed by Rayner et al. [2000]. The distribution of CP values shows that galaxies can produce CP at the same level of QSO and BL objects. Previous similar studies are that by Rayner et al. [2000], who examined 6 galaxies, none of which showing any appreciable CP level, and that by Homan and Lister [2006], who examined 8 galaxies, one of which showing CP up to -0.5% at a significance above 3σ. Although the latter does not contain any statistical test on the galaxy sample, as it has been considered too small to supply reliable information, it seems to confirm the possible presence of CP within galaxies, in agreement with our detections.

In addition, we observe a slight preference for negative CP values from galaxies, and for positive ones from BL objects (as also shown by the cumulative fraction plots Figures 7.17 to 7.19). Homan and Lister [2006] have not examined the possibility of sign preferences in their samples, anyhow, referring to the list of values that they reported, they did not measure any preference of sign from galaxies (although the only 3σ detection they reported has a negative sign), whereas the measurements from BL objects seem to show a preference for a positive sign (13 out of 22 sources have positive sign, including the only 3σ detection), as we also measured.

Anyhow, our sample of galaxies is strongly biased by the selection criteria (by excluding the extended sources from the original sample we may have broken a possible symmetry around 0 in the CP distribution) and the BL sample contains few 3σ detections, hence we do not consider the observed preferences of sign as statistically reliable.

Figure 7.5: Probability plot for the observed CP values, whole sample. The straight line indicates an ideal normal distribution.

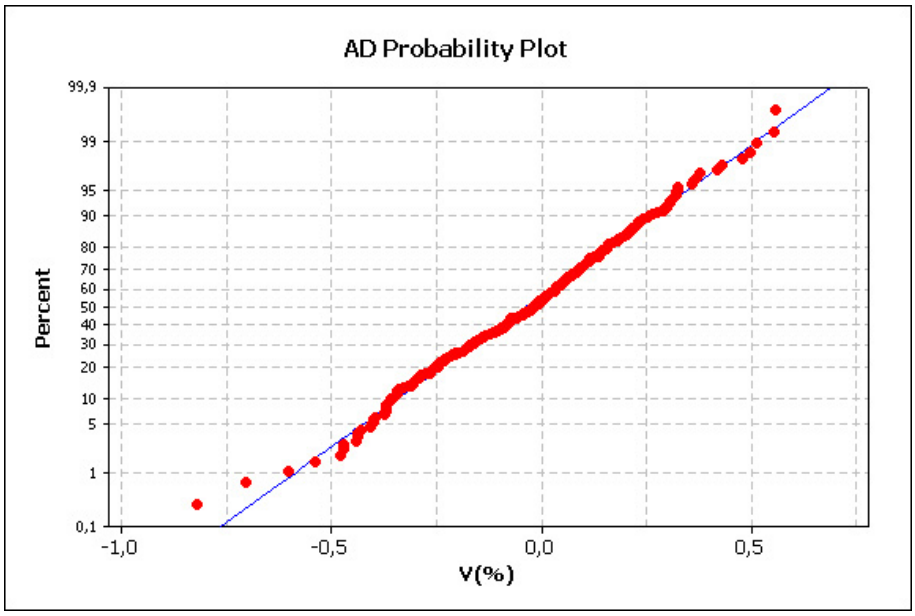

Figure 7.6: Probability plot for the observed CP values, BL. Layout as in Fig. 7.5

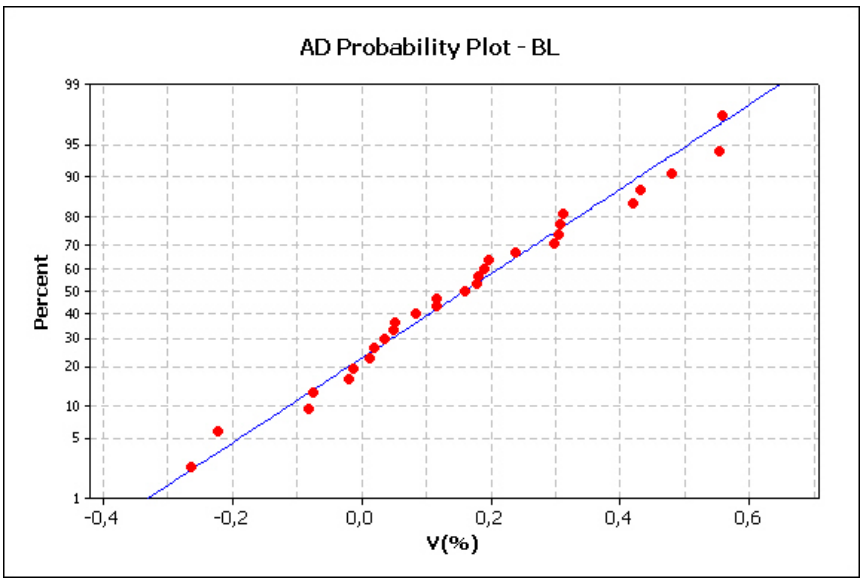

Figure 7.7: Probability plot for the observed CP values, QSO. Layout as in Fig. 7.5

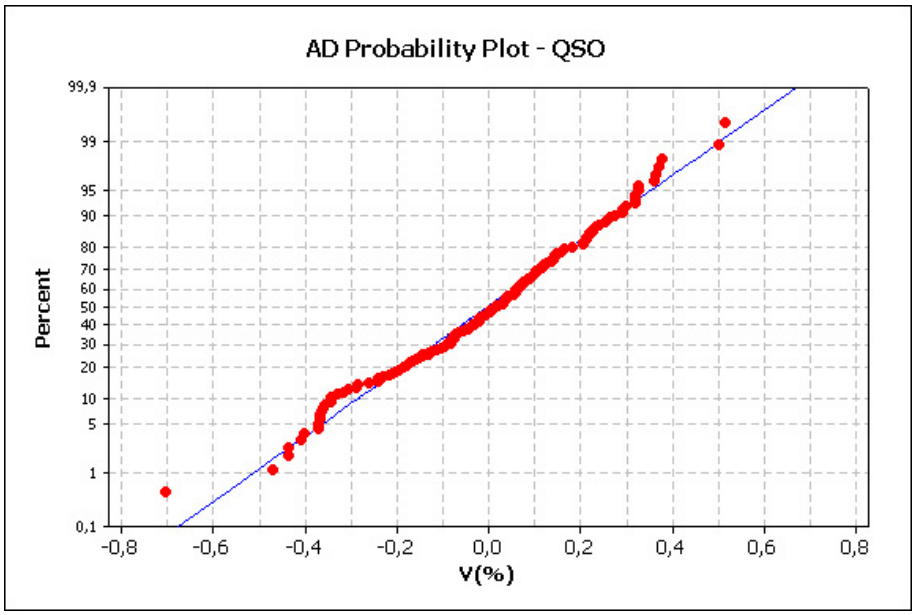

Figure 7.8: Probability plot for the observed CP values, galaxies. Layout as in Fig. 7.5

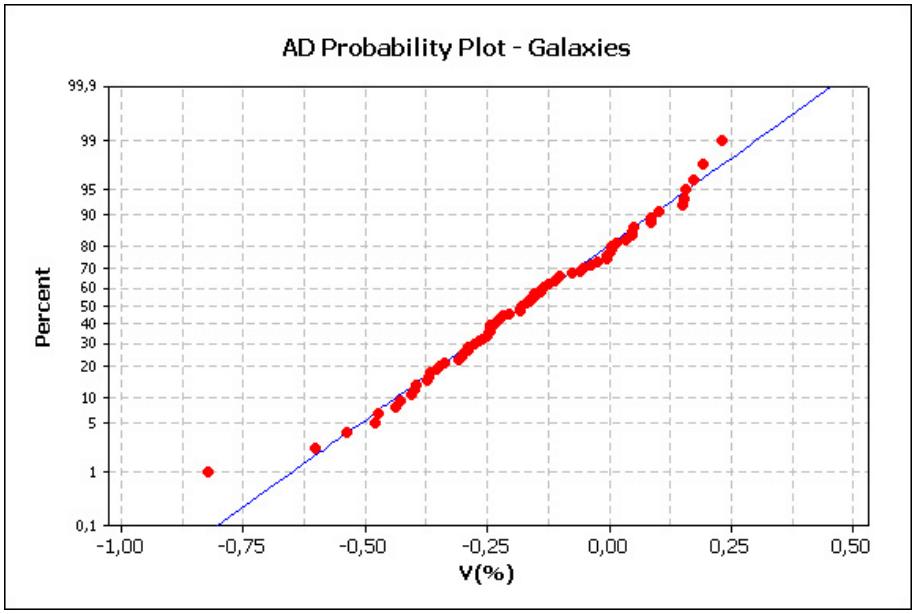

Figure 7.9: Distribution of observed CP values, whole sample. The significance of each measurement is indicated by different colours, white for $< 2\sigma$, light colour for $2 \div 3\sigma$ and dark colour for $> 3\sigma$. The total number of sources and the corresponding CP average, standard deviation and median are also indicated

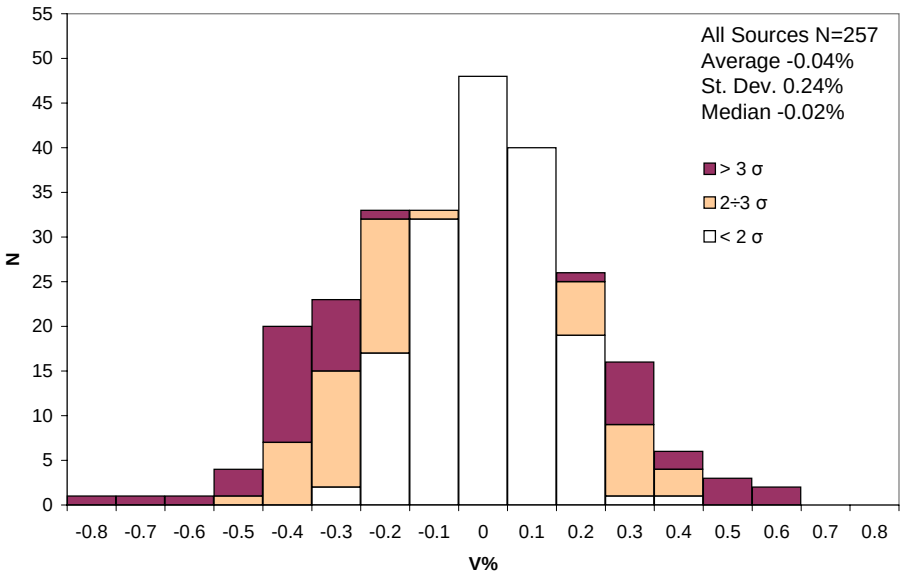

7.2.3 General Properties

In order to look for possible correlations of CP with other source properties, we have considered the spectral index α_{11-6} ($S_\nu \propto \nu^\alpha$), the redshift (both listed in Stickel et al. [1994]) and the linear polarization that we observed. We performed both the Pearson and the Kendall$-\tau$ tests for the whole sample and for each sub-class. Both tests are widely used to measure the strengths of association between two variables, but the Pearson is more efficient when variables are normally distributed, whereas the Kendall does not require any assumption related to the variables distribution.

Tables from 7.4 to 7.7 show the estimated correlation parameters (values equal to 1 and -1 would imply correlation or anti-correlation) along with the probability associated with the Pearson test (values close to 0 would support the hypothesis of correlation).

Figure 7.10: Distribution of observed CP values, galaxies. Layout as in Fig. 7.9.

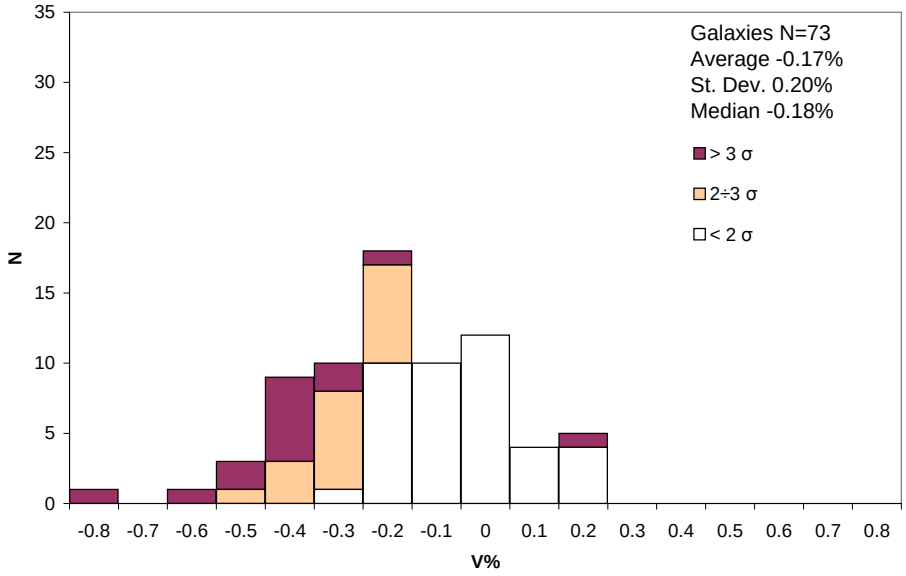

Figure 7.11: Distribution of observed CP values, QSO. Layout as in Fig. 7.9.

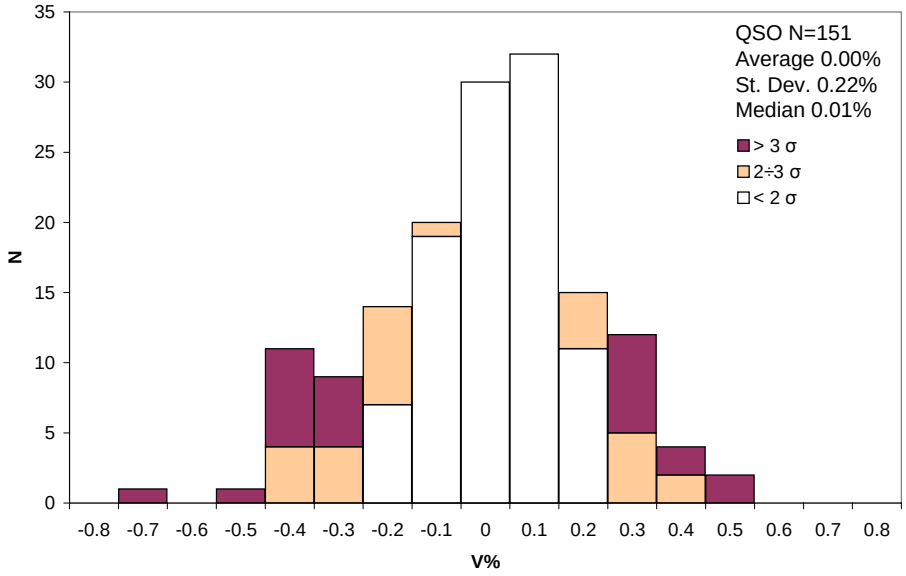

Figure 7.12: Distribution of observed CP values, BL. Layout as in Fig. 7.9.

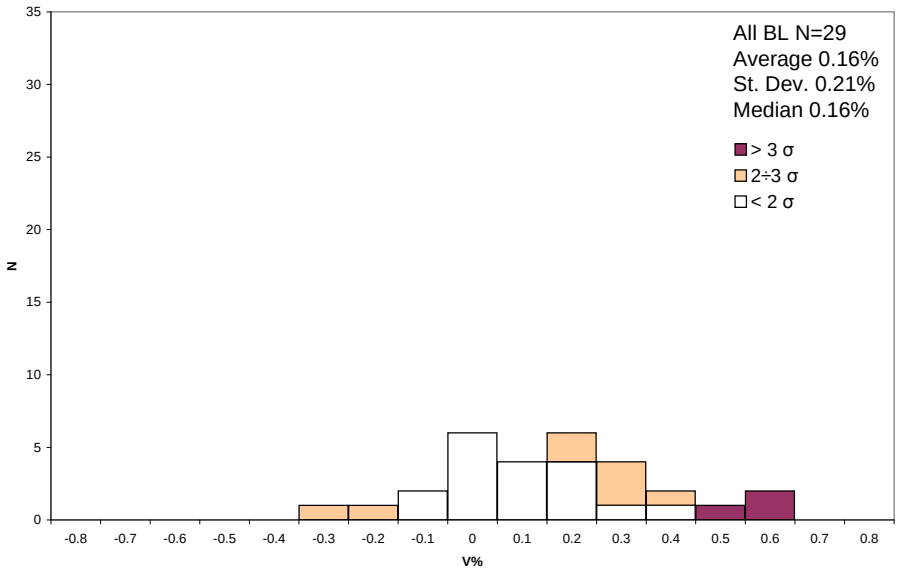

Figure 7.13: Distribution of observed CP values, BL/QSO. Layout as in Fig. 7.9.

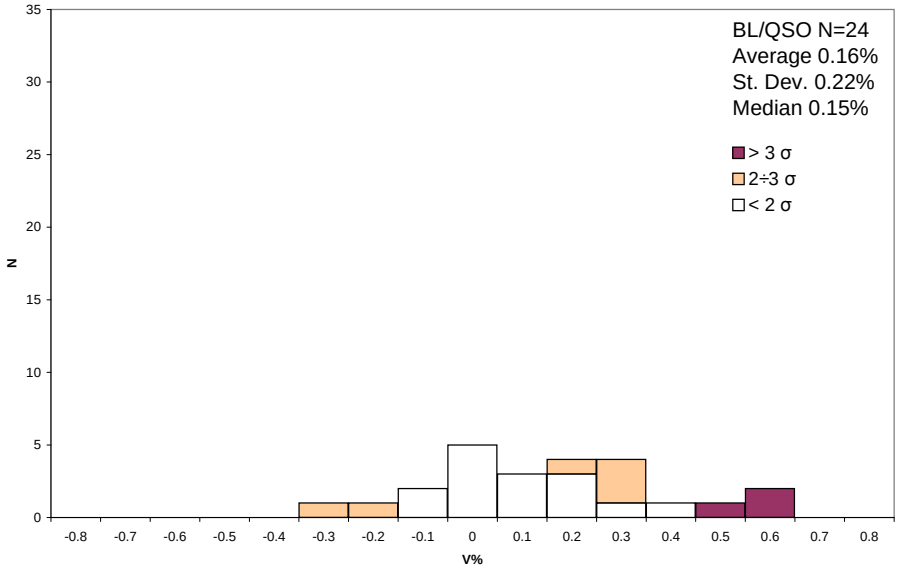

Figure 7.14: Distribution of observed CP values, BL/galaxies. Layout as in Fig. 7.9.

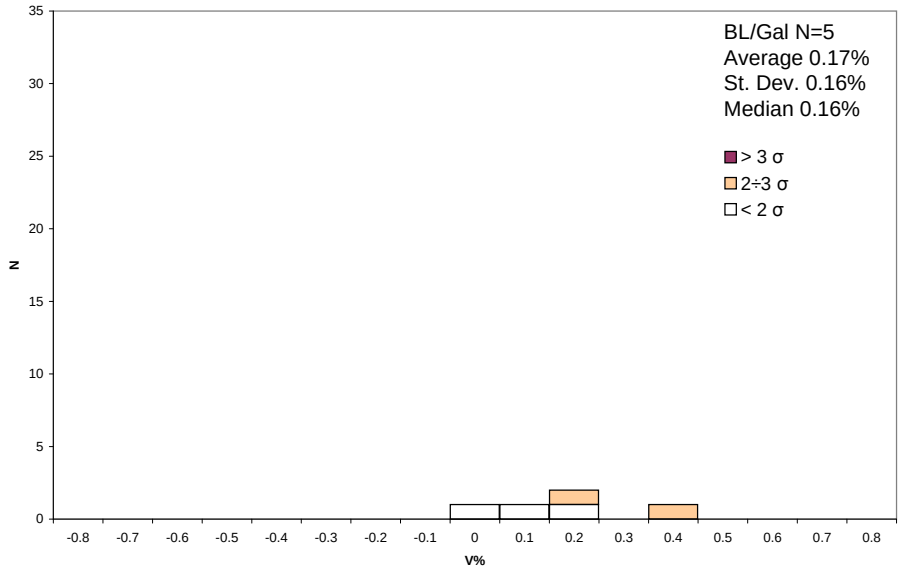

Figure 7.15: Distribution of observed CP values, FS sources. Layout as in Fig. 7.9.

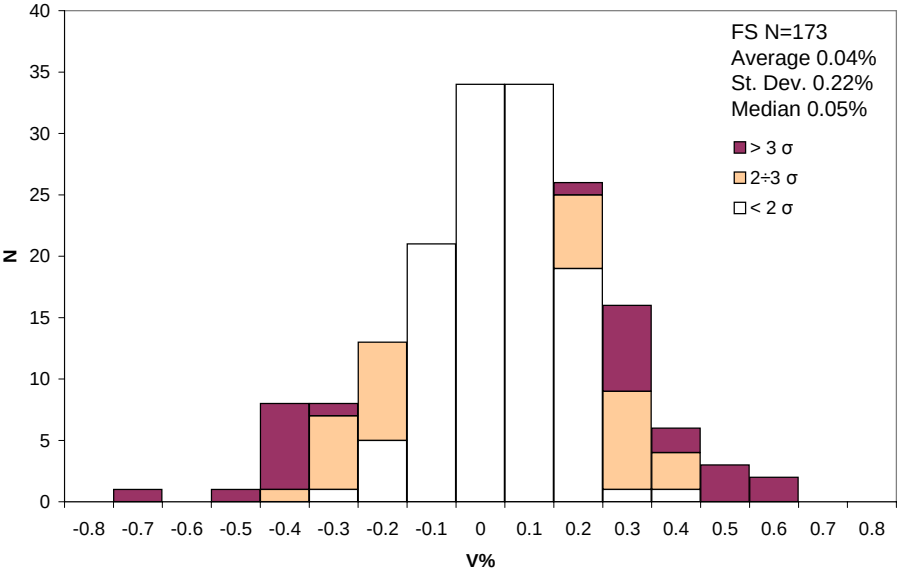

Figure 7.16: Distribution of observed CP values, SS sources. Layout as in Fig. 7.9.

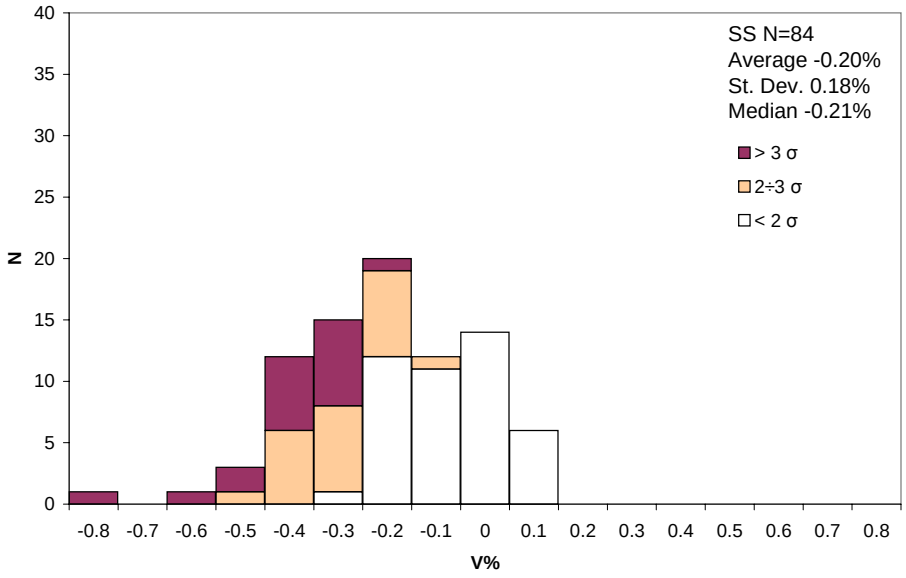

Table 7.2: AD values for different samples of sources, normality is verified for p$>$ 0.05.

Class	p
BL	0.216
QSO	0.108
G	0.856

Table 7.3: KS p-values for couple of classes, a p value $>$ 0.05 indicates similarity between the examined groups.

Couple	KS-p
G/QSO	0.000
G/BL	0.000
QSO/BL	0.015

Figure 7.17: QSO (solid line) versus galaxies (dashed line) cumulative fraction plot. The x-axis shows the percentage of CP. The median of the galaxies sample (0.5 point on the y-axis) is clearly shifted towards negative values.

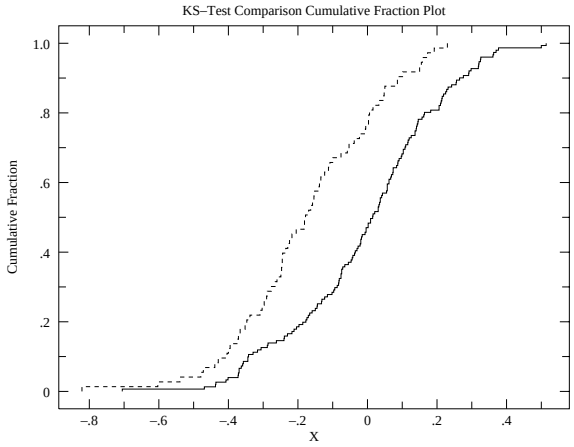

Figure 7.18: galaxies (solid line) versus BL objects (dashed line) cumulative fraction plot. Layout as in Fig. 7.17.

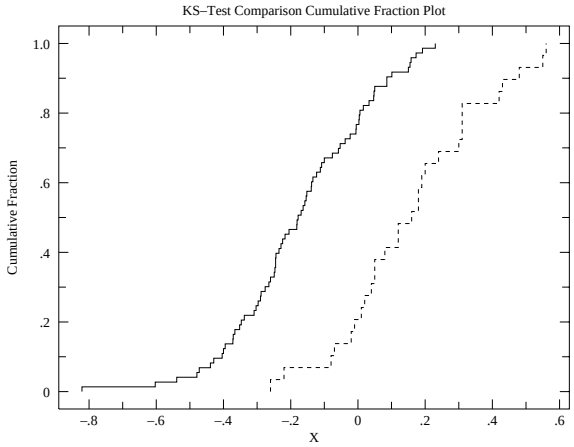

Figure 7.19: QSO (solid line) versus BL objects (dashed line) cumulative fraction plot. Layout as in Fig. 7.17.

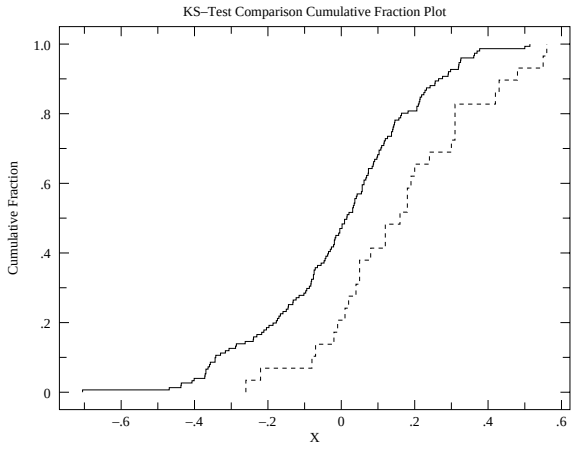

Table 7.4: Pearson-P and Kendall-τ factors for correlation with CP, whole sample. Values close to 1 and -1 indicate correlation and anti-correlation respectively. The p value related to the Pearson test, P-p, supports correlation for values close to 0.

Property	P	P-p	K-τ
Alpha	0.499	0.000	0.361
Redshift	0.117	0.079	0.104
LP	−0.019	0.760	0.044

Table 7.5: Pearson and Kendall factors for correlation with CP, galaxies. Values as in Table 7.4.

Property	P	P-p	K-τ
Alpha	0.370	0.001	0.276
Redshift	−0.082	0.518	−0.043
LP	−0.308	0.008	−0.179

Table 7.6: Pearson and Kendall factors for correlation with CP, BL. Values as in Table 7.4.

Property	P	P-p	K-τ
Alpha	0.181	0.347	0.182
Redshift	−0.368	0.122	−0.165
LP	−0.025	0.899	0.000

Table 7.7: Pearson and Kendall factors for correlation with CP, QSO. Values as in Table 7.4.

Property	P	P-p	K-τ
Alpha	0.383	0.000	0.263
Redshift	−0.016	0.848	0.007
LP	−0.020	0.806	0.019

CP versus redshift, two-point spectral index, LP

We did not find any straight correlation or anti-correlation. A weak linear dependency seems to exist with α_{11-6} for galaxies and QSO, which results in a weak correlation over the complete sample of sources (see Fig. 7.20). Also, a very weak anti-correlation with LP seems to exist for galaxies.

According to the standard definition, sources with $\alpha_{11-6} \geqslant -0.5$ are classified as flat spectrum sources (FS) while sources with $\alpha_{11-6} < -0.5$ indicate steep spectrum sources (SS), anyhow Stickel et al. [1994] lists a classification based not only on the two-point spectral index but on observations of the entire source spectra. Figs. 7.15 and 7.16 show the CP distribution according to the spectral classification by Stickel et al. [1994]. The plots mimic those showing CP distributions for galaxies and QSO, and we do not observe the correlation between high degrees of CP and FS sources. Both FS and SS sources in our sample exhibit similar levels of CP and the CP distribution for SS sources is shifted towards negative values.

7.3 New observations

During 2009 we have selected from Table A.2 a sub-sample of sources which exhibited CP larger than 0.3% and 3 mJy with a significance above 3σ. We have observed these at three different epochs with the Effelsberg telescope at 11, 6, 3.6 and 2.8 cm in order to study the source full Stokes spectra (Cenacchi et al., in prep.). We compared the new results with those observed during the survey in 2008 and here we report the comparison related to the re-observed galaxies and QSO (Table 7.8).

Despite the high variability that characterizes CP, almost all the detections were still above 3σ, besides, as a sub-sample of the survey values were taken

Table 7.8: CP results, in percentage, from the survey carried out in 2008, compared with new values observed in 2009, galaxies.

		2008	2009		
Source	Source	Survey	Apr. 29th	May 15th	May 18th
0019−00		-0.37±0.10	-0.78±0.13	-0.41±0.13	-0.44±0.06
0038+09	3C 18	-0.48±0.10	-0.24±0.11	-0.20±0.09	-0.33±0.05
0305+03	3C 78	-0.44±0.14	-0.48±0.14	-0.32±0.12	-
0307+16	3C 79	-0.54±0.11	-0.48±0.14	-0.90±0.17	-
0316+16		-0.60±0.10	-0.45±0.14	-	-
0433+29	3C 123	-0.37±0.10	-	-0.36±0.14	-

Table 7.9: CP results, in percentage, from the survey carried out in 2008, compared with new values observed in 2009, QSO.

		2008	2009		
Source	Source	Survey	Apr. 29th	May 15th	May 18th
0003−00	3C 2	-0.36±0.10	-0.35±0.12	-0.58±0.12	-0.24±0.05
0056−00		-0.37±0.11	-0.32±0.14	-0.41±0.13	-0.22±0.05
0134+32	3C 48	-0.31±0.07	-0.49±0.09	-0.32±0.14	-
0153+74		-0.47±0.10	-0.19±0.07	-0.19±0.07	-0.55±0.06
0202+14		-0.37±0.10	-0.56±0.16	-0.31±0.11	-0.47±0.06
0743−00		-0.44±0.10	-0.34±0.12	-	-
0809+48	3C 196	-0.32±0.10	-0.62±0.15	-	-
0812+36		-0.71±0.08	-0.26±0.08	-	-
2216−03		-0.40±0.10	-	-	-0.26±0.06

Figure 7.20: Observed CP percentage versus spectral index.

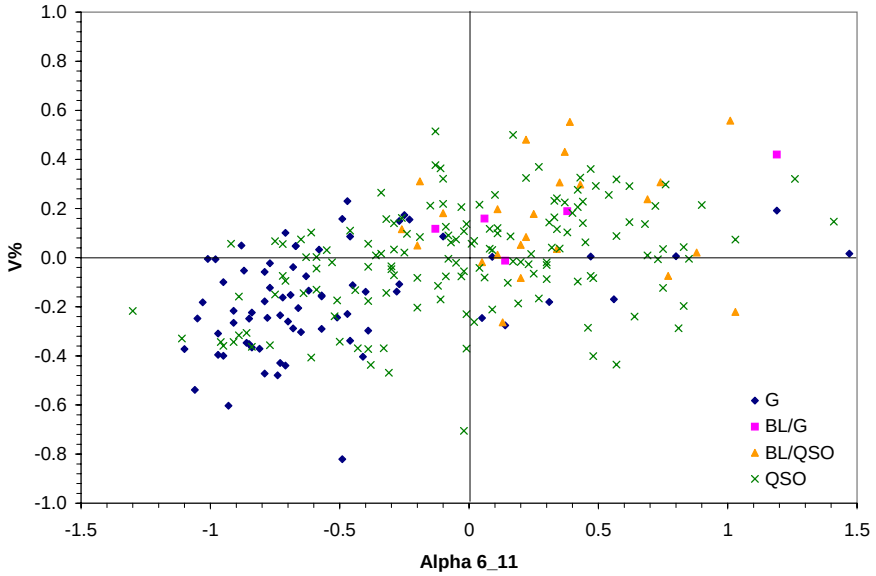

by WSRT, we consider these new results an additional confirmation of the reliability of our observation.

7.4 The Effelsberg telescope, accuracy and repeatability

During the test phase carried out in 2007 we achieved a typical accuracy in Stokes V of 1 mJy with a standard observation of nearly 10 minutes (which results in a 0.1% accuracy when observing sources with a flux of nearly 1 Jy). The survey carried out in 2008 confirmed this result, anyhow it must be stated that a proper study of the intrinsic variability of CP is still missing. In fact, we noted that some sources exhibited intra-week variation in CP and it is not yet clear how to disentangle the intrinsic variation from possible intrumental effects.

Considerations about the accuracy when measuring CP at Effelsberg

Being a proper list of CP calibrators also missing, it is hard to make statements about the repeatability of the measurements taken at Effelsberg. So far, the comparison made with the Michigan telescope is the only reliable proof that the observed CP variations are intrinsic to the sources, as the case of such a similar long-term instrumental behaviour would be quite unlikely. Hence, we consider the telescope accuracy as the most important limit to the CP measurements, with respect to the fraction of the standard deviation due to possible telescope drifts.

Hopefully, a follow-up study aimed to select possible CP calibrators, eventually carried out along with the Michigan telescope, will also allow a better

Figure 7.21: Observed CP percentage versus oberved LP percentage. The solid line corresponds to CP=LP

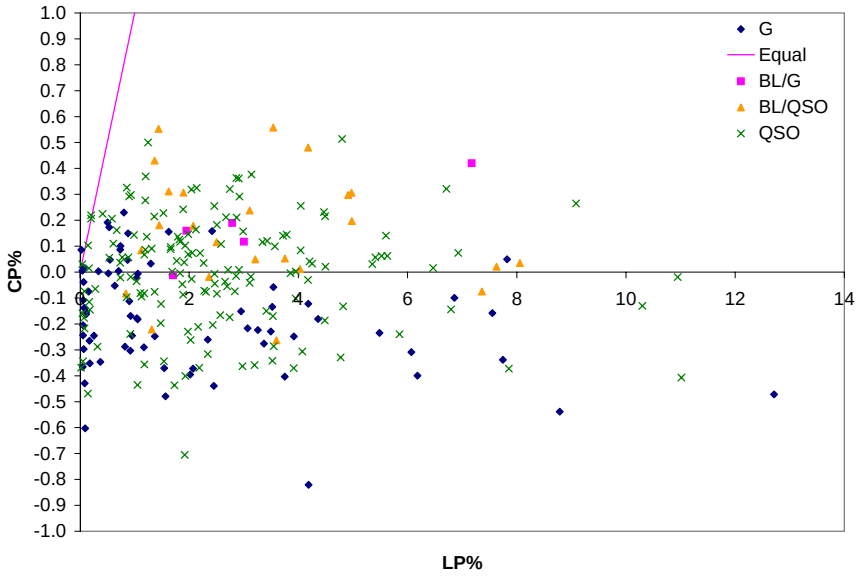

understanding of the long-term instrumental behaviour of the Effelsberg antenna, when measuring CP.

Figs. 7.22 and 7.23 show the polarimetric values observed by the Effelsberg telescope during the survey. On the basis of the distribution of the values, with respect to their significance, we consider a source to be circularly polarized when it exhibits CP larger than 0.3% in absolute value and linearly polarized when it exhibits LP larger than 0.5%.

Figure 7.22: Selection of the values observed by Effelsberg only, CP

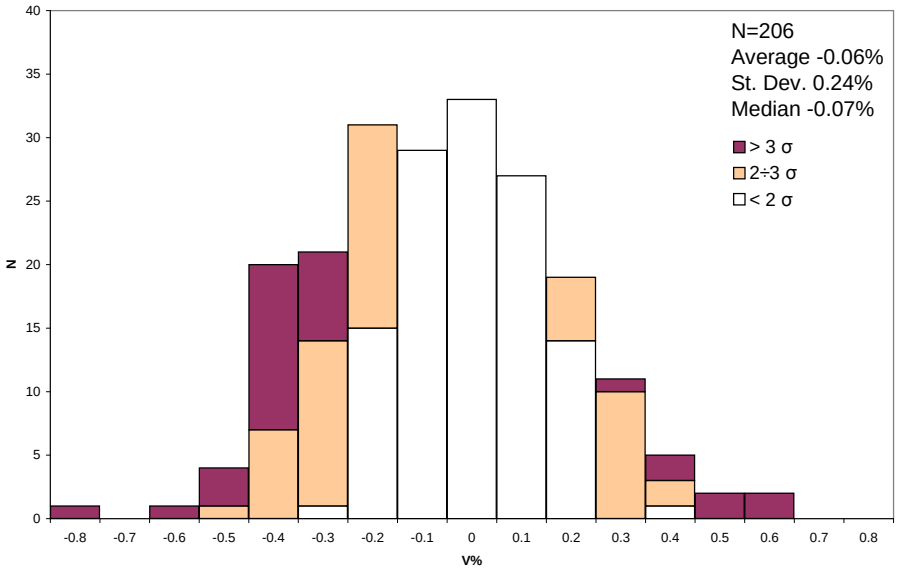

Figure 7.23: Selection of the values observed by Effelsberg only, LP

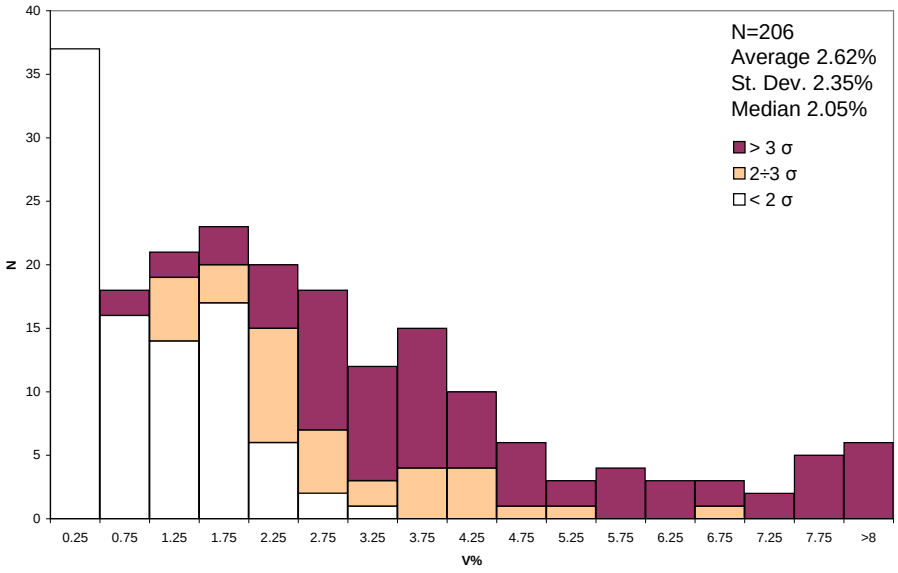

8 | Science with CP: future outlook

Contents

During 2008 we have extended our calibration procedure in the range $2.7 \div 10.5$ GHz and in 2009 we have performed full Stokes multi-frequency observations of 31 sources that appeared circularly polarized from the polarimetric 5 GHz survey (CP values $> 0.3\%$ and >3 mJy with a significance larger than 3σ). The spectra that we obtained for all 31 sources are enclosed in Appendix B.

In order to build a more detailed picture about the production of LP and CP within extra-galactic radio sources, we are currently studying possible correlations among the multi-frequency Stokes spectra that we observed and we plan future multi-epoch observations in order to study the time variability of the sources, and its effect on the full Stokes spectra.

8.1 Scientific background

The mathematical formalism that describes the polarimetric emission from synchrotron sources has been derived by Jones and O'Dell [1977] and reviewed by Wardle and Homan [2003]. In the following, we will give a brief qualitative description of the main mechanisms involved in CP production.

8.1.1 Intrinsic circular polarization

In an uni-directional magnetic field, the circularly polarized emission, originated directly via synchrotron radiation, is of the order of $\frac{1}{\Gamma} = \left(\frac{\nu_o}{\nu_B}\right)^{-\frac{1}{2}}$, where Γ is the Lorentz factor corresponding to the observed frequency ν_o, and ν_B is the Larmor frequency.

$$\begin{aligned} \nu_B &= 2.8 \cdot B\,[G]\,,[MHz] \\ &= 2.8 \cdot 10^{-6} \cdot B\,[mG]\,,[GHz] \end{aligned} \tag{8.1}$$

A more accurate expression, that also includes the relativistic motion of the source with respect to the observer, is the following:

$$m_{CP}^{int} = \frac{V}{I} = \varepsilon_{\alpha}^{V} \left(\frac{\nu_{B\perp}}{\nu_o}\right)^{\frac{1}{2}} \cot\vartheta' \tag{8.2}$$

Where:
$\varepsilon_{\alpha}^{V} = 1.8$ is a dimensionless function that covers the spectral range $\alpha = 0.5 \div 1$ within a 10% accuracy
$\nu_{B\perp} = \nu_B \cdot \sin\vartheta'$
ϑ'=angle between B and the line of sight in the source frame
$\sin\vartheta' = \delta \sin\vartheta$ = aberration factor
$\delta = [\Gamma(1 - \beta\cos\vartheta)]^{-1}$ = Doppler factor
ϑ is the angle in the observer frame (between the jet axis and the l.o.s.)
Therefore, one obtains:

$$m_c\,(\%) = 0.3 \cdot B^{\frac{1}{2}}\,(mG) \cdot \nu^{-\frac{1}{2}}\,(GHz)\,(\sin\vartheta')^{\frac{1}{2}} \cot\vartheta' \tag{8.3}$$

Or, alternatively:

$$B\,(mG) = 11.1 \cdot \nu\,(GHz) \cdot m_{CP}^{2}\,(\%)\,(\cot\vartheta')^{-2}\,(\sin\vartheta')^{-1} \tag{8.4}$$

where:
$\nu = \nu_o(1+z)\delta^{-1}$

A CP fraction of 0.5% would require a magnetic field strength $B \approx 3 \cdot \nu\,(GHz)$ mG.

E.g. a source that exhibits a CP of 0.5% at 5 GHz, with $z = 0.72$, $\delta = 6$ and $\vartheta' = 45°$ would imply, in case of intrinsic emission, $\nu \approx 1.43$ GHz and $B \approx 4.29$ mG.
A more realistic representation of a magnetic field consists in the superposition of an isotropic, tangled, field B_r and a uniform field B_u that contains a uni-directional fraction $B_{uu} = f_B B_u$. The surrounding medium can be composed of both electrons and positrons. This may be considered by introducing the following parameter

$$f_c = \frac{n^- - n^+}{n^- + n^+} \tag{8.5}$$

The intrinsic fraction of circularly polarized emission is then

$$m_{CP}^{int} = \varepsilon_{\alpha}^{V} \left(\frac{\nu_{B\perp}}{\nu}\right)^{\frac{1}{2}} \frac{B_u}{\left\langle B_{\perp}^{2}\right\rangle^{\frac{1}{2}}} (f_c \cdot f_B) \sin\epsilon \tag{8.6}$$

where:
$\epsilon = 90 - \vartheta'$
$f_c \cdot f_B = \Lambda$

The ratio $\frac{B_u}{\left\langle B_{\perp}^{2}\right\rangle^{\frac{1}{2}}}$ can be estimated from LP measurements, obtaining

$$\begin{aligned} m_{CP}^{int} &= \varepsilon_{\alpha}^{V} \left(\frac{\nu_{B\perp}}{\nu}\right)^{\frac{1}{2}} \tan\epsilon \cdot \Lambda \sqrt{\frac{m_L}{m_0}} \\ &\approx 0.3 \cdot B^{\frac{1}{2}}\,(mG) \cdot \nu^{-\frac{1}{2}}\,(GHz) \tan\epsilon\,(\sin\vartheta')^{\frac{1}{2}} \sqrt{\frac{m_L}{m_0}} \end{aligned} \tag{8.7}$$

where:
$m_L = m_0 \frac{3}{2} \xi^2 cos^2 \epsilon$ is the observed fractional linear polarization
$\xi = \frac{B_u}{B_r}$
$\langle B_\perp^2 \rangle = \frac{2}{3} B_r^2$
m_0 is the maximum possible percentage of linear polarization (=ε_Q in case of null depolarization)

High-brightness temperature sources (e.g. IDV, see Wagner and Witzel [1995], Macquart and Melrose [2000]) often show CP $\leqslant$ 1%, not consistent with the theoretical value predicted for the intrinsic emission of a power-law electron distribution. In addition, recent VLBI observations of AGN at 15 GHz lead to an estimate of the magnetic field strength in the radiating region of more than 100 mG [Vitrishchak and Gabuzda, 2007], quite beyond the expected value ($\approx$ 1 mG).

Although it is possible to apply different energy distributions, to account for an intrinsic CP [Kirk and Tsang, 2006], the CP origin can also be explained as the result of propagation effects (mode conversion).

8.1.2 The Faraday conversion

The Faraday conversion is a birefringent effect that converts linear into circular polarization.

The variation of the Stokes parameters along the line of sight in a typical frame rotated so that B is directed along one of the axes and $I_{lp} = Q$, is, according to the radiative transfer [Beckert, 2003]

$$\frac{d}{ds}\begin{pmatrix} I \\ Q \\ U \\ V \end{pmatrix} = \begin{pmatrix} \eta_I \\ \eta_Q \\ 0 \\ \eta_V \end{pmatrix} + \left[\begin{pmatrix} -\kappa_I & -\kappa_Q & 0 & -\kappa_V \\ -\kappa_Q & -\kappa_I & -\kappa_F & 0 \\ 0 & \kappa_F & -\kappa_I & -\kappa_C \\ -\kappa_V & 0 & \kappa_C & -\kappa_I \end{pmatrix} \cdot \begin{pmatrix} I \\ Q \\ U \\ V \end{pmatrix} \right] \quad (8.8)$$

where:
η =emissivity
κ = absorption coefficient.

Transport equation for the four Stokes parameters, in a properly rotated frame

The rotation coefficients (F subscript) couple Q and U, and the conversion coefficients (C subscript) couple U and V. When k_I changes sign (optically thick/thin regime), a 90° jump in LP and a change in sign in CP are expected. The emitted linearly polarized radiation can be resolved into components transverse and parallel to the magnetic field, which propagate at different speeds. On emerging from the source, there is a phase difference between the two linearly polarized components, which corresponds to circularly polarized radiation. When present, the mode conversion can give important clues about the properties of the medium crossed by the polarized radiation emitted by the source and the strength and orientation of the magnetic field [Ruszkowski, 2003].

Both Faraday conversion and rotation are linked to the presence of low-energy electrons and arise in relativistic jets (both AGN and microquasar). VLBI observations indicate that CP often originates at the base of the jets, near the core. According to this framework, part of the linearly polarized radiation emitted at the farthest side of the jet is converted into circularly polarized radiation while passing through the magnetized plasma towards the observer

Faraday conversion and helical magnetic fields

[Wardle and Homan, 2003, Gabuzda et al., 2008]. So far, the Faraday conversion seems to be the most widely accepted solution to the problem of the CP origin [Beckert, 2003, Wardle and Homan, 2003]. Helical magnetic fields represent an example of an environment that would satisfy the requirements for the observed CP and LP values [Beckert, 2003, Gabuzda, 2006], however, so far there are only few observational confirmations.

8.2 Comparison between observations and simulations, the MPIfR code

The multi-frequency full Stokes polarimetry is a powerful tool to study the radiation emission and transfer processes in the observed sources and determine the dominant mechanism for circular polarization production. CP, LP and spectral information can be used to constrain the low energy end of the relativistic particle distribution [Beckert, 2003], derive magnetic field order, strength and geometry [Gabuzda, 2006] and make assumptions about the composition of the relativistic plasma within jets [Wardle et al., 1998].

An important key to link the observed results with the source properties is represented by the chance of using a reliable simulation code that permits to describe the emitting source by comparing its observed full Stokes emission with a simulated one.

During 2008 we had the chance of comparing the results we observed from the source 0056-00 with those obtained with a model developed by Beckert & Falcke (2002) that provides the radiative transfer coefficients for polarized synchrotron radiation applied to the standard model for relativistic radio jets, assuming the presence of a helical magnetic field.

This source exhibited a change in sign of CP between 5 and 8.5 GHz, consistent with the minimum in LP and with the change in polarization angle. The model assumed an extended unpolarized synchrotron source, which dominated the flux density below nearly 5 GHz which was modeled with energy equipartition between B-field and particles, B=4 mG, $n_e = 10^{-3}$ cm^{-3}, and a typical power-law for electrons above γ=100, with p=2.45 (power-law index). The size of the emitting region was $L = 8 \cdot 10^{21}$ cm. The polarized emission would have been produced by a compact jet component of $L = 1.5 \cdot 10^{19}$ cm, B=90 mG, n_e=0.5 cm^{-3} with a well-ordered magnetic field (a tightly wound spiral) seen at an angle of 85°. This component became self-absorbed below 6 GHz and the emission was relativistically boosted with δ=6. This combination reproduced the observed level of circular polarization, the sign flip at nearly 8 GHz and the observed flux density. Within that model the minimum in LP was at lower frequencies and the simulated level of LP was too low which indicated that there might have been an additional component (even more compact) that dominated LP and produced the turn in polarization angle at higher frequencies. The observed levels of CP were: -0.14 ± 0.11% at 2.8 GHz, -0.28 ± 0.05% at 5 GHz, 0.04 ± 0.07% at 8.5 GHz, 0.31 ± 0.11% at 10.GHz.

We have re-observed this source in 2009, during three different observational epochs dedicated to a sample of sources selected from the survey carried out in 2008, and we found a similar behaviour. Also 0003-00, observed in 2009, shown a similar full Stokes pattern and a good agreement with the same model assumed by Beckert and Falcke [2002].

Figure 8.1: 0056-00 observed during 2008. Each plot contains a comparison of the observed radio continuum spectra (continuum line) and the simulated one (dashed line). Upper left, top to bottom: flux density I (the predicted values are almost coincident with the observed one), LP, CP (absolute value). Upper right, top to bottom: LP, CP. Lower left: CP. Lower right: PA.

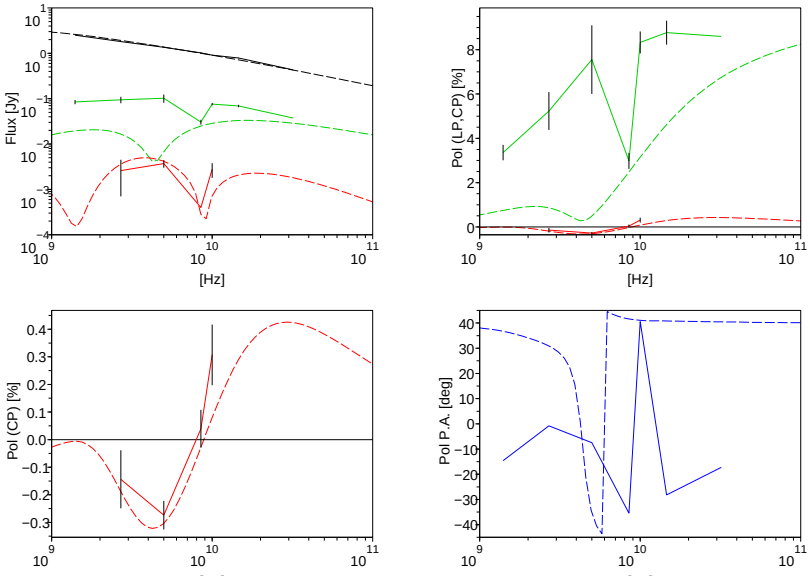

Figure 8.2: 0056-00 observed during 2009. Layout as in Fig. 8.1

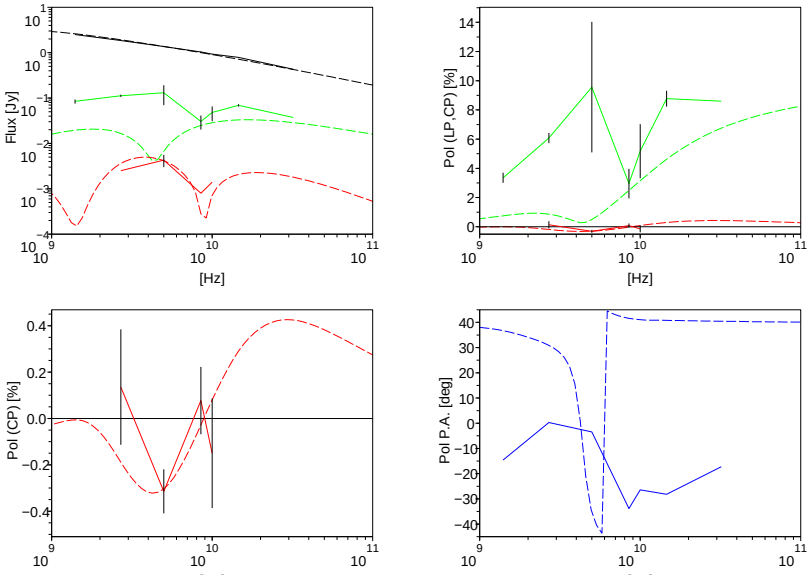

Figure 8.3: 0003-00 observed during 2009. Layout as in Fig. 8.1

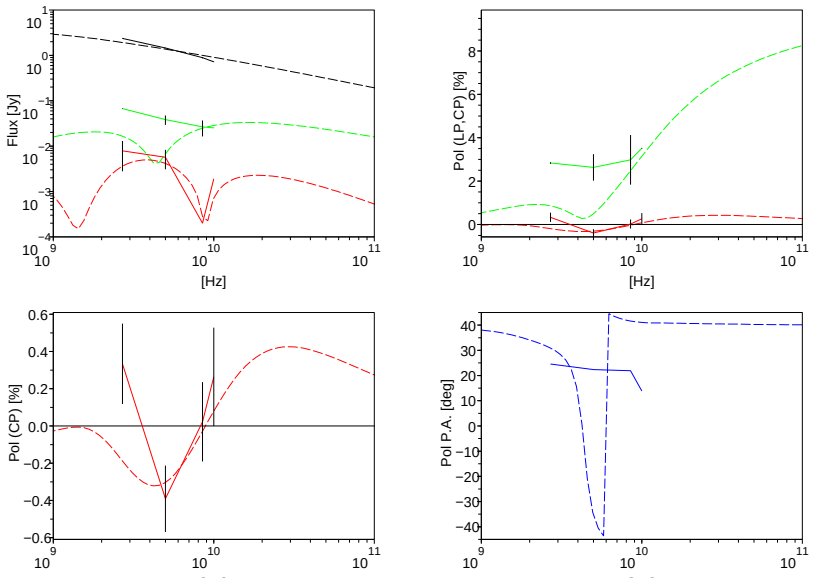

8.3 A new simulation instrument: the Michigan code radtransS

We are currently studying the use of a code developed by P. Hughes at the Michigan University, also based on the transfer equation solution but offering the chance of modeling the source geometry in much more detail.

The source is approximated as a grid of cells. For each cell the flow velocity components, particle density, pressure, spectral index, Lorentz factor, cutoff energy, magnetic field components must be defined. In addition, the position of the observer, with respect to the source, must be given. The code solves the transfer equation for each of the Stokes parameters.

Fig. 8.4 shows the result from a first very simple simulation. The source is modeled as a cube of 30x30x30 cells, along the three reference axis, the velocity of the flow throughout the jest is uniform and sub-relativistic ($v = 0.01c$ in all directions, where c is the speed of light), the particle density and pressure are also uniform. The spectral index is set to 0.75, constant within the source. The Lorentz factor and the lower cutoff energy are assumed to be 1000 and 100 respectively, also constant within the source. The magnetic field is composed by a random component superimposed to a uniform field in the x-direction, with 25% of the average energy of the random component. The source is seen at $\theta = \phi = 45°$ where θ and ϕ are polar coordinates (θ is measured from the positive z-direction, and ϕ is measured around the z-axis, starting from the x-axis).

The output shows the expected dimensionless spectra in terms of Stokes I (from 0.01 to 1), CP (from -0.5% to 0.7%) and LP (from 0 to 13%).

Fig. 8.5 show the same source but assuming a constant relativistic velocity $(0.95c)$ along the z-axis, and 0 in the other directions. The source is seen at

$\theta = 90°, \phi = 0°$, that is, the line of sight is along the x-axis, perpendicular to the velocity direction. The resulting plots show a lower Stokes I (from 0.01 to 0.3) and an higher CP (from -0.5% to 1.5%) and LP (from 0 to 15%). The three parameters peak at a lower frequencies, with respect to the first case, and the change in sign of CP is also expected at a lower frequency.

Fig. 8.6 show again the same source simulated in Fig. 8.5 but seen at $\theta = 0°$, that is, along the z-axis of the source. In this case Stokes I increases linearly from 0.01 to 100, CP ranges from -0.1 to 0.1% exhibiting a minimum at first, than the change in sign, LP is nearly 0 at all the frequencies and increases up to 8% at the higher frequency values.

Figure 8.4: Full polarimetric spectra from a non-relativistic source, modeled as a 30x30x30 cells cube. Upper left, flux density I. Upper right, fractional CP. Lower right, fractional LP. The source is seen at $\theta = \phi = 45°$.

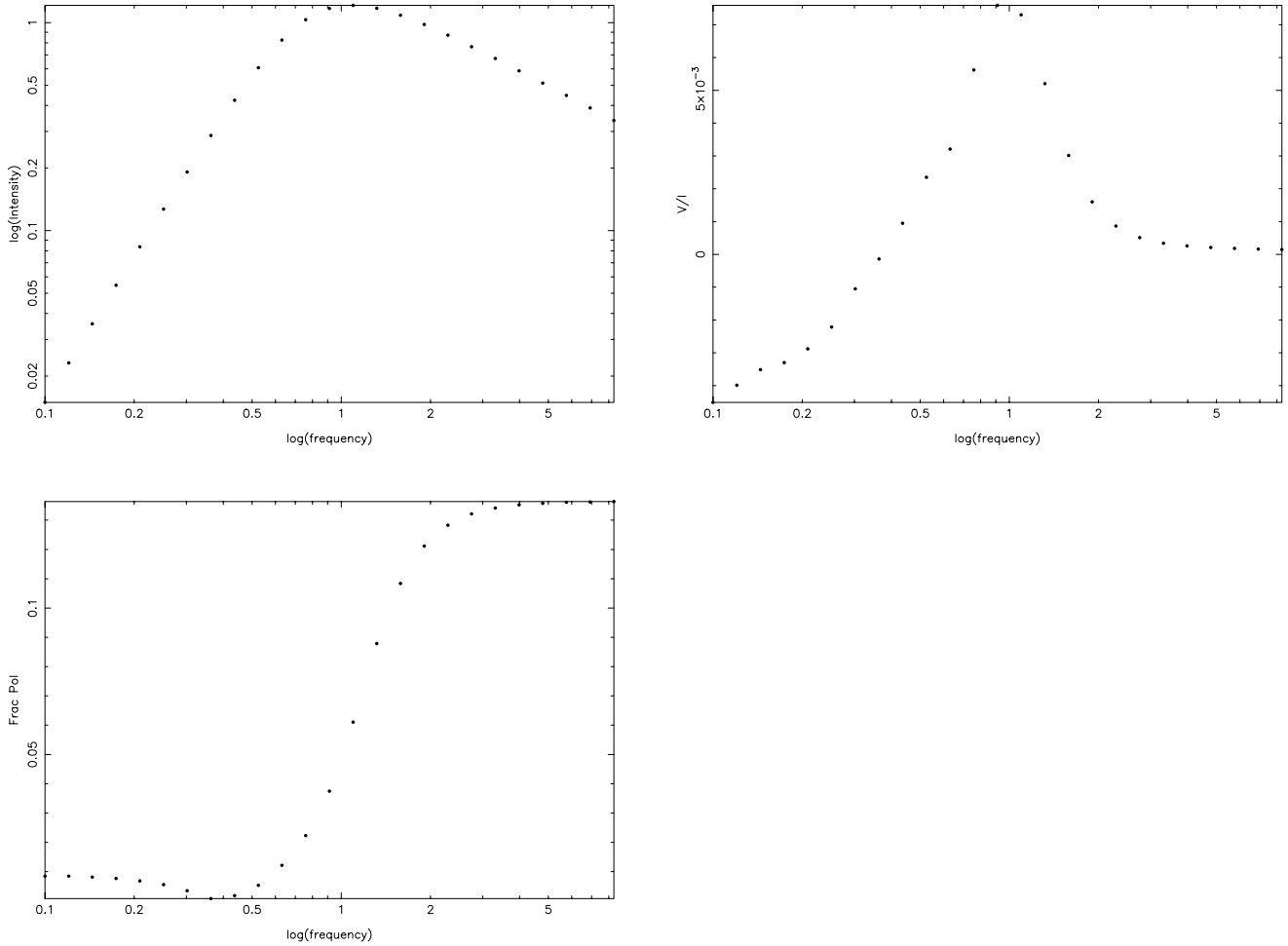

Figure 8.5: Full polarimetric spectra from a relativistic source, with ν directed along the z-axis. The source is seen at $\theta = 90°, \phi = 0°$, that is, perpendicularly to the ν direction and along the x-axis. Layout as in Fig. 8.4

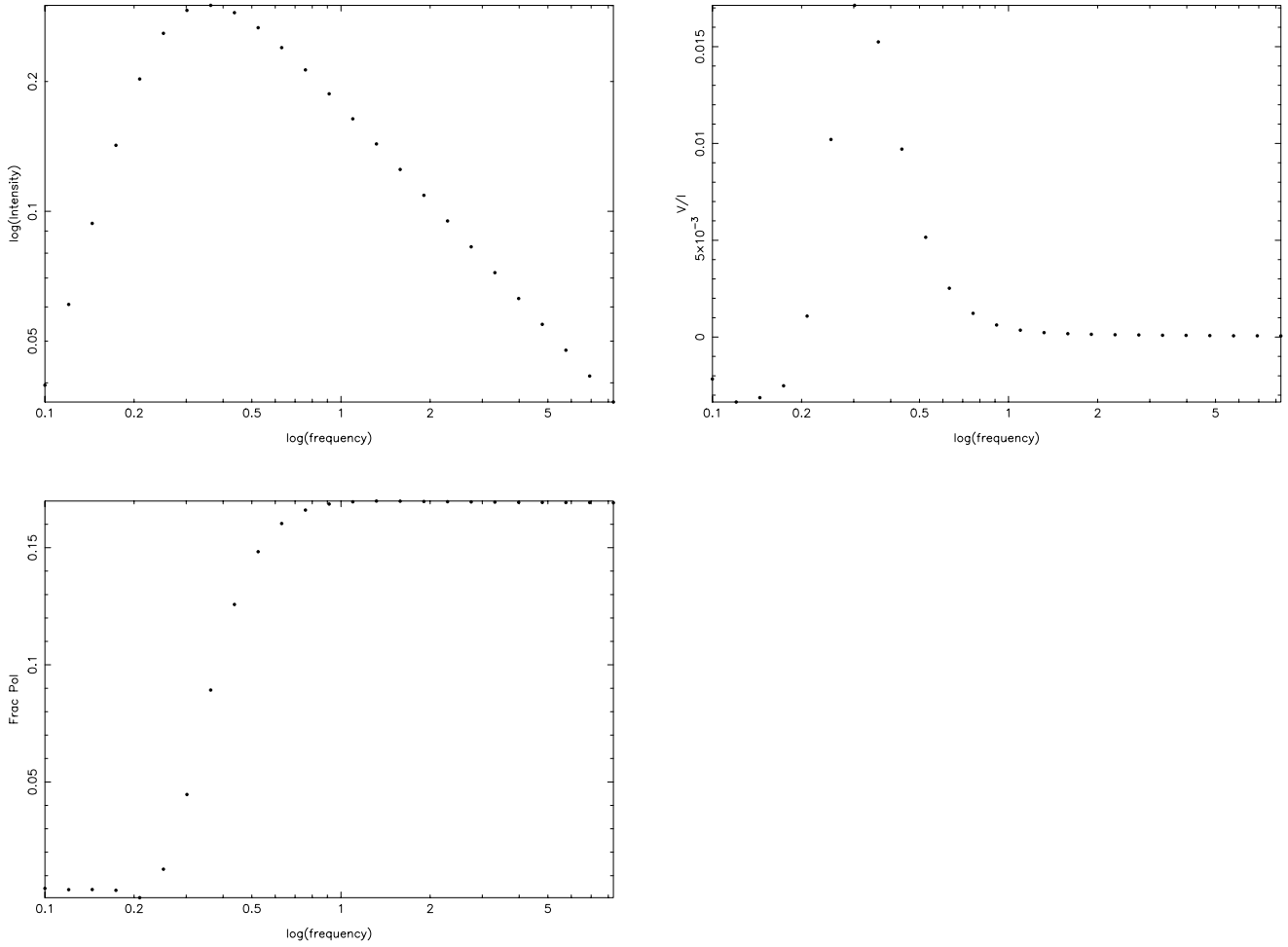

Figure 8.6: Full polarimetric spectra from a relativistic source, with ν directed along the z-axis. The source is seen at $\theta = 0^\circ$, that is, along the ν direction. Layout as in Fig. 8.4

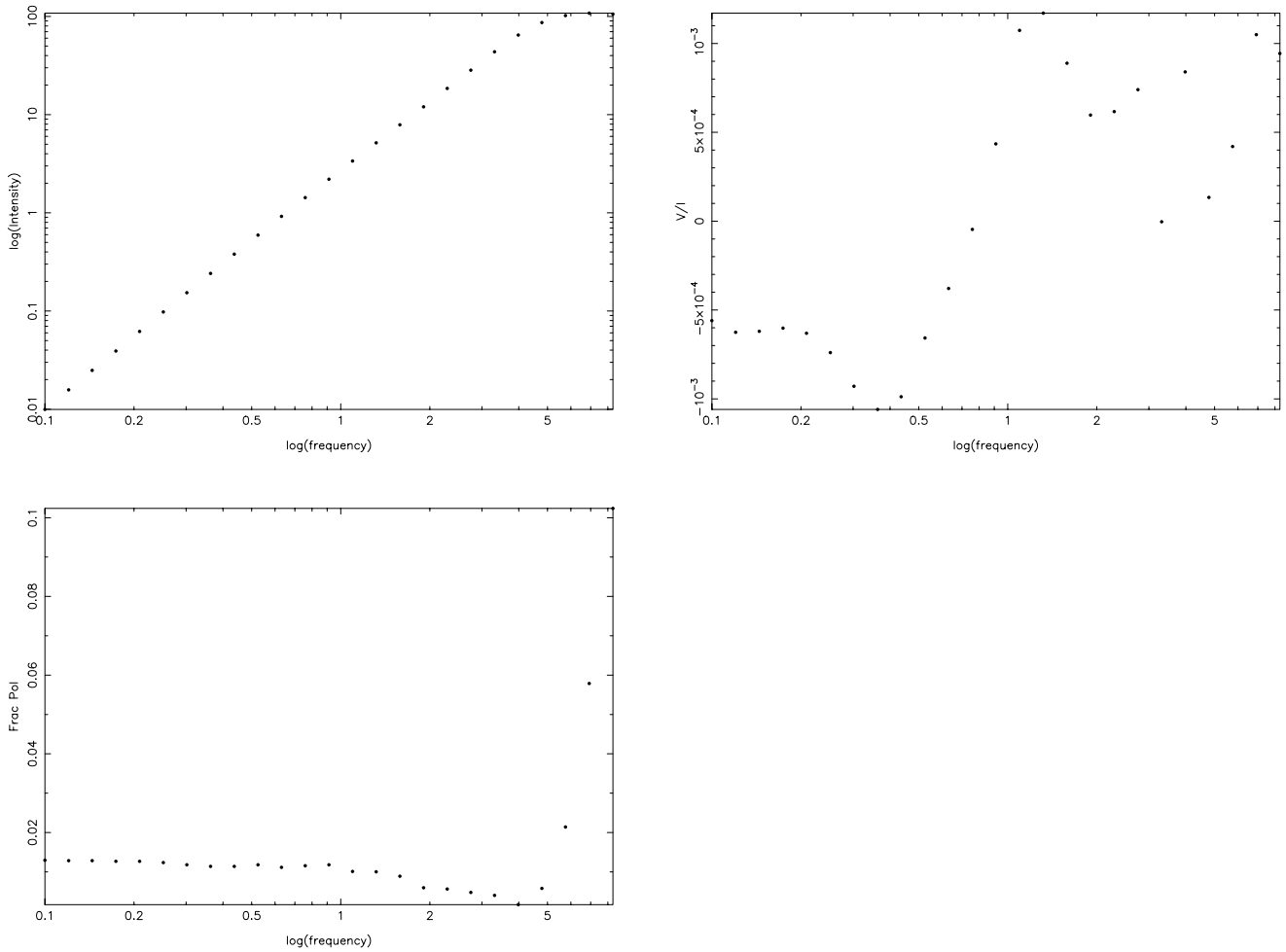

9 Conclusions

We have developed and applied a new calibration procedure for the Effelsberg 100-m radio telescope, that allows the contemporary measurement of the four Stokes parameters. The results observed at 5 GHz during the test phase are in very good agreement with those measured, completely independently, by the 26-m radio telescope of the University of Michigan, which was, before this PhD work, the only single-dish antenna used for extra-galactic full Stokes polarimetry.

A full Stokes polarimetric survey has been carried out at 5 GHz, consisting of 257 sources from the northern 1-Jy [Kühr et al., 1981] catalog, providing the first statistically complete catalog containing linear and circular polarization measurements of AGN. The statistical analysis of the results shown that galaxies can exhibit CP at the same level of QSO and BL objects. Besides, we observed that the distribution of CP for these classes is slightly shifted towards opposite sign (positive for BL objects and negative for galaxies). A similar result was found by examining the CP values listed by Homan and Lister [2006] related to 133 sample of AGN from the MOJAVE program (15 GHz).

The new calibration method has been extended to the 11, 3.6 and 2.8 cm wavelength. We used this new capability to derive, for the first time at Effelsberg, the full Stokes spectra of 31 sources, that appeared circularly polarized at 5 GHz during the survey. We compared the results obtained for the source 0056-00 with that obtained with a simulation code, that assumes a two-component radio source and the presence of a helical magnetic field along the jet, obtaining a very good agreement.

In the next future we would like to extend the calibration procedure up to 32 GHz, involving the new multi-beam receiver recently installed at Effelsberg. Possible follow-up projects include further comparison of the observed spectra with those simulated by numerical codes that supplies the expected LP and CP according to different source models (in order to obtain information about the mechanism responsible for the observed circular polarization) and the monitoring of a selected sample of source that exhibit either fast variability (in order to look for possible correlations among the Stokes parameter variations) or a long stability in time of the CP level (in order to increase the number of available CP calibrators).

A | Values from the full Stokes survey

Table A.1: Comparison EB/WSRT: observed values.

Source (1)	Source (2)	I [Jy] (3)	σ (4)	Q [Jy] (5)	σ (6)	U [Jy] (7)	σ (8)	V [Jy] (9)	σ (10)	V [%] (11)	σ (12)	P [%] (13)	σ (14)	PA [°] (15)	σ (16)
$0016{+}73^{W}$		1.486	0.030	0.004	0.001	-0.017	0.003	0.001	0.002	0.04	0.11	1.16	0.22	-38.15	2.02
$0016{+}73^{E}$		1.418	0.021	0.002	0.005	-0.017	0.006	0.001	0.001	0.09	0.08	1.20	0.42	-41.07	7.76
$0026{+}34^{W}$		1.334	0.027	0.001	0.001	0.008	0.003	0.002	0.001	0.18	0.11	0.58	0.22	40.08	3.91
$0026{+}34^{E}$		1.281	0.023	0.001	0.002	0.000	0.008	-0.001	0.001	-0.11	0.10	0.06	0.33	–	–
$0038{+}32^{W}$	3C19	1.153	0.023	0.004	0.001	-0.032	0.002	-0.002	0.001	-0.18	0.12	2.80	0.22	-41.26	0.91
$0038{+}32^{E}$		1.108	0.016	0.004	0.002	-0.032	0.006	-0.002	0.001	-0.15	0.08	2.95	0.53	-41.45	1.84
$0134{+}32^{W}$	3C48	5.633	0.113	-0.205	0.005	-0.103	0.011	-0.012	0.004	-0.21	0.07	4.07	0.14	103.33	1.22
$0134{+}32^{E}$		5.536	0.071	-0.194	0.019	-0.115	0.025	-0.017	0.004	-0.31	0.07	4.07	0.38	105.28	3.02
$0153{+}74^{W}$		1.021	0.020	0.000	0.001	0.008	0.002	-0.001	0.001	-0.06	0.09	0.79	0.18	45.81	2.32
$0153{+}74^{E}$		1.010	0.018	0.000	0.006	0.001	0.001	-0.005	0.001	-0.47	0.10	0.14	0.11	–	–
$0212{+}73^{W}$		4.379	0.088	0.000	0.001	0.018	0.007	0.010	0.003	0.22	0.07	0.41	0.17	44.74	1.31
$0212{+}73^{E}$		4.181	0.107	0.007	0.037	0.002	0.004	-0.005	0.006	-0.11	0.14	0.17	0.83	–	–
$0738{+}31^{W}$		1.883	0.038	-0.050	0.001	0.020	0.004	0.000	0.002	-0.03	0.10	2.88	0.12	78.95	1.86
$0738{+}31^{E}$		1.888	0.028	-0.046	0.008	0.015	0.006	-0.003	0.002	-0.17	0.08	2.57	0.39	80.78	3.51
$0804{+}49^{W}$		0.629	0.013	-0.018	0.001	0.003	0.001	-0.001	0.001	-0.24	0.13	2.86	0.14	85.25	1.95
$0804{+}49^{E}$		0.650	0.012	-0.019	0.004	-0.001	0.002	0.002	0.001	0.36	0.11	2.91	0.62	90.89	3.37
$0828{+}49^{W}$		0.475	0.010	-0.005	0.001	-0.005	0.001	0.000	0.001	0.06	0.18	1.49	0.22	112.87	4.03
$0828{+}49^{E}$		0.509	0.009	-0.003	0.003	-0.008	0.002	0.002	0.001	0.31	0.11	1.62	0.47	125.20	10.31
$0831{+}55^{W}$		5.181	0.105	0.000	0.001	0.020	0.010	0.003	0.004	0.06	0.08	0.40	0.19	45.00	1.08
$0831{+}55^{E}$		5.447	0.139	-0.001	0.047	0.001	0.006	0.005	0.008	0.09	0.15	0.02	0.49	–	–
$0833{+}58^{W}$		1.035	0.021	0.023	0.001	-0.016	0.002	0.000	0.001	0.01	0.11	2.68	0.15	-17.80	1.92
$0833{+}58^{E}$		1.046	0.027	0.021	0.010	-0.020	0.002	0.003	0.002	0.32	0.15	2.74	0.67	-22.17	6.82
$0836{+}71^{W}$		1.930	0.039	-0.118	0.003	-0.055	0.004	0.001	0.002	0.06	0.09	6.75	0.20	102.58	0.81
$0836{+}71^{E}$		1.983	0.051	-0.120	0.020	-0.062	0.015	-0.003	0.003	-0.14	0.15	6.80	0.99	103.77	3.51
$0850{+}58^{W}$		0.767	0.016	0.003	0.001	0.018	0.002	0.002	0.001	0.30	0.14	2.41	0.22	40.18	1.41
$0850{+}58^{E}$		0.798	0.020	0.005	0.007	0.017	0.002	0.000	0.001	0.03	0.14	2.26	0.30	37.54	10.68
$0859{+}47^{W}$		1.558	0.032	-0.026	0.001	0.046	0.003	0.004	0.001	0.27	0.08	3.37	0.17	59.54	0.86
$0859{+}47^{E}$		1.645	0.042	-0.023	0.011	0.037	0.010	0.003	0.002	0.21	0.15	2.67	0.64	60.86	7.03

Table A.1: Comparison EB/WSRT: observed values *(contd).*

Source (1)	Source (2)	I [Jy] (3)	σ (4)	Q [Jy] (5)	σ (6)	U [Jy] (7)	σ (8)	V [Jy] (9)	σ (10)	V [%] (11)	σ (12)	P [%] (13)	σ (14)	PA [°] (15)	σ (16)
$0906+43^W$	3C216	1.612	0.032	-0.030	0.001	0.010	0.003	0.001	0.001	0.09	0.08	1.94	0.08	80.76	2.26
$0906+43^E$		1.698	0.043	-0.029	0.009	0.000	0.013	-0.007	0.002	-0.44	0.14	1.73	0.51	90.16	12.31
$0917+62^W$		1.371	0.028	-0.012	0.001	0.024	0.002	0.000	0.001	-0.02	0.09	1.92	0.16	57.99	1.31
$0917+62^E$		1.431	0.037	-0.010	0.011	0.024	0.007	0.002	0.002	0.12	0.15	1.84	0.52	56.71	11.26
$0945+40^W$		1.804	0.036	0.021	0.001	0.067	0.003	0.002	0.001	0.11	0.08	3.91	0.20	36.39	0.53
$0945+40^E$		1.850	0.047	0.022	0.007	0.062	0.015	0.002	0.003	0.10	0.15	3.57	0.80	35.27	3.61
$0945+66^W$		1.170	0.024	-0.006	0.001	-0.023	0.002	0.000	0.001	0.04	0.09	2.03	0.17	128.24	1.00
$0945+66^E$		1.217	0.031	-0.003	0.007	-0.029	0.009	0.002	0.002	0.16	0.15	2.42	0.71	132.27	6.48
$0954+65^W$		1.342	0.027	0.067	0.002	0.016	0.003	-0.002	0.001	-0.12	0.11	5.09	0.17	6.56	1.23
$0954+65^E$		1.344	0.035	0.065	0.013	0.014	0.009	0.004	0.002	0.31	0.16	4.97	0.94	5.98	3.78
$1749+70^W$		0.629	0.013	-0.015	0.001	-0.002	0.001	-0.001	0.001	-0.17	0.14	2.45	0.14	94.65	2.40
$1749+70^E$		0.605	0.011	-0.015	0.003	-0.004	0.003	0.001	0.001	0.12	0.11	2.50	0.53	98.01	5.48
$1800+44^W$		1.317	0.026	0.017	0.001	0.035	0.002	0.006	0.001	0.42	0.10	2.97	0.18	32.48	0.97
$1800+44^E$		1.280	0.023	0.014	0.003	0.022	0.011	0.004	0.001	0.32	0.11	2.04	0.76	29.01	7.08
$1803+78^W$		2.919	0.058	-0.055	0.002	0.048	0.005	0.008	0.000	0.27	0.01	2.51	0.14	69.30	1.65
$1803+78^E$		2.777	0.050	-0.048	0.013	0.031	0.012	0.005	0.003	0.18	0.10	2.07	0.46	73.67	5.99
$1928+73^W$		3.696	0.074	-0.080	0.002	0.041	0.006	0.007	0.003	0.18	0.08	2.43	0.10	76.57	1.86
$1928+73^E$		3.664	0.066	-0.071	0.024	0.012	0.005	-0.008	0.004	-0.23	0.10	1.98	0.63	85.34	2.44
$2007+77^W$		0.895	0.018	0.009	0.001	-0.023	0.002	0.001	0.001	0.02	0.02	0.52	0.04	-34.14	1.10
$2007+77^E$		0.868	0.016	0.013	0.006	-0.024	0.004	0.002	0.001	0.24	0.11	3.11	0.51	-30.50	5.77
$2200+42^W$		2.619	0.052	0.032	0.001	-0.058	0.005	-0.004	0.002	-0.16	0.07	2.55	0.17	-30.56	1.08
$2200+42^E$		2.569	0.038	0.027	0.008	-0.072	0.012	0.003	0.002	0.12	0.09	3.00	0.47	-34.57	3.17
$2201+31^W$		2.283	0.046	-0.005	0.001	0.017	0.005	0.004	0.002	0.19	0.08	0.77	0.19	52.56	2.43
$2201+31^E$		2.397	0.035	0.004	0.003	0.000	0.010	0.000	0.002	0.01	0.08	0.16	0.13	–	–
$2255+41^W$		0.990	0.020	-0.002	0.001	0.004	0.002	0.000	0.001	-0.03	0.13	0.41	0.23	56.86	9.33
$2255+41^E$		0.956	0.014	0.000	0.004	0.000	0.004	0.000	0.001	0.03	0.08	0.04	0.45	–	–

Table A.1: Comparison EB/WSRT: observed values *(contd).*

Source (1)	Source (2)	I [Jy] (3)	σ (4)	Q [Jy] (5)	σ (6)	U [Jy] (7)	σ (8)	V [Jy] (9)	σ (10)	V [%] (11)	σ (12)	P [%] (13)	σ (14)	PA [°] (15)	σ (16)
2323+43^{W}		0.953	0.019	0.006	0.001	0.011	0.002	-0.001	0.001	-0.06	0.11	1.33	0.17	29.80	2.52
2323+43^{E}		0.944	0.014	0.005	0.004	0.007	0.004	-0.001	0.001	-0.11	0.08	0.90	0.44	28.34	14.07
2342+82^{W}		1.334	0.027	-0.004	0.001	0.010	0.002	0.001	0.001	0.09	0.08	0.80	0.16	55.97	2.84
2342+82^{E}		1.309	0.019	-0.001	0.005	0.000	0.005	-0.002	0.001	-0.16	0.08	0.04	0.37	—	—
2351+45^{W}		1.475	0.030	-0.013	0.001	0.012	0.003	0.000	0.001	0.02	0.09	1.16	0.14	68.62	3.73
2351+45^{E}		1.432	0.021	-0.010	0.004	0.003	0.006	0.000	0.001	-0.02	0.08	0.74	0.31	81.28	16.66
2352+49^{W}		1.379	0.028	0.000	0.001	0.008	0.003	0.002	0.001	0.18	0.09	0.56	0.19	43.53	2.67
2352+49^{E}		1.346	0.020	0.000	0.006	0.001	0.003	-0.002	0.001	-0.14	0.08	0.08	0.31	—	—

NOTES- W: Measurements from Westerbork. *E*: Measurements from Effelsberg. Col.(1):IAU name. Col.(2):Other name. Col.(3),(4): Stokes I and accuracy. Col.(5),(6): Stokes Q and accuracy. Col.(7),(8): Stokes U and accuracy. Col.(9),(10): Stokes V and accuracy. Col.(11),(12): Fractional circular polarization and accuracy. Col.(13),(14): Fractional linear polarization and accuracy. Col.(15),(16): Polarization angle and accuracy, values for P$<$0.5% are not listed.

Table A.2: Complete results.

Source (1)	Source (2)	I [Jy] (3)	σ (4)	Q [Jy] (5)	σ (6)	U [Jy] (7)	σ (8)	V [Jy] (9)	σ (10)	V [%] (11)	σ (12)	N σ (13)	P [%] (14)	σ (15)	PA [°] (16)	σ (17)	T (18)	O (19)	z (20)	α_{11-6} (21)	S (22)	FR (23)
0003−00	3C 2	1.418	0.026	-0.032	0.011	-0.028	0.005	-0.005	0.001	**-0.36**	**0.10**	3.62	2.97	0.63	110.69	5.57	E	qso	1.0370	-0.84	ss	
0003−06		2.295	0.042	0.025	0.013	0.039	0.007	-0.006	0.002	-0.26	0.10	2.63	2.03	0.40	28.49	7.23	E	qso	0.3470	0.02	fs	2
0010+40		0.847	0.015	-0.002	0.002	0.014	0.005	0.001	0.001	0.16	0.10	1.55	1.62	0.64	49.29	3.83	E	g	0.2550	-0.23	fs	
0016+73		1.418	0.021	0.002	0.005	-0.017	0.006	0.001	0.001	0.09	0.08	1.03	1.20	0.42	-41.07	7.76	E	qso	1.7810	0.16	fs	
0019−00		1.088	0.020	0.000	0.006	0.000	0.005	-0.004	0.001	**-0.37**	**0.10**	3.59	0.05	0.45	-	-	E	g	?	-0.84	ss	
0026+34		1.281	0.023	0.001	0.002	0.000	0.008	-0.001	0.001	-0.11	0.10	1.08	0.06	0.33	-	-	E	g	?	-0.27	fs	
0034−01	3C 15	1.546	0.028	0.005	0.008	0.085	0.010	-0.004	0.002	-0.23	0.11	2.15	5.48	0.63	43.25	2.81	E	g	0.0730	-0.73	ss	1,2
0035−02	3C 17	2.396	0.043	0.012	0.014	-0.018	0.008	-0.007	0.002	**-0.30**	**0.10**	3.05	0.92	0.43	-28.13	16.27	E	g	0.2197	-0.65	ss	1
0038+09	3C 18	1.622	0.029	-0.023	0.009	0.010	0.007	-0.008	0.002	**-0.48**	**0.10**	4.91	1.56	0.52	78.07	8.63	E	g	0.1880	-0.74	ss	2
0038+32	3C 19	1.108	0.016	0.004	0.002	-0.032	0.006	-0.002	0.001	-0.15	0.08	1.83	2.95	0.53	-41.45	1.84	E	g	0.4820	-0.69	ss	2
0048−09		0.972	0.018	0.042	0.008	-0.022	0.004	0.003	0.001	0.30	0.12	2.59	4.91	0.73	-13.75	3.13	E	bl/qso	?	0.43	fs	
0055+30		0.936	0.024	0.007	0.004	0.000	0.007	0.001	0.001	0.09	0.14	0.62	0.74	0.44	2.02	30.83	E	g	0.0167	-0.10	fs	1,2
0055−01	3C 29	1.870	0.048	0.172	0.029	-0.165	0.018	-0.009	0.004	-0.47	0.21	2.20	12.71	1.33	-21.90	2.85	E	g	0.0447	-0.79	ss	1
0056−00		1.321	0.024	-0.101	0.013	0.023	0.009	-0.005	0.001	**-0.37**	**0.11**	3.32	7.85	0.98	83.48	2.43	E	qso	0.7170	-0.39	fs	
0106+01		1.421	0.026	-0.032	0.010	-0.044	0.007	0.000	0.001	0.00	0.10	0.04	3.86	0.56	116.83	4.58	E	qso	2.1070	-0.08	fs	2
0108+38		1.386	0.028	0.003	0.001	0.009	0.002	0.000	0.001	0.00	0.08	0.06	0.71	0.16	36.78	2.82	W	g	0.3230	0.47	fs	
0112−01		0.808	0.021	-0.006	0.006	0.031	0.005	-0.003	0.001	-0.37	0.15	2.49	3.91	0.65	50.12	5.02	E	qso	1.3810	-0.01	fs	
0116+08		1.155	0.030	0.004	0.007	0.013	0.007	-0.003	0.002	-0.29	0.14	2.02	1.17	0.63	36.77	14.92	E	g	0.5936	-0.57	ss	
0116+31		1.530	0.031	0.001	0.001	0.012	0.002	0.004	0.001	0.23	0.08	3.01	0.80	0.16	42.90	1.83	W	g	0.0590	-0.47	fs	
0119+04		1.110	0.020	0.019	0.006	0.029	0.006	0.000	0.001	-0.04	0.10	0.40	3.11	0.50	28.14	4.63	E	qso	0.6370	0.04	fs	
0119+11		3.374	0.061	-0.016	0.016	-0.070	0.015	0.006	0.004	0.16	0.11	1.55	2.12	0.46	128.54	6.40	E	qso	0.5700	0.33	fs	
0122−00		1.068	0.019	0.017	0.006	0.024	0.004	-0.001	0.001	-0.06	0.10	0.53	2.70	0.45	27.49	5.15	E	qso	1.0700	-0.02	fs	
0127+23	3C 43	1.119	0.020	0.036	0.006	-0.012	0.006	-0.002	0.001	-0.15	0.10	1.47	3.41	0.52	-9.54	4.16	E	qso	1.4590	-0.75	ss	2?
0133+20	3C 47	1.102	0.020	0.021	0.004	0.048	0.006	-0.004	0.001	**-0.33**	**0.10**	3.42	4.77	0.50	33.01	2.53	E	qso	0.4250	-1.11	ss	2
0133+47		3.211	0.064	0.012	0.001	0.093	0.005	0.009	0.002	0.29	0.07	4.47	2.92	0.17	41.30	0.36	W	qso	0.8590	0.62	fs	
0134+32	3C 48	5.536	0.071	-0.194	0.019	-0.115	0.025	-0.017	0.004	**-0.31**	**0.07**	4.15	4.07	0.38	105.28	3.02	E	qso	0.3670	-0.86	ss	
0138−09		0.843	0.015	-0.061	0.008	0.020	0.005	0.000	0.001	0.02	0.11	0.18	7.63	0.93	80.95	2.31	E	bl/qso	>0.501	0.88	fs	
0146+05		1.316	0.024	0.002	0.007	-0.004	0.006	-0.004	0.001	-0.29	0.10	2.92	0.32	0.46	-	-	E	qso	2.3450	0.81	fs	
0149+21		0.877	0.016	-0.010	0.003	-0.003	0.006	-0.001	0.001	-0.08	0.11	0.78	1.18	0.41	98.63	15.79	E	qso	1.3200	-0.20	fs	
0153+74		1.010	0.018	0.000	0.006	0.001	0.001	-0.005	0.001	**-0.47**	**0.10**	4.63	0.14	0.11	-	-	E	qso	2.3380	-0.31	fs	
0202+14		2.077	0.038	0.000	0.007	0.000	0.011	-0.008	0.002	**-0.37**	**0.10**	3.75	0.02	0.40	-	-	E	qso	?	-0.43	fs	
0202+31		1.816	0.046	-0.020	0.003	-0.008	0.015	0.007	0.003	0.37	0.15	2.41	1.20	0.35	100.43	19.07	E	qso	1.4660	0.27	fs	
0212+73		4.181	0.107	0.007	0.037	0.002	0.004	-0.005	0.006	-0.11	0.14	0.81	0.17	0.83	-	-	E	qso	2.3670	-0.12	fs	
0218+35		1.876	0.038	0.073	0.002	0.019	0.003	0.000	0.001	0.01	0.07	0.16	4.03	0.12	7.39	1.14	W	bl/qso	>0.686	0.11	fs	
0221+06		0.632	0.011	0.013	0.004	0.012	0.004	0.000	0.001	0.01	0.12	0.08	2.71	0.60	21.41	6.36	E	qso	0.5114	0.69	fs	
0223+34		1.996	0.040	-0.004	0.001	0.011	0.003	0.002	0.001	0.11	0.07	1.60	0.61	0.15	55.33	3.11	W	qso	?	-0.46	fs	
0229+13		2.154	0.039	-0.002	0.008	-0.047	0.013	-0.008	0.002	**-0.37**	**0.10**	3.74	2.18	0.58	133.74	4.62	E	qso	2.0650	-0.33	fs	
0234+28		3.706	0.067	-0.035	0.004	0.051	0.024	0.004	0.004	0.10	0.10	0.94	1.66	0.53	62.02	6.35	E	qso	1.2100	-0.24	fs	
0235+16		2.637	0.039	-0.031	0.006	0.015	0.015	-0.006	0.002	-0.22	0.08	2.71	1.31	0.32	77.05	11.40	E	bl/qso	0.9400	1.03	fs	
0238−08		0.879	0.016	0.002	0.004	0.004	0.004	0.002	0.001	0.19	0.10	1.89	0.51	0.48	31.33	27.00	E	g	0.0050	1.19	fs	2
0240−00	3C 71	1.851	0.047	-0.002	0.010	-0.007	0.012	-0.006	0.003	-0.35	0.14	2.55	0.37	-	-	42.50	E	g	0.0034	-0.86	ss	2
0248+43		1.341	0.027	-0.005	0.001	-0.001	0.002	0.003	0.001	0.23	0.08	2.76	0.41	0.07	-	-	W	qso	1.3160	0.37	fs	
0256+07		0.501	0.013	-0.028	0.004	-0.002	0.004	0.000	0.001	0.06	0.17	0.37	5.63	0.90	92.31	4.12	E	qso	0.8930	0.45	fs	
0305+03	3C 78	3.023	0.077	-0.074	0.021	0.007	0.020	-0.013	0.004	**-0.44**	**0.14**	3.24	2.45	0.69	87.35	7.81	E	g	0.0288	-0.71	ss	1
0307+16	3C 79	1.198	0.022	0.076	0.009	0.072	0.011	-0.006	0.001	**-0.54**	**0.11**	4.77	8.79	0.87	21.71	2.82	E	g	0.2559	-1.06	ss	2
0316+16		2.861	0.052	-0.002	0.007	-0.001	0.017	-0.017	0.003	**-0.60**	**0.10**	6.10	0.09	0.31	-	-	E	g	?	-0.93	ss	
0316+41	3C 84	14.954	0.382	0.010	0.046	0.004	0.119	0.0024	0.021	0.02	0.14	0.11	0.07	0.40	-	-	E	g	0.0172	1.47	fs	1

Table A.2: Complete results *(contd)*.

Source (1)	Source (2)	I [Jy] (3)	σ (4)	Q [Jy] (5)	σ (6)	U [Jy] (7)	σ (8)	V [Jy] (9)	σ (10)	V [%] (11)	σ (12)	N σ (13)	P [%] (14)	σ (15)	PA [°] (16)	σ (17)	T (18)	O (19)	z (20)	α_{11-6} (21)	S (22)	FR (23)
0319+12		1.684	0.031	-0.086	0.012	0.066	0.011	0.000	0.002	0.02	0.11	0.14	6.47	0.71	71.24	3.06	E	qso	2.6620	-0.34	fs	
0332+07		0.424	0.008	-0.011	0.003	-0.005	0.003	0.001	0.000	0.21	0.12	1.80	2.87	0.76	102.08	7.09	E	qso	?	0.72	fs	
0336−01		2.452	0.063	-0.041	0.016	-0.022	0.016	-0.002	0.003	-0.09	0.14	0.61	1.89	0.64	103.86	9.80	E	qso	0.8520	0.30	fs	
0347+05		1.159	0.030	-0.040	0.007	0.008	0.010	-0.001	0.002	-0.06	0.15	0.40	3.54	0.63	84.50	6.66	E	g	0.3390	-0.79	ss	2
0400+25		1.907	0.035	0.025	0.006	-0.060	0.012	0.002	0.002	0.12	0.10	1.15	3.43	0.59	-33.53	3.15	E	qso	2.1090	0.11	fs	
0402+37		1.001	0.018	0.000	0.003	0.001	0.007	-0.003	0.001	-0.30	0.10	2.95	0.07	0.57	-	-	E	g	0.0540	-0.39	fs	
0403+76		2.907	0.053	0.002	0.013	0.003	0.015	-0.004	0.003	-0.15	0.10	1.52	0.11	0.51	-	-	E	g	0.5985	-0.57	ss	
0404+03	3C 105	1.818	0.047	0.011	0.011	0.058	0.013	-0.004	0.003	-0.22	0.15	1.53	3.26	0.69	39.71	5.34	E	g	0.0860	-0.84	ss	2
0410+11	3C 109	1.276	0.033	-0.018	0.007	0.041	0.010	-0.002	0.002	-0.13	0.14	0.95	3.52	0.77	56.99	5.01	E	g	0.3056	-0.62	ss	2
0420−01		3.688	0.094	-0.008	0.022	-0.027	0.024	0.002	0.005	0.06	0.14	0.39	0.78	0.63	126.51	22.02	E	qso	0.9150	0.01	fs	
0428+20		2.293	0.041	-0.001	0.004	0.001	0.014	-0.006	0.002	-0.24	0.10	2.48	0.06	0.55	-	-	E	g	0.2190	-0.51	ss	
0430+05	3C 120	4.247	0.063	0.155	0.022	-0.101	0.011	-0.008	0.004	-0.18	0.08	2.15	4.36	0.47	-16.49	2.37	E	g	0.0331	0.31	fs	1
0433+29	3C 123	16.167	0.292	-0.001	0.022	-0.249	0.038	-0.060	0.016	**-0.37**	**0.10**	3.78	1.54	0.24	134.86	2.54	E	g	0.2177	-0.81	ss	2
0440−00		2.231	0.057	0.051	0.021	0.001	0.002	-0.002	0.003	-0.07	0.14	0.50	2.28	0.94	0.44	1.38	E	qso	0.8440	-0.29	fs	
0446+11		0.909	0.023	-0.004	0.008	-0.007	0.001	-0.002	0.001	-0.17	0.14	1.20	0.93	0.45	119.99	23.34	E	g	?	0.56	fs	
0453+22	3C 132.0	1.159	0.030	0.077	0.015	0.020	0.002	-0.001	0.002	-0.10	0.15	0.69	6.86	1.31	7.21	1.59	E	g	0.2140	-0.95	ss	2
0454+84		0.219	0.006	0.000	0.002	0.003	0.000	0.001	0.001	0.43	0.24	1.81	1.37	0.19	42.85	18.55	E	bl/qso	0.1120	0.37	fs	1
0457+02		1.015	0.026	0.002	0.009	-0.001	0.002	-0.001	0.001	-0.15	0.14	1.03	0.18	0.80	-	-	E	qso	2.3840	-0.64	ss	
0458−02		1.025	0.026	0.013	0.009	-0.003	0.002	0.001	0.001	0.09	0.14	0.64	1.31	0.84	-7.35	6.57	E	qso	2.2860	-0.08	fs	
0500+01		1.733	0.044	0.001	0.014	-0.001	0.004	-0.003	0.002	-0.18	0.14	1.26	0.07	0.63	-	-	E	qso	?	-0.39	fs	
0518+16	3C 138.0	4.186	0.077	0.400	0.056	-0.162	0.018	-0.005	0.005	-0.13	0.13	1.02	10.30	1.28	-11.00	1.80	E	qso	0.7590	-0.59	ss	
0528+13		3.759	0.068	0.072	0.013	-0.079	0.013	-0.003	0.004	-0.07	0.10	0.72	2.84	0.36	-23.79	3.59	E	qso	2.0670	0.47	fs	
0538+49	3C 147.0	7.871	0.158	0.013	0.001	0.040	0.009	0.004	0.004	0.06	0.05	1.23	0.54	0.11	36.01	1.95	W	qso	0.5450	-0.72	ss	
0539−05		1.563	0.040	-0.026	0.014	0.018	0.003	0.002	0.002	0.15	0.15	0.99	1.98	0.76	72.76	7.85	E	qso	0.8390	1.41	fs	
0602+67		0.833	0.015	-0.001	0.004	0.005	0.003	0.002	0.001	0.21	0.11	1.96	0.58	0.34	49.68	21.43	E	qso	?	0.42	fs	
0605+48	3C 153.0	1.350	0.025	-0.015	0.005	0.051	0.008	-0.003	0.001	-0.25	0.10	2.44	3.92	0.61	53.27	3.09	E	g	0.2771	-0.85	ss	2
0605−08		1.215	0.031	0.003	0.010	0.026	0.003	-0.003	0.002	-0.21	0.14	1.47	2.16	0.27	42.19	11.19	E	qso	0.8720	0.09	fs	
0615+82		0.736	0.013	-0.001	0.003	-0.001	0.002	0.002	0.001	0.21	0.11	1.95	0.20	0.31	-	-	E	qso	0.7100	-0.03	fs	
0707+47		0.673	0.014	-0.021	0.001	0.005	0.001	0.003	0.001	0.38	0.13	2.92	3.14	0.16	83.15	1.90	W	qso	1.2920	-0.13	fs	
0710+43		1.580	0.032	-0.001	0.001	0.008	0.003	0.003	0.001	0.17	0.09	1.91	0.53	0.19	47.39	2.89	W	g	0.5180	-0.25	fs	
0711+35		0.524	0.011	-0.008	0.001	0.018	0.001	0.001	0.001	0.14	0.14	1.00	3.72	0.22	57.82	1.12	W	qso	1.6200	-0.29	fs	
0716+71		1.260	0.019	0.013	0.009	0.005	0.006	0.001	0.001	0.08	0.09	0.98	1.12	0.70	10.26	13.79	E	bl/qso	?	0.22	fs	
0735+17		0.921	0.014	0.020	0.005	-0.008	0.003	0.000	0.001	-0.02	0.09	0.21	2.36	0.56	-10.26	4.23	E	bl/qso	>0.424	0.05	fs	
0736+01		0.936	0.017	0.022	0.007	0.039	0.003	0.005	0.001	**0.51**	**0.12**	4.32	4.80	0.43	30.61	3.79	E	qso	0.1910	-0.13	fs	
0738+31		1.888	0.028	-0.046	0.008	0.015	0.006	-0.003	0.002	-0.17	0.08	2.00	2.57	0.39	80.78	3.51	E	qso	0.6310	0.27	fs	
0742+10		2.963	0.054	0.000	0.018	-0.002	0.004	-0.009	0.003	**-0.30**	**0.10**	3.04	0.07	0.16	-	-	E	ef	?	-0.11	fs	
0743−00		1.982	0.036	0.004	0.012	0.021	0.003	-0.009	0.002	**-0.44**	**0.10**	4.35	1.05	0.20	39.59	16.50	E	qso	0.9940	0.57	fs	
0745+24		1.189	0.012	-0.018	0.003	-0.024	0.003	-0.001	0.001	-0.08	0.06	1.40	2.51	0.24	116.51	2.76	E	qso	0.4090	0.48	fs	1,2
0748+12		3.874	0.040	-0.017	0.006	0.031	0.007	0.011	0.002	0.29	0.06	4.75	0.90	0.17	59.15	4.80	E	qso	0.8890	0.49	fs	
0804+49		0.650	0.012	-0.019	0.004	-0.001	0.002	0.002	0.001	0.36	0.11	3.40	2.91	0.62	90.89	3.37	E	qso	1.4330	0.47	fs	
0805−07		0.824	0.021	0.007	0.007	0.023	0.002	0.001	0.001	0.16	0.15	1.04	2.99	0.38	36.30	8.09	E	qso	1.8370	-0.32	fs	
0809+48	3C 196.0	4.357	0.079	-0.047	0.011	-0.090	0.025	-0.014	0.004	**-0.32**	**0.10**	3.12	2.34	0.53	121.14	4.32	E	qso	0.8710	-0.89	ss	2
0812+36		0.838	0.017	-0.007	0.001	0.014	0.001	-0.006	0.001	**-0.71**	**0.08**	8.44	1.92	0.10	57.92	1.24	W	qso	1.0250	-0.02	fs	
0814+42		1.224	0.025	0.011	0.001	-0.014	0.002	0.002	0.001	0.18	0.10	1.81	1.45	0.16	-26.83	2.48	W	bl/qso	0.258 ?	-0.10	fs	
0820+22		1.499	0.027	0.001	0.009	-0.048	0.005	0.001	0.002	0.05	0.11	0.47	3.21	0.36	-44.53	5.23	E	bl/qso	0.9510	-0.20	fs	
0823+03		1.153	0.021	0.005	0.007	0.085	0.006	-0.001	0.001	-0.07	0.12	0.62	7.36	0.53	43.47	2.35	E	bl/qso	0.5060	0.77	fs	
0828+49		0.509	0.009	-0.003	0.003	-0.008	0.002	0.002	0.001	0.31	0.11	2.82	1.62	0.47	125.20	10.31	E	bl/qso	0.5480	-0.19	fs	
0831+55		5.447	0.139	-0.001	0.047	0.001	0.006	0.005	0.008	0.09	0.15	0.59	0.02	0.49	-	-	E	g	0.2412	-0.46	fs	

Table A.2: Complete results *(contd).*

Source (1)	Source (2)	I [Jy] (3)	σ (4)	Q [Jy] (5)	σ (6)	U [Jy] (7)	σ (8)	V [Jy] (9)	σ (10)	V [%] (11)	σ (12)	N σ (13)	P [%] (14)	σ (15)	PA [°] (16)	σ (17)	T (18)	O (19)	z (20)	α_{11-6} (21)	S (22)	FR (23)
0833+58		1.046	0.027	0.021	0.010	-0.020	0.002	0.003	0.002	0.32	0.15	2.11	2.74	0.67	-22.17	6.82	E	qso	2.1010	1.26	fs	
0836+71		1.983	0.051	-0.120	0.020	-0.062	0.015	-0.003	0.003	-0.14	0.15	0.95	6.80	0.99	103.77	3.51	E	qso	2.1720	-0.32	fs	2
0838+13	3C 207	1.408	0.026	0.029	0.009	0.024	0.003	-0.001	0.001	-0.04	0.10	0.36	2.66	0.53	19.87	4.89	E	qso	0.6840	-0.39	ss	2
0839+18		0.789	0.014	-0.005	0.006	-0.015	0.003	0.001	0.001	0.07	0.12	0.59	1.98	0.45	125.83	9.84	E	qso	1.2720	0.02	fs	
0850+58		0.798	0.020	0.005	0.007	0.017	0.002	0.000	0.001	0.03	0.14	0.24	2.26	0.30	37.54	10.68	E	qso	1.3220	0.75	fs	
0851+20		2.037	0.037	0.031	0.013	-0.097	0.009	0.004	0.003	0.20	0.13	1.48	4.98	0.46	-36.14	3.48	E	bl/qso	0.3060	0.11	fs	
0859+47		1.645	0.042	-0.023	0.011	0.037	0.010	0.003	0.002	0.21	0.15	1.43	2.67	0.64	60.86	7.03	E	qso	1.4620	-0.15	fs	1
0906+01		1.236	0.022	-0.041	0.009	-0.038	0.003	0.003	0.001	0.22	0.11	2.01	4.49	0.55	111.28	3.24	E	qso	1.0180	0.04	fs	
0906+43	3C 216.0	1.698	0.043	-0.029	0.009	0.000	0.013	-0.007	0.002	**-0.44**	**0.14**	3.07	1.73	0.51	90.16	12.31	E	qso	0.6680	-0.38	fs	
0917+62		1.431	0.037	-0.010	0.011	0.024	0.007	0.0017	0.002	0.12	0.15	0.79	1.84	0.52	56.71	11.26	E	qso	1.4460	0.08	fs	
0923+39		10.404	0.210	-0.181	0.004	0.140	0.014	0.008	0.006	0.07	0.06	1.29	2.20	0.10	71.13	1.41	W	qso	0.6980	1.03	fs	2
0941−08		1.148	0.029	0.001	0.010	-0.001	0.001	-0.002	0.002	-0.16	0.15	1.12	0.11	0.70	-	-	E	g	?	-0.72	ss	
0945+40		1.850	0.047	0.022	0.007	0.062	0.015	0.0018	0.003	0.10	0.15	0.65	3.57	0.80	35.27	3.61	E	qso	1.2520	0.11	fs	
0945+66		1.217	0.031	-0.003	0.007	-0.029	0.009	0.0019	0.002	0.16	0.15	1.06	2.42	0.71	132.27	6.48	E	g	?	-0.49	fs	
0947+14	3C 228	1.157	0.030	-0.059	0.014	-0.040	0.003	-0.005	0.002	-0.40	0.14	2.77	6.18	1.01	107.01	3.28	E	g	0.5524	-0.95	ss	2
0951+69	3C 231.0	3.458	0.088	0.000	0.013	-0.002	0.027	-0.007	0.005	-0.21	0.14	1.50	0.06	0.77	-	-	E	g	0.0009	-0.66	ss	1
0953+25		0.954	0.024	0.017	0.009	-0.002	0.001	0.000	0.001	0.04	0.14	0.30	1.77	0.90	-3.32	2.39	E	qso	0.7120	0.83	fs	
0954+55		1.777	0.037	0.066	0.002	0.029	0.003	0.001	0.001	0.08	0.07	1.15	4.04	0.14	11.80	1.00	W	qso	0.9010	-0.19	fs	
0954+65		1.344	0.035	0.065	0.013	0.014	0.009	0.004	0.002	0.31	0.16	1.96	4.97	0.94	5.98	3.78	E	bl/qso	0.3670	0.35	fs	
0958+29	3C 234	1.385	0.035	0.028	0.013	0.006	0.002	-0.005	0.002	-0.37	0.14	2.74	2.07	0.93	6.34	3.51	E	g	0.1848	-1.10	ss	2
1003+35	3C 236.0	1.434	0.029	0.007	0.001	-0.003	0.003	0.001	0.001	0.05	0.09	0.54	0.55	0.12	-11.80	8.96	W	g	0.0989	-0.67	ss	2
1030+41		0.688	0.014	-0.002	0.001	0.006	0.001	-0.001	0.001	-0.10	0.12	0.78	0.85	0.21	54.01	4.58	W	qso	1.1200	0.42	fs	
1031+56		1.153	0.023	0.008	0.001	0.007	0.002	0.002	0.001	0.15	0.09	1.64	0.88	0.13	20.54	4.51	W	g	0.4590	-0.27	fs	
1039+02		0.968	0.025	-0.019	0.009	0.004	0.002	-0.003	0.001	-0.31	0.14	2.17	1.95	0.90	84.23	3.81	E	ef	?	-0.83	ss	
1039+81		1.267	0.026	-0.002	0.001	0.000	0.003	0.001	0.001	0.10	0.11	0.91	0.15	0.10	-	-	W	qso	1.2540	0.38	fs	
1040+12	3C 245.0	1.273	0.033	0.060	0.014	0.127	0.010	-0.005	0.003	-0.41	0.20	2.00	11.01	0.92	32.41	2.74	E	qso	1.0290	-0.61	ss	2
1049+21		0.694	0.018	0.013	0.006	0.001	0.002	0.002	0.001	0.24	0.15	1.66	1.89	0.88	1.19	3.78	E	qso	1.3000	0.34	fs	
1055+01		3.358	0.086	-0.140	0.036	-0.022	0.006	0.001	0.005	0.04	0.15	0.28	4.21	1.06	94.43	1.67	E	qso	0.8920	0.32	fs	
1055+20		1.136	0.029	-0.013	0.010	-0.025	0.003	-0.001	0.002	-0.04	0.15	0.30	2.47	0.47	121.40	9.09	E	qso	1.1100	-0.59	ss	
1116+12		1.296	0.033	-0.016	0.010	-0.034	0.007	0.000	0.002	0.01	0.15	0.06	2.91	0.56	122.39	7.05	E	qso	2.1180	-0.36	fs	
1117+14		1.036	0.026	0.001	0.007	0.000	0.005	-0.001	0.001	-0.07	0.14	0.52	0.08	0.70	-	-	E	qso	?	-0.72	ss	
1145−07		0.844	0.022	0.010	0.007	0.015	0.003	0.003	0.001	0.32	0.15	2.18	2.14	0.54	28.28	9.71	E	qso	1.3420	0.22	fs	
1147+24		0.780	0.020	0.011	0.006	-0.003	0.004	0.004	0.001	**0.55**	**0.15**	3.58	1.44	0.70	-8.88	10.87	E	bl/qso	?	0.39	fs	
1148−00		1.797	0.046	-0.003	0.015	-0.087	0.009	-0.002	0.003	-0.13	0.15	0.86	4.82	0.53	133.88	4.79	E	qso	1.9820	-0.44	fs	
1150+81		1.706	0.034	0.024	0.001	0.019	0.003	0.002	0.001	0.13	0.08	1.62	1.82	0.13	19.25	2.24	W	qso	1.2500	-0.09	fs	
1157+73	3C 268.1	2.328	0.048	0.034	0.004	-0.043	0.006	-0.006	0.003	-0.26	0.11	2.41	2.34	0.22	-25.88	2.38	W	g	0.9737	-0.70	ss	2
1203+64	3C 268.3	1.166	0.023	-0.007	0.001	0.000	0.002	-0.001	0.001	-0.05	0.09	0.60	0.64	0.08	90.73	7.10	W	g	0.3710	-0.87	ss	2
1213+35		1.126	0.023	-0.066	0.002	0.078	0.002	0.003	0.001	0.26	0.09	3.02	9.08	0.26	65.16	0.57	W	qso	0.8510	-0.34	fs	
1216+48		0.655	0.013	0.006	0.001	0.027	0.001	0.000	0.001	-0.03	0.13	0.24	4.17	0.22	38.28	0.92	W	qso	1.0760	0.30	fs	
1222+13	3C 272.1	2.394	0.061	0.083	0.024	-0.166	0.015	-0.008	0.004	-0.34	0.17	2.03	7.75	0.74	-31.66	3.46	E	g	0.0031	-0.46	fs	1
1226+02	3C 273.0	37.854	0.969	1.137	0.355	-0.971	0.138	-0.039	0.057	-0.10	0.15	0.68	3.95	0.76	-20.25	4.85	E	qso	0.1580	0.15	fs	
1228+12	3C 274.0	60.167	1.538	0.500	0.487	0.377	0.216	-0.107	0.082	-0.18	0.14	1.30	1.04	0.68	18.50	15.55	E	g	0.0043	-0.79	ss	1
1229−02		0.834	0.021	0.031	0.008	-0.017	0.003	0.000	0.001	0.03	0.15	0.22	4.25	0.88	-14.63	3.93	E	qso	1.0450	-0.29	ss	2
1237−10		1.500	0.038	0.024	0.013	0.063	0.007	0.000	0.002	0.02	0.15	0.14	4.49	0.53	34.53	5.34	E	qso	0.7530	-0.25	fs	
1239−04	3C 275.0	1.002	0.026	-0.014	0.008	0.002	0.003	-0.002	0.001	-0.25	0.14	1.72	1.37	0.83	86.24	6.81	E	g	0.4800	-1.05	ss	2
1243−07		0.749	0.019	0.009	0.006	0.008	0.002	0.002	0.001	0.23	0.14	1.59	1.53	0.66	20.62	11.24	E	qso	1.2860	0.44	fs	
1250+56	3C 277.1	0.762	0.015	0.021	0.001	0.003	0.001	-0.001	0.001	-0.17	0.11	1.57	2.74	0.16	3.91	1.95	W	qso	0.3210	-0.51	ss	2

Table A.2: Complete results *(contd)*.

Source (1)	Source (2)	I [Jy] (3)	σ (4)	Q [Jy] (5)	σ (6)	U [Jy] (7)	σ (8)	V [Jy] (9)	σ (10)	V [%] (11)	σ (12)	N σ (13)	P [%] (14)	σ (15)	PA [°] (16)	σ (17)	T (18)	O (19)	z (20)	α_{11-6} (21)	S (22)	FR (23)
1251+27	3C 277.3	1.238	0.032	0.051	0.011	0.010	0.007	-0.002	0.002	-0.12	0.14	0.86	4.18	0.88	5.79	4.18	E	g	0.0857	-0.77	ss	2
1252+11		0.749	0.019	0.018	0.006	-0.006	0.003	0.001	0.001	0.11	0.14	0.75	2.58	0.81	-9.16	5.46	E	qso	0.8710	-0.02	fs	
1253−05	3C 279.0	11.983	0.307	-0.091	0.096	0.064	0.044	-0.002	0.017	-0.02	0.15	0.13	0.93	0.69	72.47	16.95	E	qso	0.5360	0.30	fs	
1302−10		0.561	0.014	-0.003	0.005	-0.006	0.002	0.003	0.001	**0.50**	**0.16**	3.19	1.25	0.49	120.92	16.91	E	qso	0.2860	0.17	fs	
1306−09		1.965	0.050	0.012	0.016	0.011	0.007	-0.006	0.003	-0.29	0.14	2.02	0.82	0.63	21.72	21.13	E	g?	0.4640	-0.68	ss	
1308+32		0.890	0.018	0.032	0.001	0.009	0.002	0.000	0.001	0.05	0.10	0.51	3.75	0.14	7.59	1.36	W	bl/qso	0.9970	0.20	fs	
1323+32		2.225	0.045	0.028	0.001	0.006	0.004	0.001	0.002	0.03	0.08	0.43	1.30	0.07	5.93	3.48	W	g	0.3690	-0.58	ss	
1328+25	3C 287	3.196	0.082	0.074	0.025	-0.102	0.019	0.000	0.005	0.00	0.15	0.02	3.95	0.67	-26.95	5.28	E	qso	1.0550	-0.59	ss	
1328+30	3C 286	7.516	0.199	0.335	0.070	0.752	0.073	-0.001	0.012	-0.02	0.16	0.12	10.95	1.01	33.00	2.46	E	qso	0.8460	-0.53	ss	
1335−06		1.038	0.027	0.033	0.010	0.003	0.003	-0.004	0.001	-0.36	0.14	2.60	3.20	0.96	2.20	2.94	E	qso	0.6250	-0.95	ss	2
1345+12		2.825	0.072	0.002	0.022	-0.002	0.011	-0.004	0.004	-0.14	0.14	0.98	0.09	0.66	-	-	E	g	0.1209	-0.40	fs	
1350+31	3C 293	1.521	0.031	0.011	0.002	0.008	0.003	0.001	0.001	0.05	0.08	0.58	0.87	0.14	18.42	5.03	W	g	0.0452	-0.67	ss	1,2
1352−10		1.043	0.027	0.022	0.009	-0.014	0.004	0.002	0.002	0.18	0.15	1.24	2.51	0.77	-15.89	6.23	E	qso	0.3320	0.40	fs	
1354+19		1.747	0.045	-0.071	0.013	0.065	0.014	0.001	0.003	0.06	0.16	0.39	5.52	0.78	68.84	4.02	E	qso	0.7200	-0.07	fs	2
1358+62		1.682	0.034	0.013	0.001	0.012	0.003	0.000	0.001	-0.02	0.08	0.29	1.04	0.12	20.84	3.57	W	g	0.4310	-0.77	ss	
1404+28		2.503	0.064	0.001	0.007	-0.001	0.020	0.000	0.004	0.01	0.15	0.04	0.04	0.44	-	-	E	g	0.0768	0.80	fs	
1406−07		0.787	0.020	0.028	0.008	-0.022	0.003	-0.001	0.001	-0.19	0.15	1.24	4.48	0.80	-19.23	4.29	E	qso	1.4940	0.19	fs	
1409+52	3C 295.0	6.549	0.132	0.052	0.003	0.046	0.001	0.000	0.005	-0.01	0.08	0.08	1.06	0.05	20.71	0.98	W	g	0.4614	-0.98	ss	2
1413+34		1.035	0.021	0.008	0.001	0.007	0.001	-0.001	0.001	-0.09	0.06	1.47	1.05	0.07	20.86	1.81	W	?	?	-0.56	ss	
1416+06	3C 298.0	1.449	0.037	0.008	0.011	-0.021	0.006	-0.005	0.002	-0.34	0.14	2.43	1.54	0.46	-34.34	13.89	E	qso	1.4390	-0.96	ss	
1418+54		1.017	0.020	0.003	0.001	0.028	0.002	0.002	0.001	0.19	0.10	1.94	2.79	0.19	41.81	0.80	W	bl/g	0.1520	0.38	fs	
1420+19	3C 300	1.044	0.027	-0.018	0.007	-0.011	0.007	-0.004	0.001	**-0.40**	**0.14**	2.92	2.02	0.66	105.19	9.05	E	g	0.2700	-0.97	ss	2
1434+03		1.288	0.033	0.022	0.011	0.015	0.003	-0.003	0.002	-0.26	0.14	1.79	2.09	0.74	17.23	7.34	E	?	?	-0.65	ss	
1435+63		1.376	0.028	0.030	0.001	-0.014	0.002	-0.003	0.001	-0.20	0.09	2.37	2.43	0.12	-12.72	1.97	W	qso	2.0680	-0.20	fs	
1442+10		0.985	0.025	-0.014	0.008	0.012	0.003	0.001	0.001	0.10	0.15	0.71	1.93	0.68	69.56	8.97	E	qso	3.5305	-0.61	ss	
1453−10		1.510	0.039	0.010	0.013	0.015	0.002	-0.005	0.002	-0.36	0.14	2.60	1.18	0.51	27.61	17.53	E	qso	0.9380	-0.77	ss	2
1458+71	3C 309.1	3.329	0.067	0.035	0.001	-0.013	0.002	-0.003	0.001	-0.09	0.03	2.91	1.13	0.05	-10.35	1.65	W	qso	0.9050	-0.71	ss	2
1502+10		1.464	0.026	0.020	0.011	-0.014	0.003	0.001	0.002	0.09	0.11	0.80	1.66	0.65	-17.34	8.10	E	qso	0.5630	0.57	fs	
1504+37		0.756	0.015	0.022	0.001	-0.012	0.003	-0.002	0.001	-0.28	0.16	1.71	3.37	0.22	-14.44	2.60	W	g	0.6740	0.14	fs	
1508−05		2.137	0.039	-0.011	0.013	0.019	0.003	-0.001	0.002	-0.03	0.10	0.34	1.03	0.33	59.73	14.67	E	qso	1.1910	-0.30	fs	
1510−08		2.423	0.044	-0.015	0.014	0.019	0.003	0.003	0.003	0.14	0.10	1.38	0.99	0.38	63.95	13.80	E	qso	0.3610	0.31	fs	
1518+04		1.112	0.016	0.000	0.006	-0.001	0.001	-0.002	0.001	-0.22	0.09	2.33	0.08	0.15	-	-	E	qso	?	-1.30	ss	
1529+24	3C 321	1.052	0.016	0.082	0.009	0.004	0.001	0.001	0.001	0.05	0.09	0.55	7.82	0.85	1.45	0.49	E	g	0.0960	-0.88	ss	2
1532+01		0.799	0.014	0.007	0.004	0.005	0.002	-0.001	0.001	-0.08	0.11	0.75	1.10	0.41	16.39	8.57	E	qso	1.4350	0.06	fs	
1538+14		1.645	0.030	0.102	0.017	-0.084	0.007	0.001	0.002	0.04	0.12	0.29	8.06	0.83	-19.79	2.54	E	bl/qso	0.6050	0.34	fs	
1546+02		2.596	0.047	-0.092	0.015	0.000	0.006	-0.007	0.003	-0.29	0.10	2.80	3.55	0.58	89.94	1.81	E	qso	0.4120	0.46	fs	
1548+05		3.601	0.092	-0.016	0.032	-0.192	0.016	0.001	0.006	0.03	0.16	0.19	5.35	0.47	132.67	4.68	E	qso	1.4220	0.09	fs	
1555+00		0.430	0.008	-0.006	0.002	-0.013	0.002	0.000	0.000	0.12	0.12	1.00	3.34	0.51	123.39	4.02	E	qso	1.7700	0.34	fs	
1600+33		1.626	0.033	0.000	0.001	0.012	0.003	0.002	0.001	0.10	0.08	1.33	0.74	0.16	44.85	1.76	W	g	?	-0.71	fs	
1602+01	3C 327.1	1.120	0.020	0.004	0.005	0.011	0.002	-0.002	0.001	-0.18	0.10	1.84	1.06	0.24	35.29	11.15	E	g	0.4628	-1.03	ss	2
1606+10		1.560	0.028	-0.012	0.007	0.014	0.003	0.004	0.002	0.28	0.11	2.53	1.20	0.31	65.92	8.05	E	qso	1.2260	0.42	fs	
1607+26		1.780	0.032	0.002	0.002	-0.002	0.006	-0.005	0.002	-0.27	0.10	2.65	0.17	0.23	-	-	E	g	0.4730	-0.91	ss	
1611+34		3.952	0.079	0.070	0.002	0.067	0.006	0.010	0.003	0.26	0.07	3.69	2.46	0.12	21.76	1.38	W	qso	1.4010	0.10	fs	
1624+41		1.098	0.022	0.001	0.001	0.007	0.002	0.002	0.001	0.16	0.09	1.72	0.67	0.18	41.95	3.16	W	qso	2.5500	-0.26	fs	2
1633+38		2.812	0.056	0.008	0.001	0.069	0.005	0.000	0.002	-0.01	0.08	0.09	2.46	0.18	41.64	0.53	W	qso	1.8140	0.73	fs	2
1634+62	3C 343.0	1.560	0.031	-0.008	0.000	0.011	0.002	0.001	0.001	0.06	0.06	1.02	0.89	0.10	62.13	2.30	W	qso	0.9880	-0.92	ss	
1637+57		1.557	0.031	-0.028	0.001	0.010	0.003	0.001	0.001	0.04	0.09	0.43	1.91	0.09	80.32	2.40	W	qso	0.7500	0.35	fs	
1637+62	3C 343.1	1.226	0.025	0.000	0.001	0.006	0.002	0.000	0.001	0.00	0.09	0.06	0.52	0.17	43.72	3.87	W	g	0.7500	-1.01	ss	2

Table A.2: Complete results *(contd)*.

Source (1)	Source (2)	I [Jy] (3)	σ (4)	Q [Jy] (5)	σ (6)	U [Jy] (7)	σ (8)	V [Jy] (9)	σ (10)	V [%] (11)	σ (12)	N σ (13)	P [%] (14)	σ (15)	PA [°] (16)	σ (17)	T (18)	O (19)	z (20)	α_{11-6} (21)	S (22)	FR (23)
1638+12		1.187	0.018	0.001	0.004	0.001	0.001	-0.001	0.001	-0.08	0.08	0.90	0.16	0.22	-	-	E	g	?	-0.63	ss	
1638+39		1.995	0.040	0.051	0.002	0.025	0.004	0.000	0.002	-0.01	0.09	0.16	2.86	0.13	13.25	1.68	W	qso	1.6660	0.17	fs	2
1641+17	3C 346	1.411	0.021	0.012	0.007	-0.007	0.002	-0.003	0.001	-0.24	0.08	3.03	0.95	0.43	-15.58	8.78	E	g	0.1610	-0.78	ss	1
1641+39	3C 345	5.898	0.118	0.012	0.003	0.238	0.012	0.015	0.005	0.26	0.08	3.25	4.04	0.22	43.58	0.36	W	qso	0.5940	0.54	fs	2
1642+69		1.263	0.025	-0.082	0.002	0.020	0.002	0.004	0.001	**0.32**	**0.08**	4.13	6.71	0.20	83.16	0.68	W	qso	0.7510	-0.10	fs	2
1648+01		0.777	0.014	-0.033	0.006	0.011	0.001	0.002	0.001	0.23	0.11	2.17	4.47	0.80	81.04	1.77	E	qso	?	0.33	fs	
1652+39		1.450	0.029	0.028	0.040	0.000	0.002	0.002	0.001	0.16	0.07	2.14	1.95	2.73	-0.12	2.18	W	bl/gal	0.0337	0.06	fs	2
1655+07		1.432	0.026	0.012	0.009	0.003	0.002	0.005	0.002	**0.33**	**0.11**	3.01	0.86	0.62	7.23	7.10	E	qso	0.6210	0.43	fs	
1656+05		1.142	0.021	0.064	0.010	0.001	0.001	0.002	0.001	0.14	0.10	1.34	5.60	0.86	0.41	0.50	E	qso	0.8790	0.44	fs	
1721−02		0.749	0.014	-0.026	0.006	-0.010	0.001	-0.003	0.001	**-0.40**	**0.10**	3.89	3.75	0.73	100.72	2.53	E	g	0.0330	-0.41	fs	
1725+04		0.658	0.012	0.006	0.004	0.003	0.001	0.002	0.001	0.30	0.11	2.82	0.93	0.57	13.05	8.99	E	qso	0.2930	0.76	fs	
1732+38		0.893	0.018	0.007	0.001	-0.015	0.001	0.000	0.001	0.00	0.09	0.05	1.83	0.15	-31.95	1.51	W	qso	0.9760	0.85	fs	
1739+52		0.975	0.020	0.005	0.001	0.011	0.002	0.001	0.001	0.14	0.09	1.44	1.22	0.17	33.58	2.21	W	qso	1.3790	0.68	fs	
1741−03		4.937	0.089	0.073	0.031	0.006	0.006	-0.006	0.005	-0.12	0.10	1.23	1.48	0.63	2.30	2.40	E	qso	1.0570	0.75	fs	
1749+09		1.600	0.029	-0.040	0.012	-0.040	0.005	0.009	0.002	**0.56**	**0.11**	4.95	3.54	0.59	112.51	4.74	E	bl/qso	0.3220	1.01	fs	
1749+70		0.605	0.011	-0.015	0.003	-0.004	0.003	0.001	0.001	0.12	0.11	1.08	2.50	0.53	98.01	5.48	E	bl/qso	0.7700	-0.26	fs	1
1751+44		0.663	0.013	-0.001	0.001	0.009	0.001	0.001	0.001	0.21	0.14	1.57	1.36	0.20	49.74	2.96	W	qso	0.8710	0.90	fs	
1800+44		1.280	0.023	0.014	0.003	0.022	0.011	0.004	0.001	0.32	0.11	2.95	2.04	0.76	29.01	7.08	E	qso	0.6630	0.57	fs	
1803+78		2.777	0.050	-0.048	0.013	0.031	0.012	0.005	0.003	0.18	0.10	1.71	2.07	0.46	73.67	5.99	E	bl/qso	0.6840	0.25	fs	1
1807+69	3C 371.0	1.768	0.035	0.023	0.001	0.019	0.003	0.000	0.002	-0.01	0.09	0.14	1.70	0.13	19.66	2.34	W	bl/g	0.0510	0.14	fs	2
1823+56		1.368	0.027	-0.003	0.001	0.057	0.003	0.007	0.001	**0.48**	**0.09**	5.17	4.18	0.22	46.40	0.47	W	bl/qso	0.6640	0.22	fs	1
1828+48	3C 380	5.081	0.102	0.017	0.002	0.057	0.008	0.003	0.003	0.07	0.07	0.98	1.18	0.16	36.76	1.36	W	qso	0.6910	-0.75	ss	2
1829+29		1.170	0.021	0.002	0.007	-0.001	0.003	-0.004	0.001	**-0.35**	**0.10**	3.48	0.18	0.59	-	-	E	g	0.8420	-0.85	ss	
1830+28		1.086	0.020	-0.017	0.006	0.011	0.003	-0.001	0.001	-0.05	0.10	0.48	1.87	0.52	73.75	6.05	E	qso	0.5940	-0.30	fs	
1928+73		3.664	0.066	-0.071	0.024	0.012	0.005	-0.008	0.004	-0.23	0.10	2.31	1.98	0.63	85.34	2.44	E	qso	0.3020	-0.01	fs	1,2
1954+51		1.104	0.022	-0.015	0.001	0.013	0.002	0.002	0.001	0.14	0.10	1.32	1.79	0.14	70.30	2.53	W	qso	1.2300	-0.01	fs	1,2
2007+77		0.868	0.016	0.013	0.006	-0.024	0.004	0.0021	0.001	0.24	0.11	2.22	3.11	0.51	-30.50	5.77	E	bl/qso	0.3420	0.69	fs	
2008−06		1.408	0.025	0.001	0.008	0.000	0.003	-0.001	0.001	-0.04	0.10	0.38	0.06	0.53	-	-	E	g	?	-0.68	ss	
2021+61		3.296	0.066	-0.009	0.001	0.006	0.006	0.000	0.003	0.00	0.08	0.04	0.34	0.11	72.40	12.48	W	g	0.2266	0.09	fs	
2029+12		0.938	0.017	-0.018	0.006	0.003	0.004	0.003	0.001	0.31	0.10	2.95	1.89	0.68	85.69	5.90	E	bl/qso	1.215?	0.74	fs	
2044−02	3C 422.0	0.895	0.016	0.002	0.004	-0.008	0.003	-0.002	0.001	-0.24	0.10	2.40	0.92	0.32	-38.56	15.09	E	qso	0.9420	-0.52	ss	
2113+29		0.921	0.017	0.026	0.003	-0.024	0.005	0.001	0.001	0.14	0.10	1.39	3.78	0.48	-21.28	3.73	E	qso	1.5140	0.62	fs	
2121+24	3C 433	3.705	0.055	0.079	0.013	-0.211	0.018	-0.011	0.003	**-0.31**	**0.09**	3.58	6.07	0.48	-34.71	1.71	E	g	0.1016	-0.97	ss	1,2
2128+04		1.900	0.049	-0.001	0.014	-0.001	0.009	-0.008	0.003	**-0.43**	**0.14**	3.10	0.08	0.67	-	-	E	g	0.9900	-0.73	ss	
2131−02		2.398	0.043	-0.062	0.017	-0.060	0.011	-0.006	0.002	-0.26	0.10	2.54	3.60	0.61	111.82	4.77	E	bl/qso	0.557?	0.13	fs	
2134+00		9.931	0.180	-0.139	0.059	-0.046	0.031	-0.020	0.010	-0.20	0.10	1.97	1.48	0.57	99.17	6.72	E	qso	1.9360	0.83	fs	
2136+14		2.709	0.049	-0.004	0.014	0.004	0.010	0.006	0.003	0.22	0.10	2.10	0.20	0.44	-	-	E	qso	2.4270	-0.10	fs	
2144+09		0.686	0.012	-0.013	0.004	0.006	0.003	0.000	0.001	-0.03	0.10	0.26	2.04	0.53	78.24	5.87	E	qso	1.1130	0.23	fs	
2145+06		5.707	0.084	-0.014	0.014	-0.008	0.021	-0.004	0.005	-0.06	0.08	0.80	0.28	0.28	-	-	E	qso	0.9900	0.25	fs	
2149+05		0.842	0.015	-0.001	0.005	-0.002	0.002	-0.002	0.001	-0.25	0.10	2.39	0.26	0.30	-	-	E	g	0.7400	0.05	fs	
2150+17		0.683	0.012	0.003	0.004	-0.005	0.004	-0.001	0.001	-0.08	0.11	0.77	0.84	0.59	-31.38	19.23	E	bl/qso	?	0.20	fs	
2200+42		2.569	0.038	0.027	0.008	-0.072	0.012	0.003	0.002	0.12	0.09	1.38	3.00	0.47	-34.57	3.17	E	bl/g	0.0688	-0.13	fs	1
2201+31		2.397	0.035	0.004	0.003	0.000	0.010	0.000	0.002	0.01	0.08	0.18	0.16	0.13	-	-	E	qso	0.2980	0.24	fs	2
2209+08		0.730	0.019	-0.039	0.009	0.002	0.002	0.000	0.001	0.06	0.14	0.40	5.41	1.20	88.83	1.28	E	qso	0.4840	-0.39	ss	2
2210+01		1.088	0.020	0.000	0.006	-0.001	0.002	-0.004	0.001	**-0.34**	**0.10**	3.49	0.05	0.21	-	-	E	qso	?	-0.91	ss	
2216−03		2.564	0.046	-0.042	0.015	0.026	0.005	-0.010	0.003	**-0.40**	**0.10**	4.03	1.93	0.51	74.09	5.29	E	qso	0.9010	0.48	fs	

Table A.2: Complete results *(contd).*

Source (1)	Source (2)	I [Jy] (3)	σ (4)	Q [Jy] (5)	σ (6)	U [Jy] (7)	σ (8)	V [Jy] (9)	σ (10)	V [%] (11)	σ (12)	N σ (13)	P [%] (14)	σ (15)	PA [°] (16)	σ (17)	T (18)	O (19)	z (20)	α_{11-6} (21)	S (22)	FR (23)
2223+21		1.282	0.023	-0.039	0.008	-0.080	0.008	0.001	0.001	0.07	0.11	0.66	6.93	0.65	121.83	2.59	E	qso	1.9490	-0.65	ss	2
2223−05	3C 446.0	6.265	0.093	0.204	0.036	-0.086	0.006	-0.011	0.005	-0.17	0.08	2.06	3.53	0.54	-11.48	1.98	E	qso	1.4040	-0.11	fs	
2227−08		3.102	0.046	-0.021	0.017	-0.068	0.005	-0.002	0.003	-0.08	0.08	0.91	2.31	0.23	126.53	6.37	E	qso	1.5610	-0.03	fs	
2230+11		4.649	0.069	0.019	0.008	0.163	0.012	-0.016	0.004	**-0.34**	**0.08**	4.12	3.52	0.26	41.66	1.45	E	qso	1.0370	-0.50	ss	2
2234+28		1.139	0.021	0.001	0.003	0.008	0.003	0.000	0.001	0.04	0.10	0.36	0.74	0.29	41.06	9.73	E	qso	0.7950	0.08	fs	
2247+11		0.850	0.022	0.004	0.008	0.064	0.006	-0.001	0.001	-0.16	0.17	0.93	7.55	0.68	43.04	3.40	E	g	0.0243	-0.57	ss	1
2247+14		1.105	0.014	-0.011	0.004	-0.015	0.003	0.000	0.001	0.00	0.07	0.03	1.69	0.29	116.07	5.23	E	qso	0.2370	-0.63	fs	
2251+15	3C 454.3	9.532	0.141	0.547	0.063	0.107	0.015	-0.023	0.008	-0.24	0.09	2.76	5.85	0.66	5.55	0.99	E	qso	0.8590	0.64	fs	
2254+07		0.348	0.006	0.000	0.002	0.025	0.002	0.001	0.001	0.42	0.15	2.73	7.17	0.61	44.89	2.70	E	bl/gal	0.1900	1.19	fs	
2255+41		0.956	0.014	0.000	0.004	0.000	0.004	0.000	0.001	0.03	0.08	0.37	0.04	0.45	-	-	E	qso	1.1490	-0.55	ss	
2314+03	3C 459	1.329	0.024	0.040	0.009	0.007	0.002	-0.003	0.001	-0.22	0.10	2.12	3.07	0.65	4.68	1.61	E	g	0.2199	-0.91	ss	2
2318+04		0.491	0.009	-0.009	0.003	0.011	0.001	0.002	0.001	0.36	0.12	3.11	2.86	0.43	63.78	5.10	E	qso	0.6230	-0.11	fs	
2319+27		1.081	0.016	-0.025	0.006	-0.022	0.004	0.000	0.001	-0.02	0.09	0.20	3.13	0.51	110.79	4.35	E	qso	1.2530	0.20	fs	
2323+43		0.944	0.014	0.005	0.004	0.007	0.004	-0.001	0.001	-0.11	0.08	1.39	0.90	0.44	28.34	14.07	E	g	0.1450	-0.45	ss	
2324+40	3C 462.0	0.981	0.015	0.030	0.005	0.017	0.005	-0.002	0.001	-0.23	0.08	2.75	3.50	0.50	14.68	3.96	E	g	0.3940	-0.47	ss	
2324−02		0.900	0.016	0.004	0.005	0.037	0.003	-0.007	0.001	**-0.82**	**0.11**	7.63	4.19	0.39	41.83	3.89	E	g	0.1880	-0.49	ss	
2328+10		1.173	0.021	-0.004	0.006	0.024	0.005	0.001	0.001	0.07	0.10	0.72	2.06	0.40	50.18	7.53	E	qso	1.4890	-0.05	fs	
2342+82		1.309	0.019	-0.001	0.005	0.000	0.005	-0.002	0.001	-0.16	0.08	1.95	0.04	0.37	-	-	E	qso	0.7350	-0.89	ss	
2344+09		1.454	0.026	0.006	0.008	-0.019	0.004	-0.001	0.001	-0.08	0.10	0.75	1.37	0.32	-35.94	11.29	E	qso	0.6730	-0.09	fs	
2351+45		1.432	0.021	-0.010	0.004	0.003	0.006	0.000	0.001	-0.02	0.08	0.25	0.74	0.31	81.28	16.66	E	qso	1.9920	-0.05	fs	2
2352+49		1.346	0.020	0.000	0.006	0.001	0.003	-0.002	0.001	-0.14	0.08	1.71	0.08	0.31	-	-	E	g	0.2370	-0.28	fs	

NOTES— Col.(1):IAU name. Col.(2):Other name. Col.(3),(4): Stokes I and accuracy. Col.(5),(6): Stokes Q and accuracy. Col.(7),(8): Stokes U and accuracy. Col.(9),(10): Stokes V and accuracy. Col.(11),(12): Fractional circular polarization and accuracy. Values $\geqslant 0.3$ with a significance $\geqslant 3\sigma$ and corresponding to $V \geqslant 3\,\mathrm{mJy}$ are bold faced. Col.(13): Detection level of fractional CP. Col.(14),(15): Fractional linear polarization and accuracy. Col.(16),(17): Polarization angle and accuracy, values for P<0.5% are not listed. Col.(18): telescope that carried out the measurements. Col.(19): Optical classification. Col.(20): Redshift. Col. (21): Spectral index. Col.(22): Spectral type. Col.(23): Fanaroff-Riley class. Cols. from 19 to 23 from Stickel et al. [1994]

B | Observed Full Stokes spectra

In the following, the complete list of spectra observed in 2009 is presented. The selection criteria was mainly established in order to:

- Build the full Stokes spectra from sources that from the survey exhibited CP larger than 0.3% and 3 mJy, with a significance of at least 3σ, as a preliminary study for a future more detailed multi-epoch observation
- Check the values obtained at 6cm from the survey, particularly those coming from Galaxies
- Check again the consistency of the measurements taken by Effelsberg and WSRT

Figure B.1: Full Stokes spectra from 0003-00

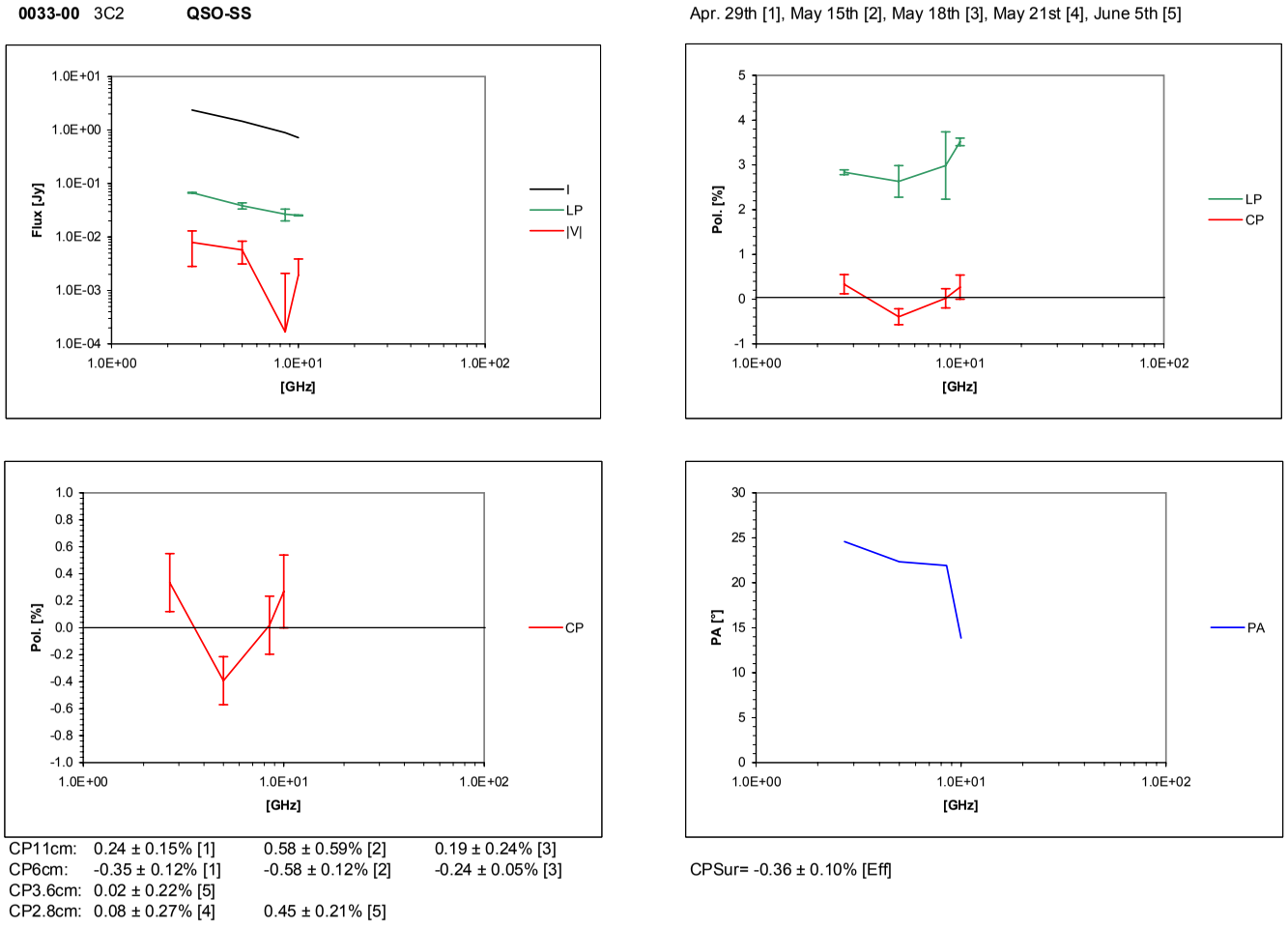

Figure B.2: Full Stokes spectra from 0019-00

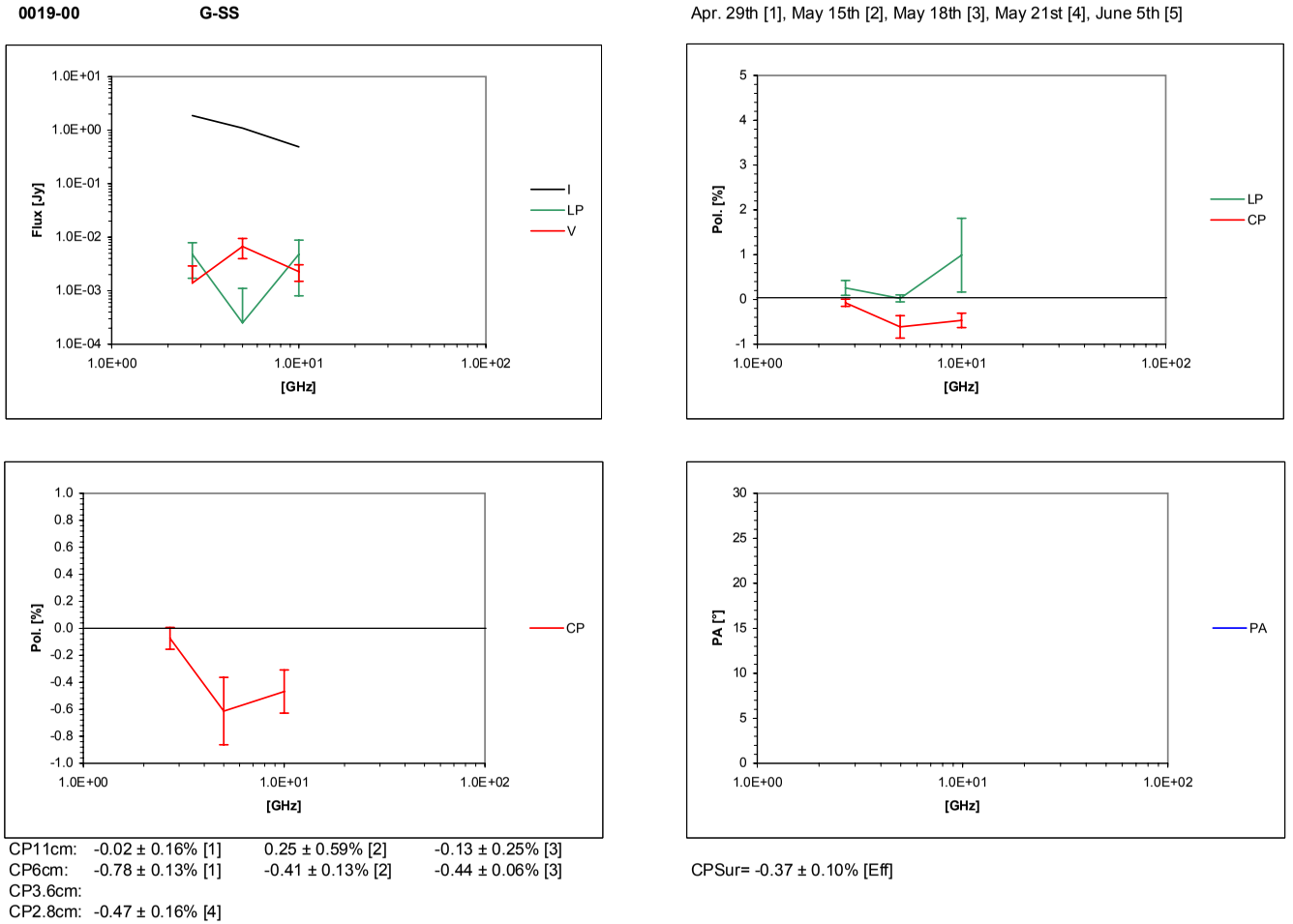

Figure B.3: Full Stokes spectra from 0038+09

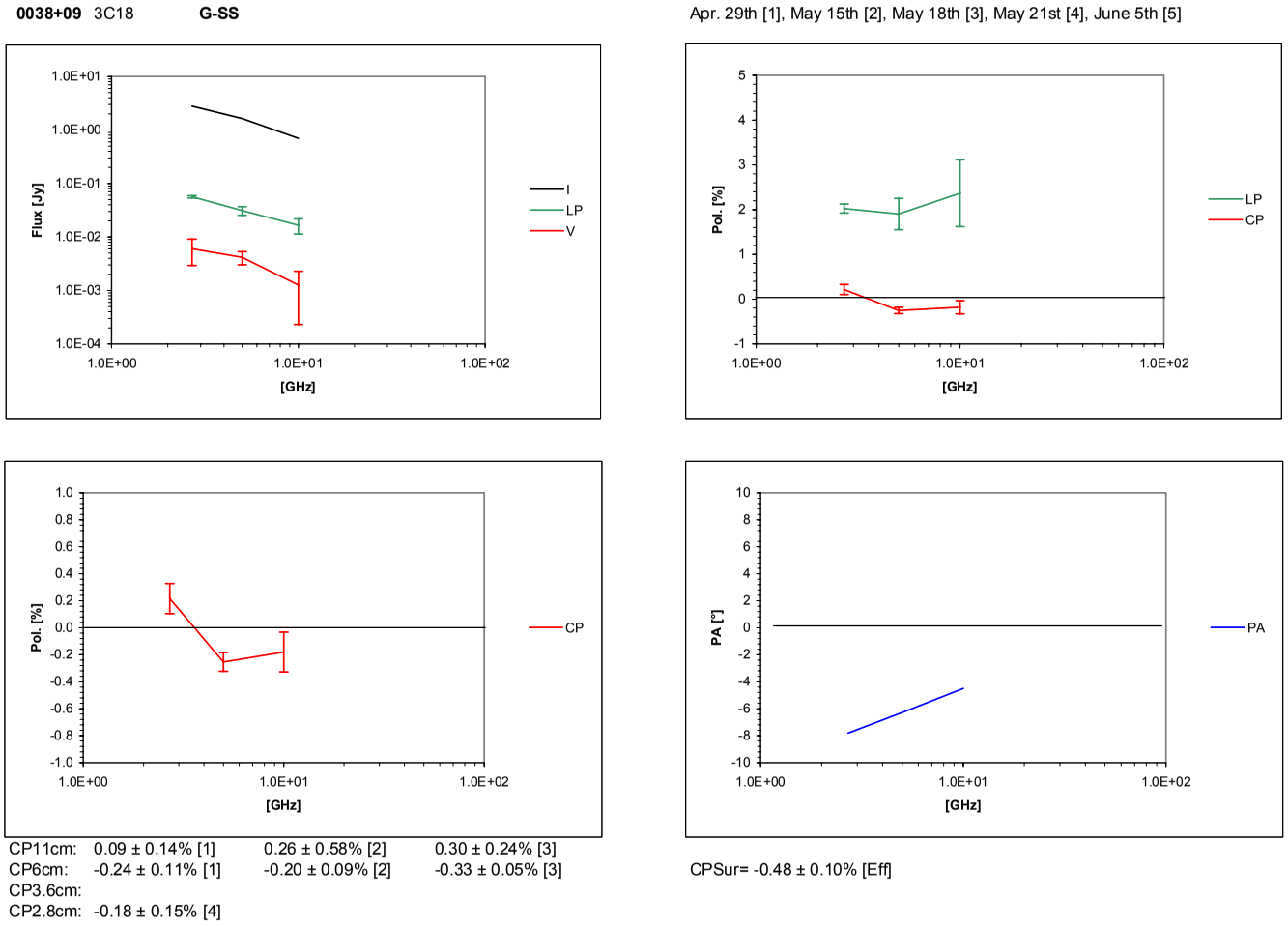

Figure B.4: Full Stokes spectra from 0056-00

0056-00 **QSO-FS**

Apr. 29th [1], May 15th [2], May 18th [3], May 21st [4], June 5th [5]

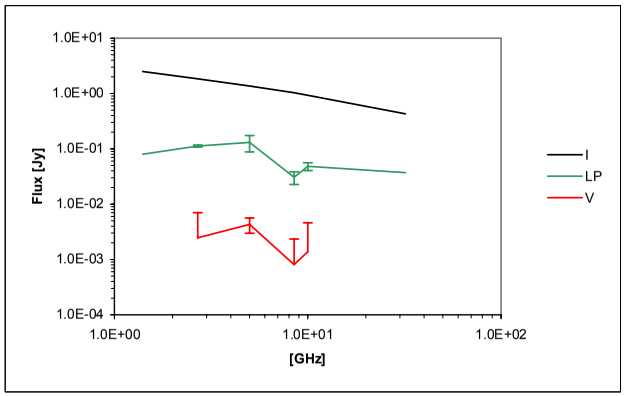

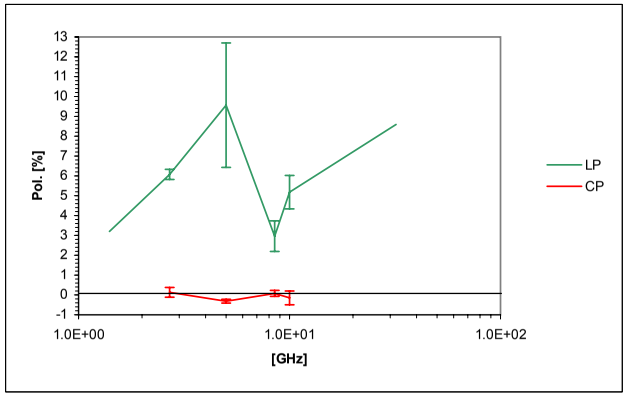

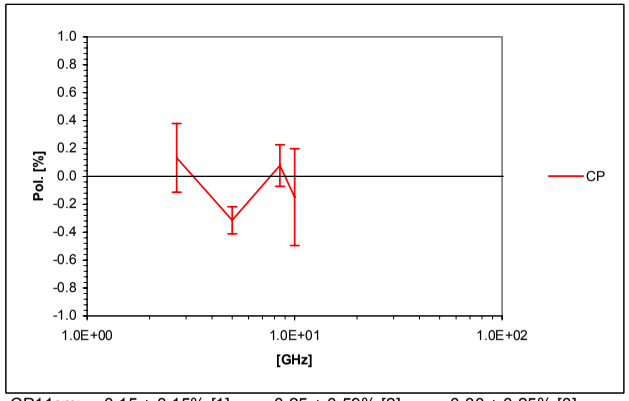

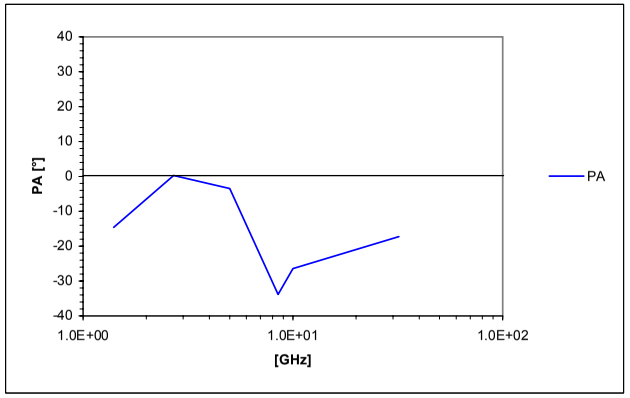

CP11cm:	-0.15 ± 0.15% [1]	0.25 ± 0.59% [2]	0.30 ± 0.25% [3]
CP6cm:	-0.32 ± 0.14% [1]	-0.41 ± 0.13% [2]	-0.22 ± 0.05% [3]
CP3.6cm:	0.08 ± 0.15% [5]		
CP2.8cm:	-0.39 ± 0.20% [4]	0.10 ± 0.26% [5]	

CPSur= -0.37 ± 0.11% [Eff]

Figure B.5: Full Stokes spectra from 0134+32

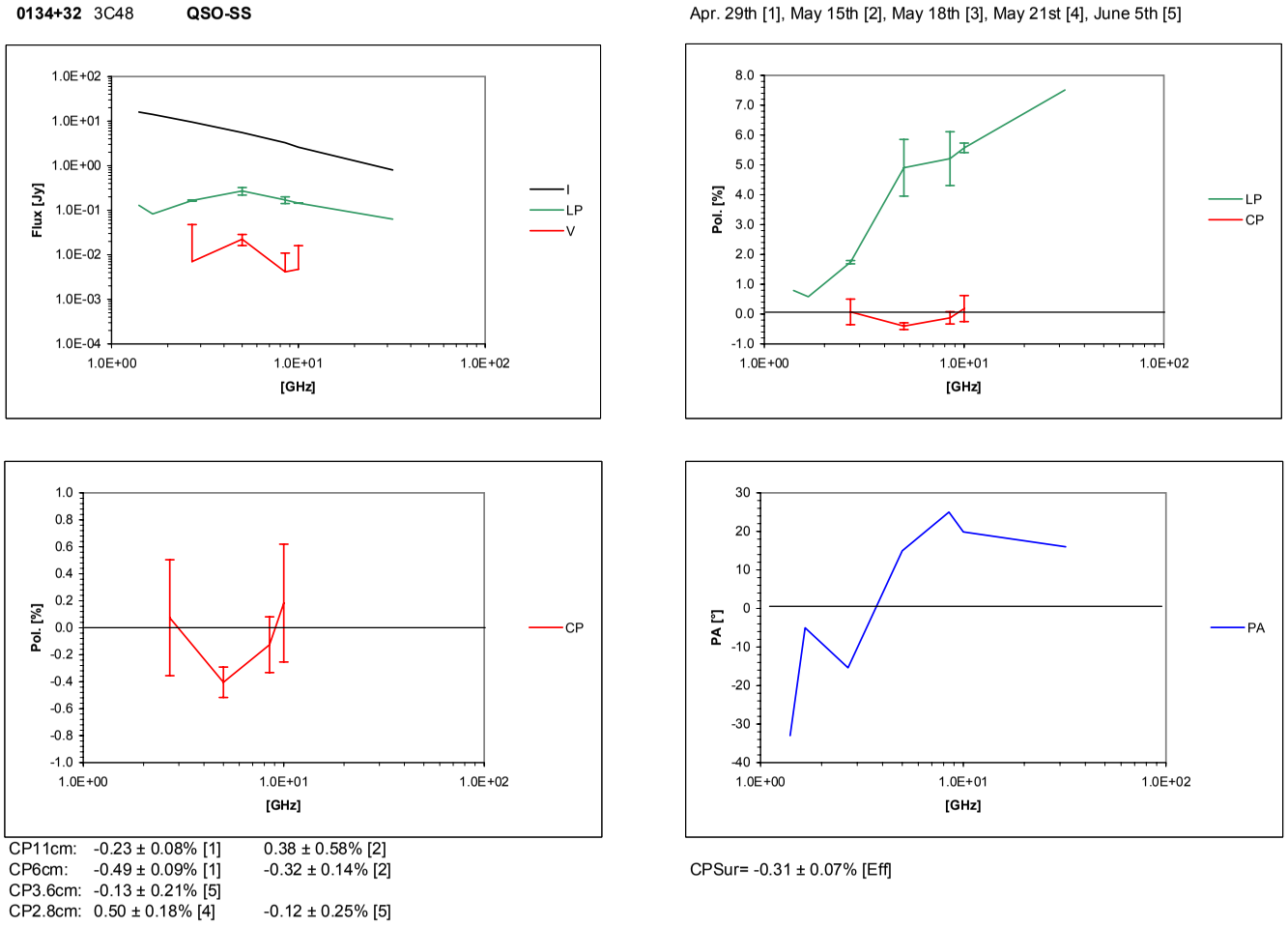

Figure B.6: Full Stokes spectra from 0153+74

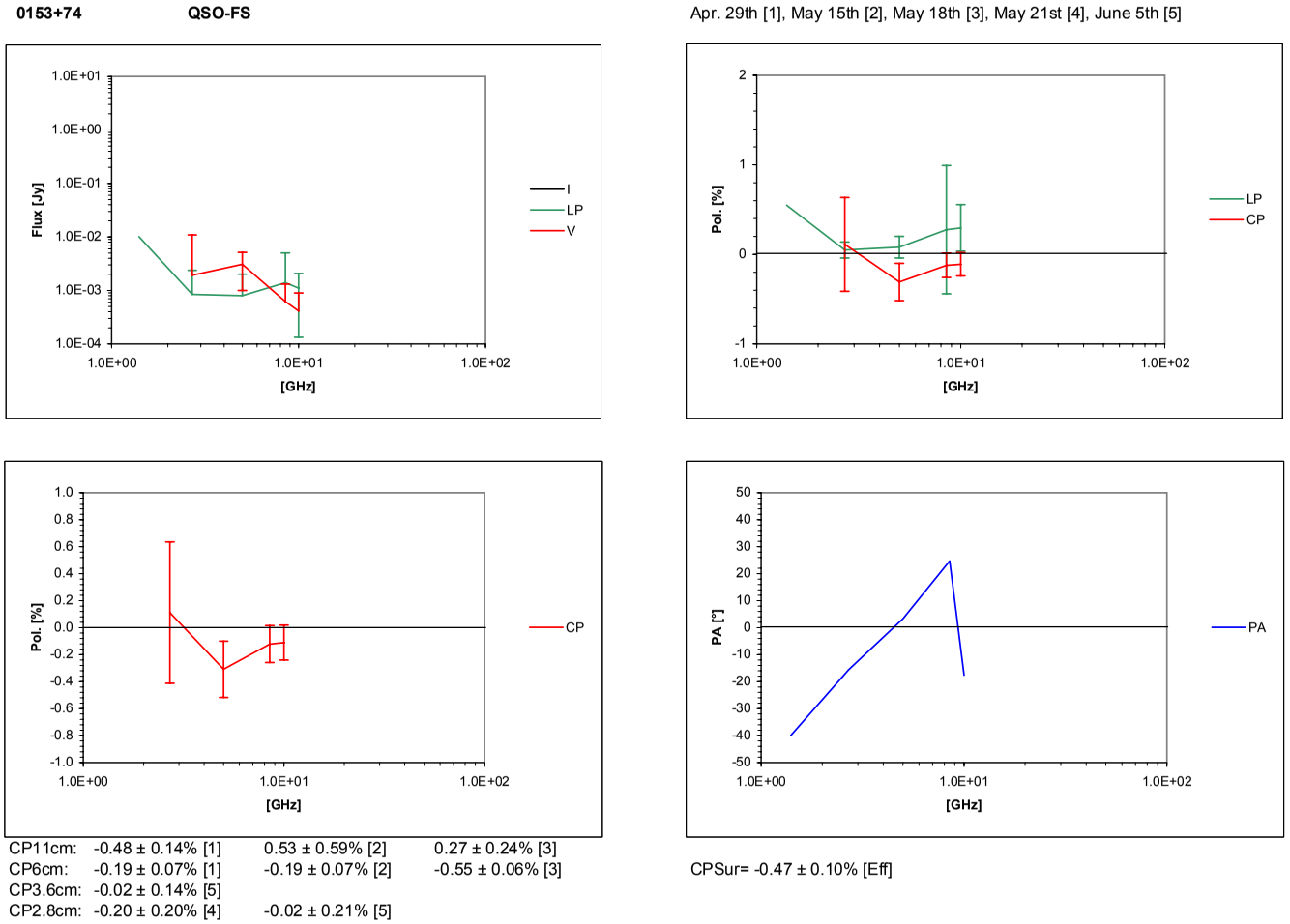

CP11cm: -0.48 ± 0.14% [1] 0.53 ± 0.59% [2] 0.27 ± 0.24% [3]
CP6cm: -0.19 ± 0.07% [1] -0.19 ± 0.07% [2] -0.55 ± 0.06% [3]
CP3.6cm: -0.02 ± 0.14% [5]
CP2.8cm: -0.20 ± 0.20% [4] -0.02 ± 0.21% [5]

CPSur= -0.47 ± 0.10% [Eff]

Figure B.7: Full Stokes spectra from 0202+14

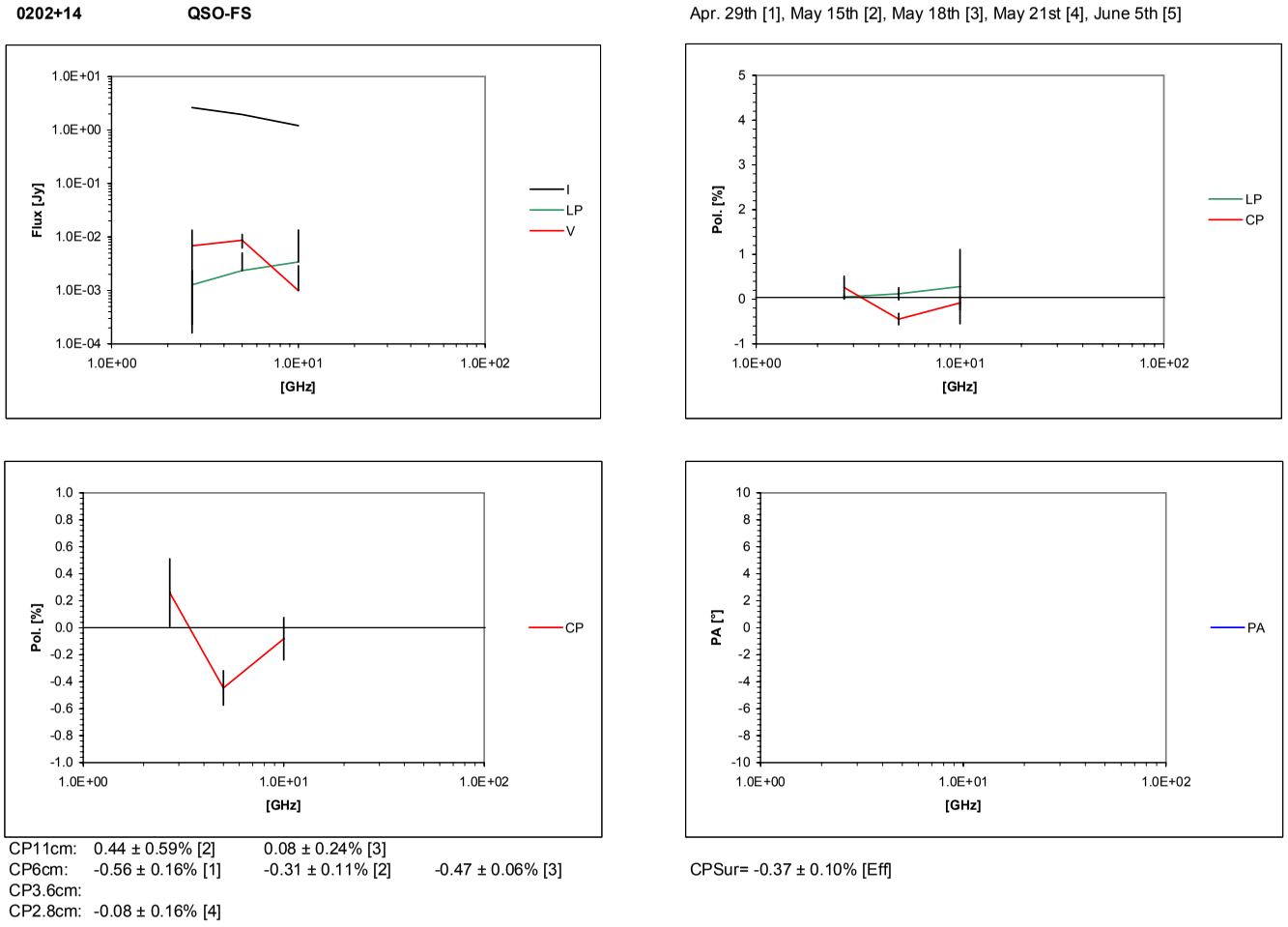

Figure B.8: Full Stokes spectra from 0202+31

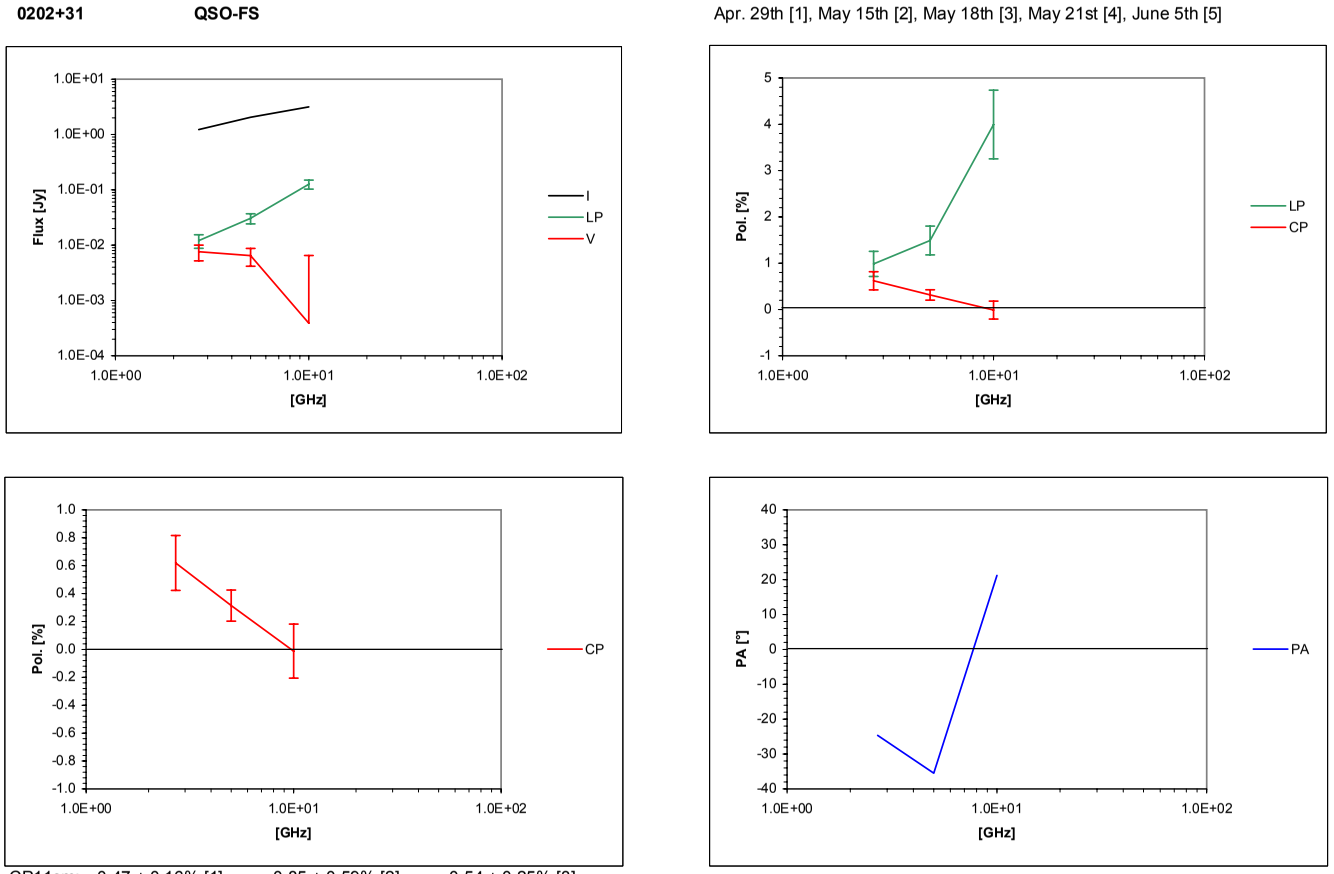

CP11cm: 0.47 ± 0.16% [1] 0.85 ± 0.59% [2] 0.54 ± 0.25% [3]
CP6cm: 0.26 ± 0.20% [1] 0.44 ± 0.22% [2] 0.24 ± 0.14% [3]
CP3.6cm:
CP2.8cm: -0.01 ± 0.19% [4]

CPSur= 0.37 ± 0.15% [Eff]

Figure B.9: Full Stokes spectra from 0212+73

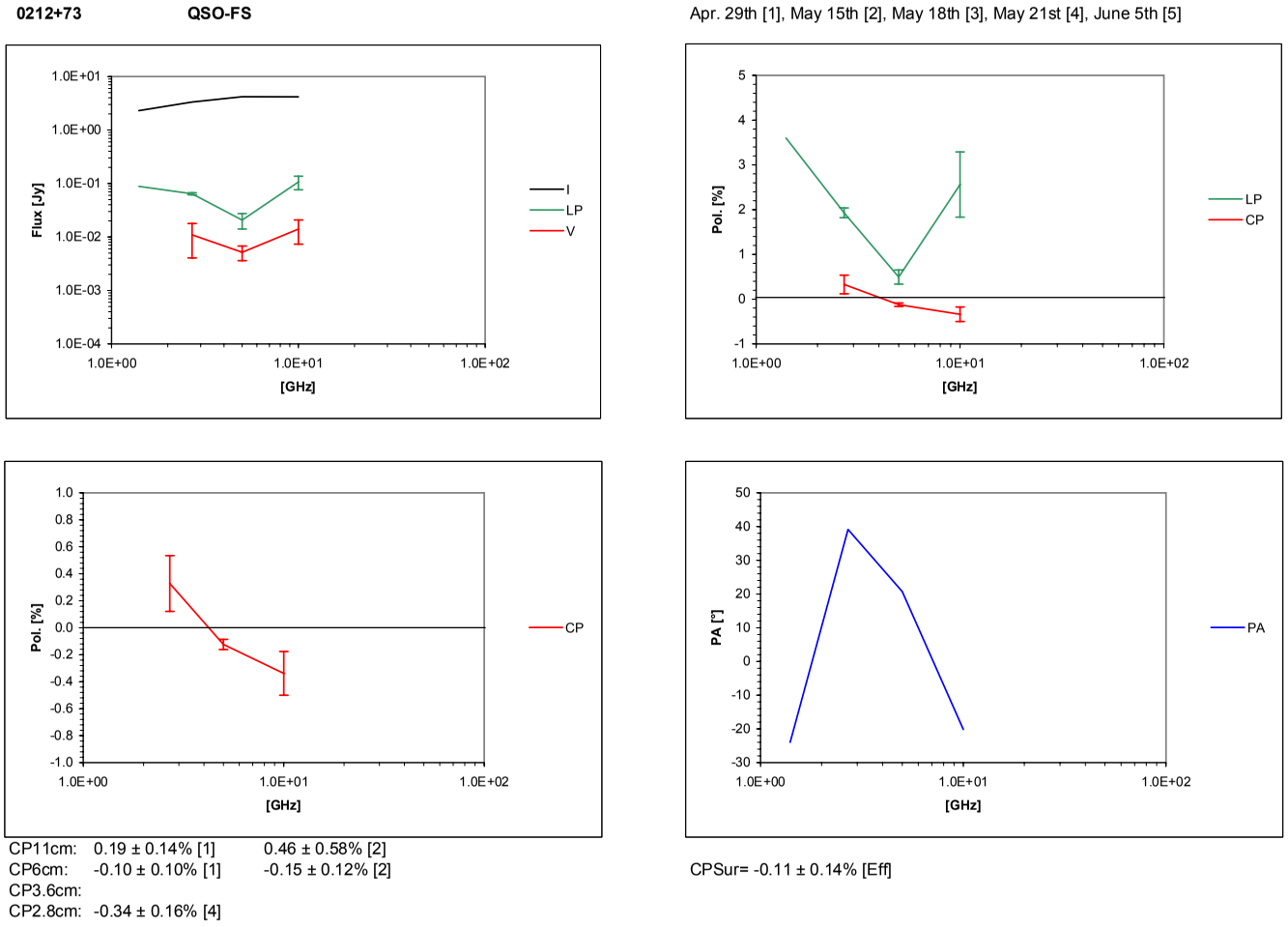

Figure B.10: Full Stokes spectra from 0229+13

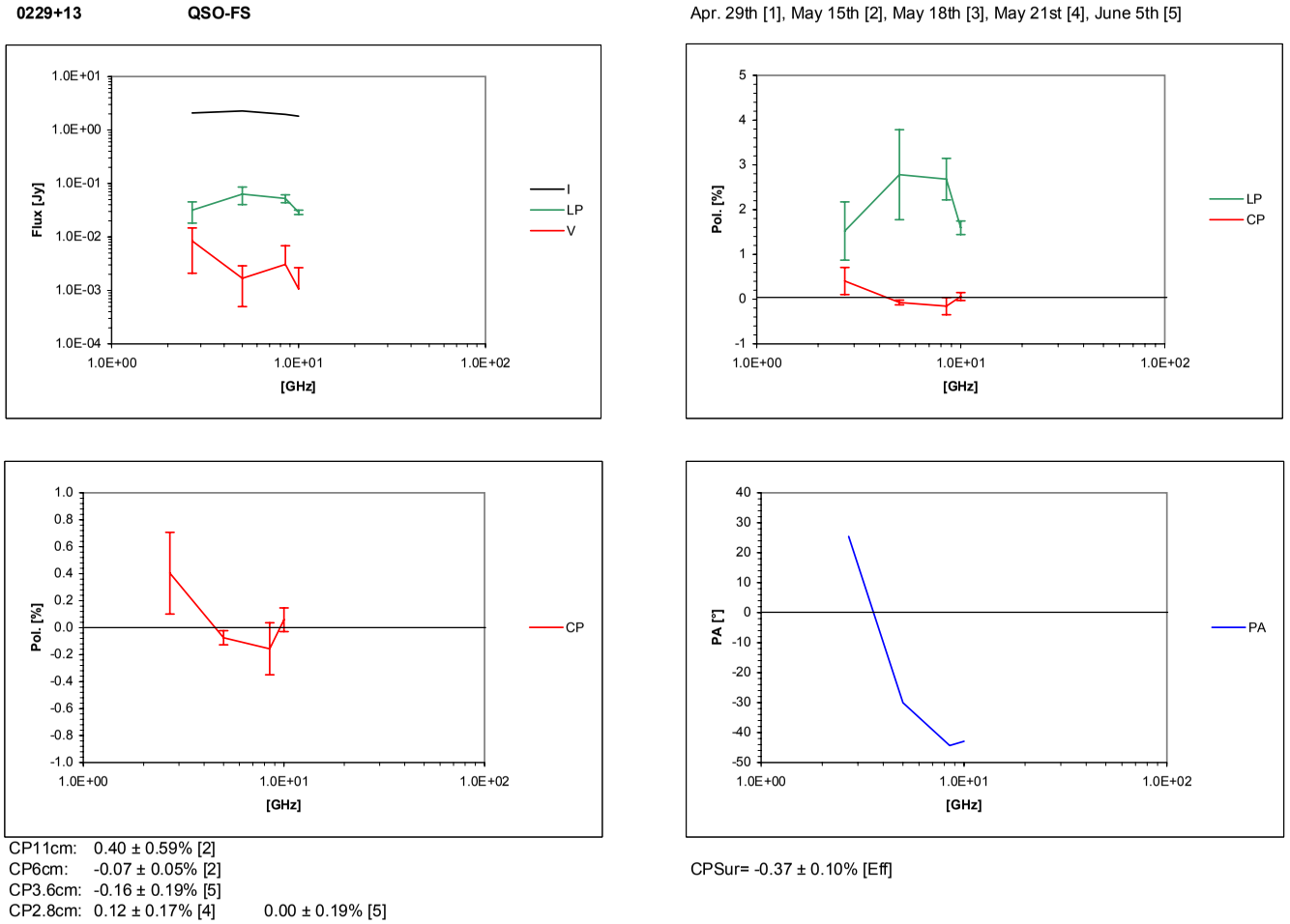

CP11cm: 0.40 ± 0.59% [2]
CP6cm: -0.07 ± 0.05% [2]
CP3.6cm: -0.16 ± 0.19% [5]
CP2.8cm: 0.12 ± 0.17% [4] 0.00 ± 0.19% [5]

CPSur= -0.37 ± 0.10% [Eff]

Figure B.11: Full Stokes spectra from 0305+03

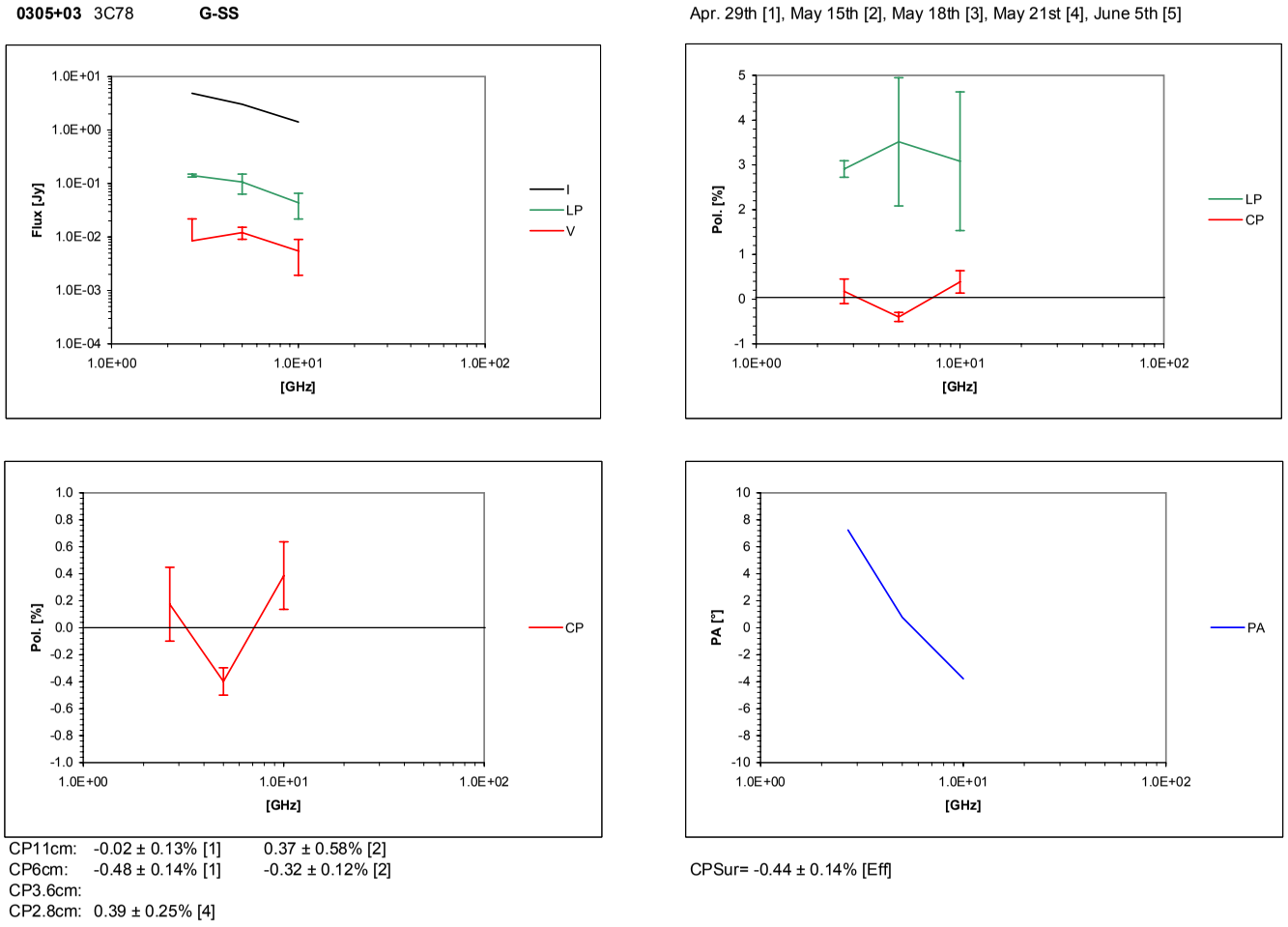

Figure B.12: Full Stokes spectra from 0307+16

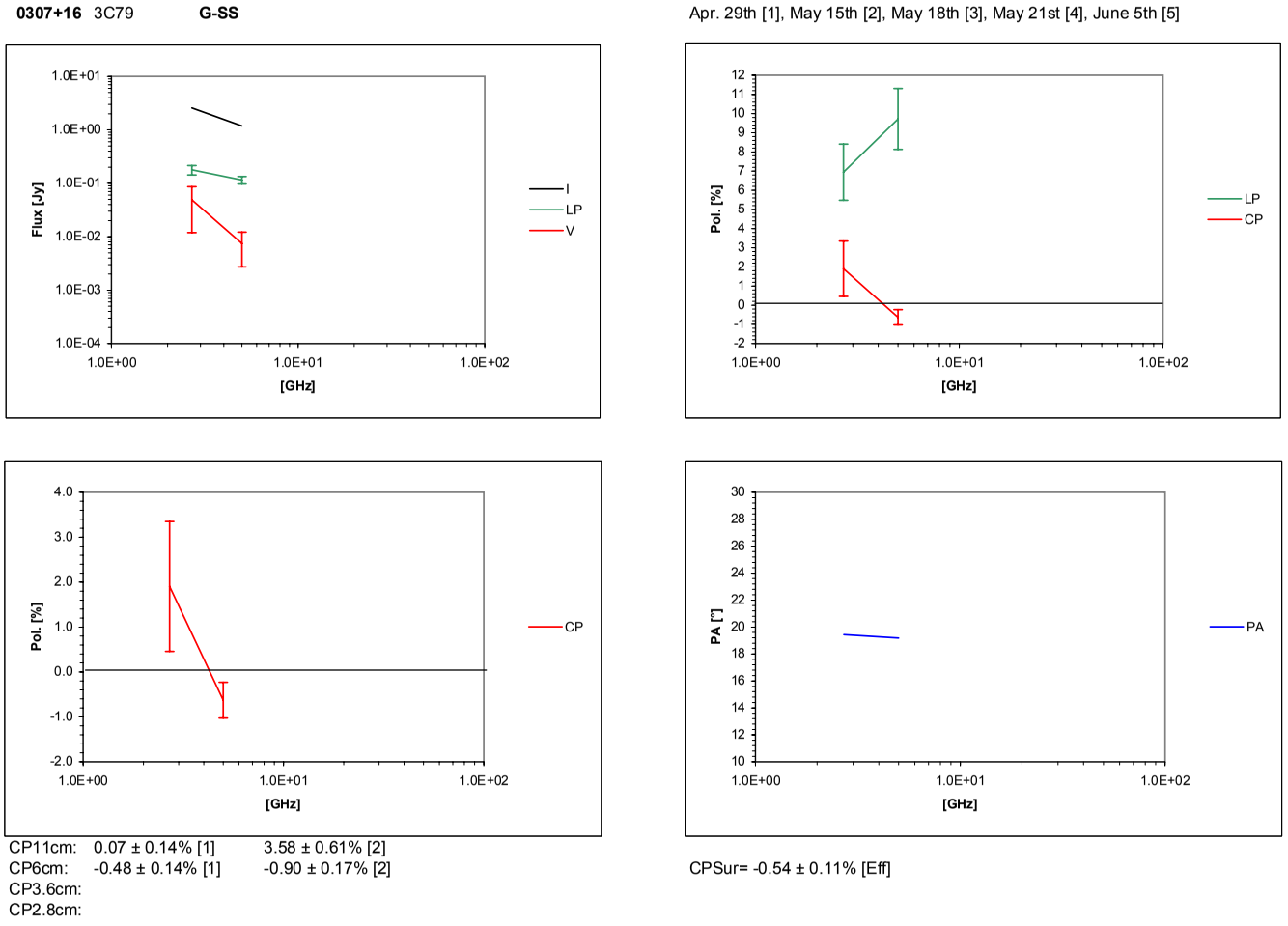

CP11cm: 0.07 ± 0.14% [1] 3.58 ± 0.61% [2]
CP6cm: -0.48 ± 0.14% [1] -0.90 ± 0.17% [2]
CP3.6cm:
CP2.8cm:

CPSur= -0.54 ± 0.11% [Eff]

Figure B.13: Full Stokes spectra from 0316+16

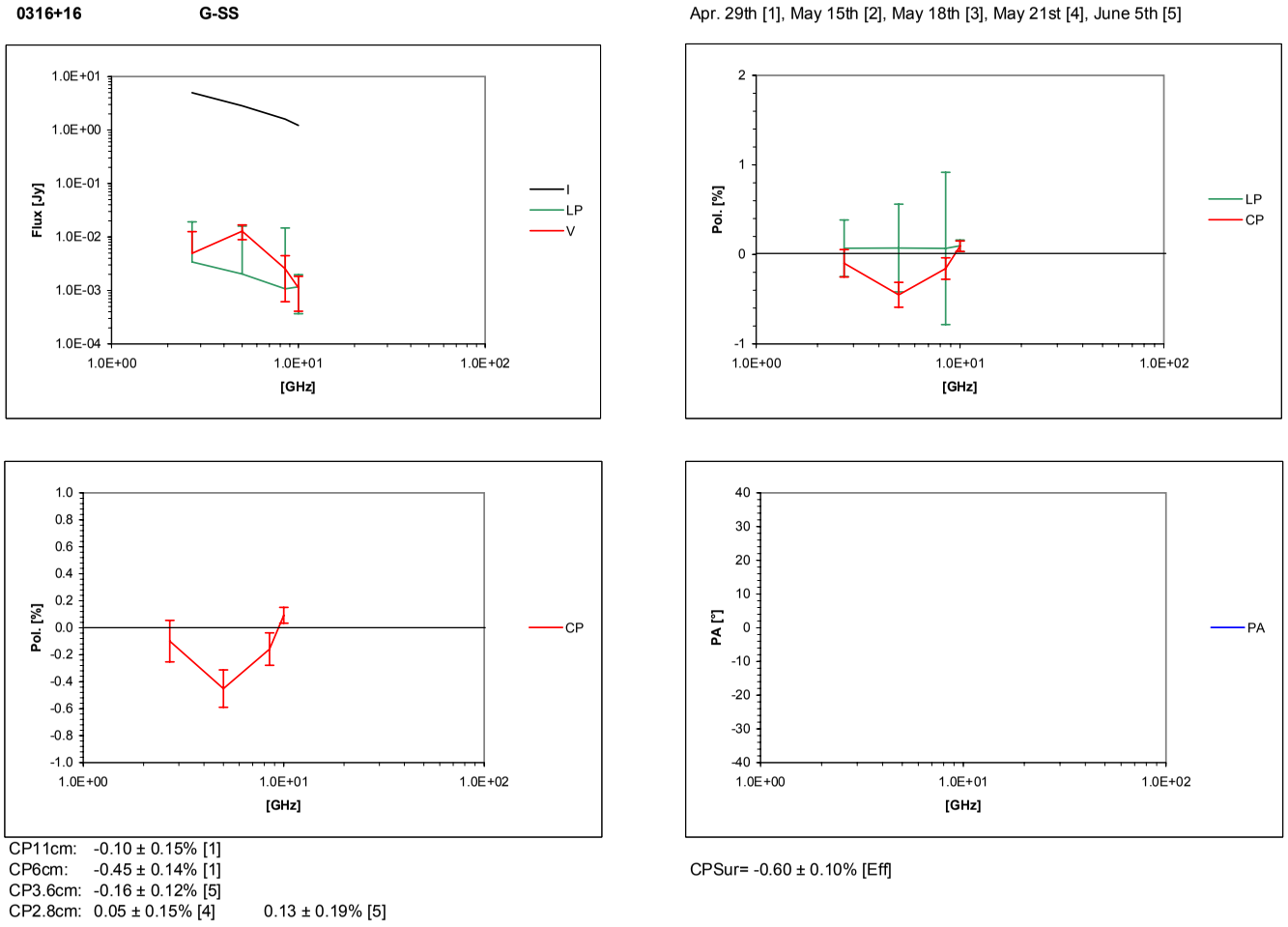

Figure B.14: Full Stokes spectra from 0433+29

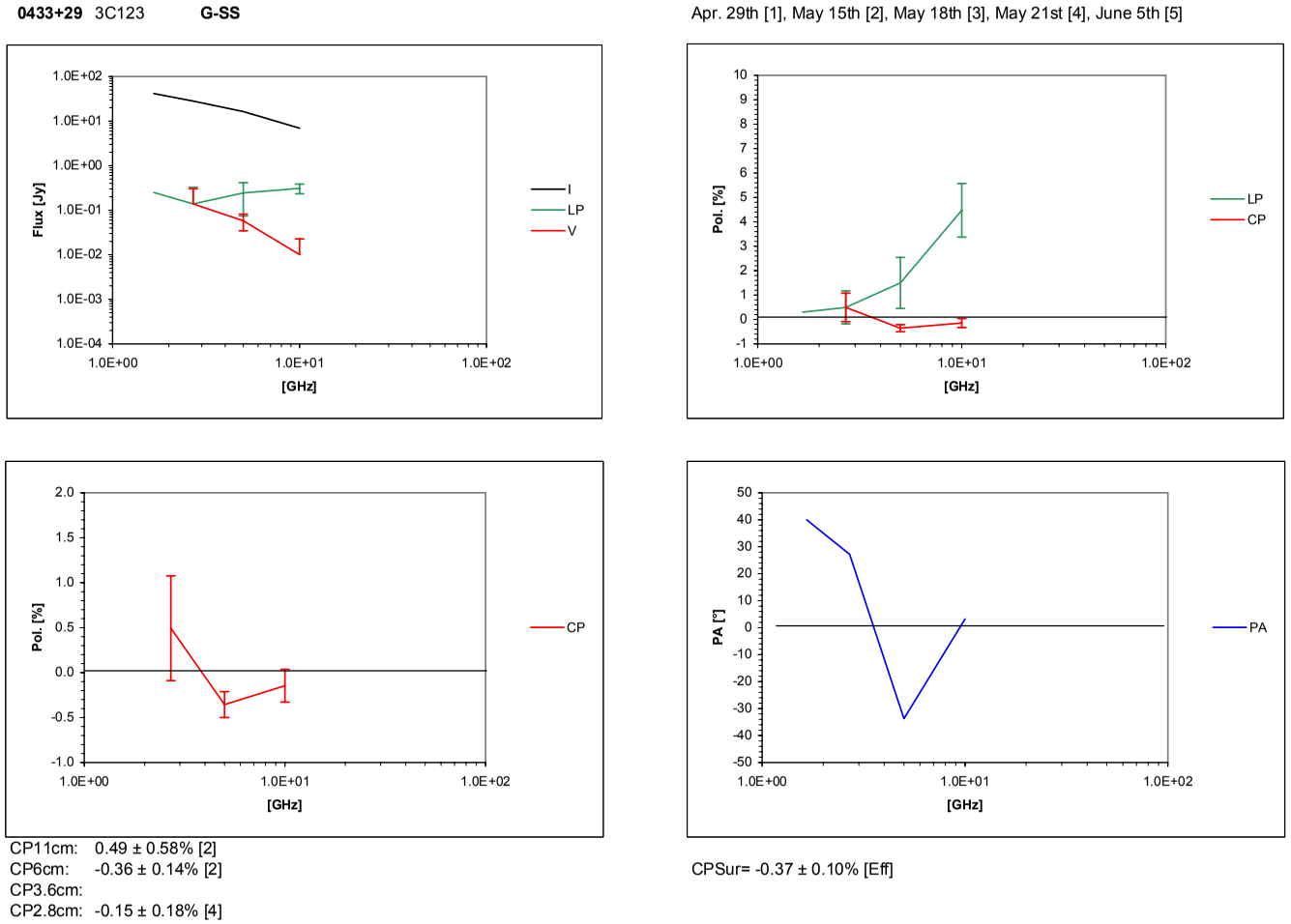

CP11cm: 0.49 ± 0.58% [2]
CP6cm: -0.36 ± 0.14% [2]
CP3.6cm:
CP2.8cm: -0.15 ± 0.18% [4]

CPSur= -0.37 ± 0.10% [Eff]

Figure B.15: Full Stokes spectra from 0538+49

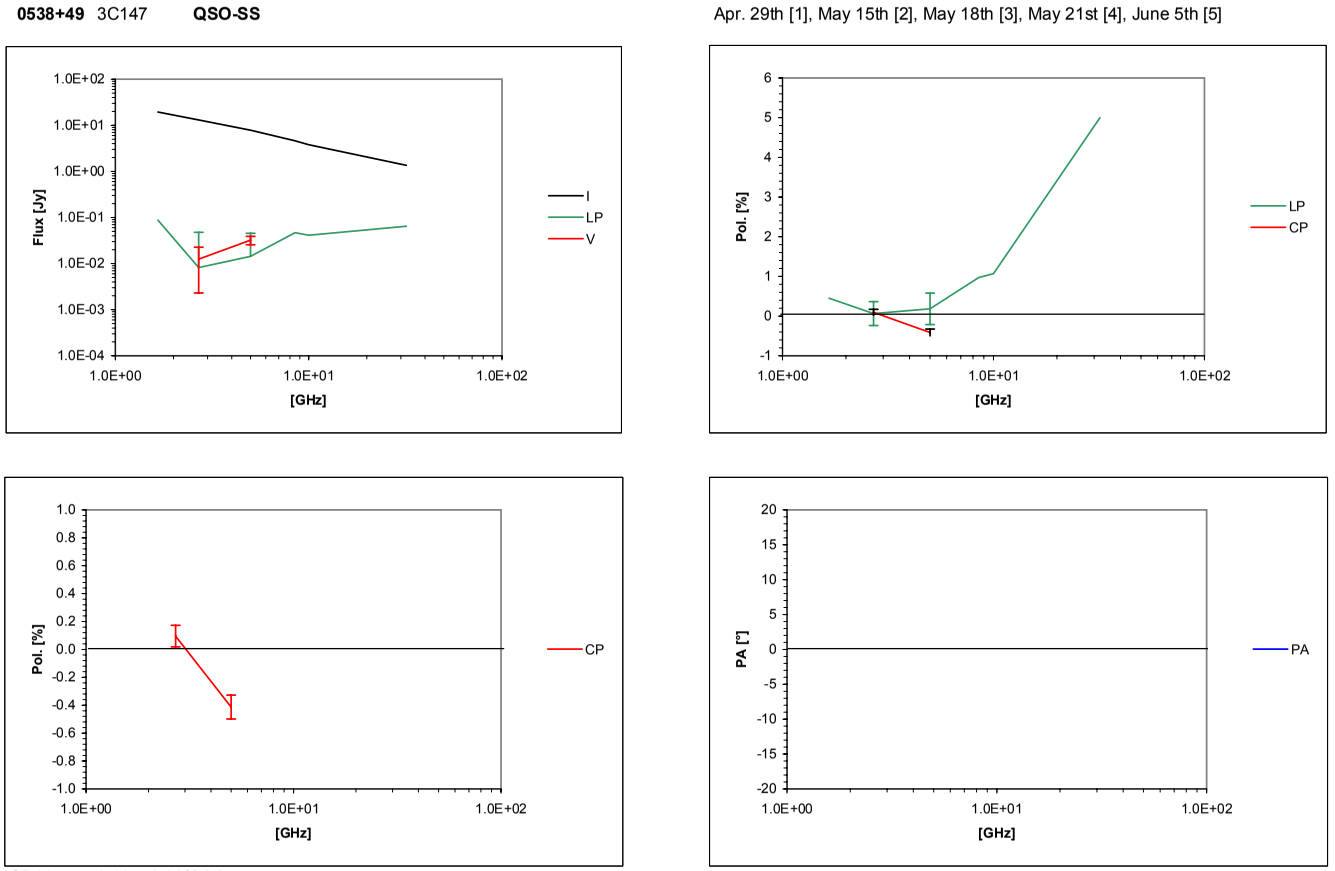

Figure B.16: Full Stokes spectra from 0736+01

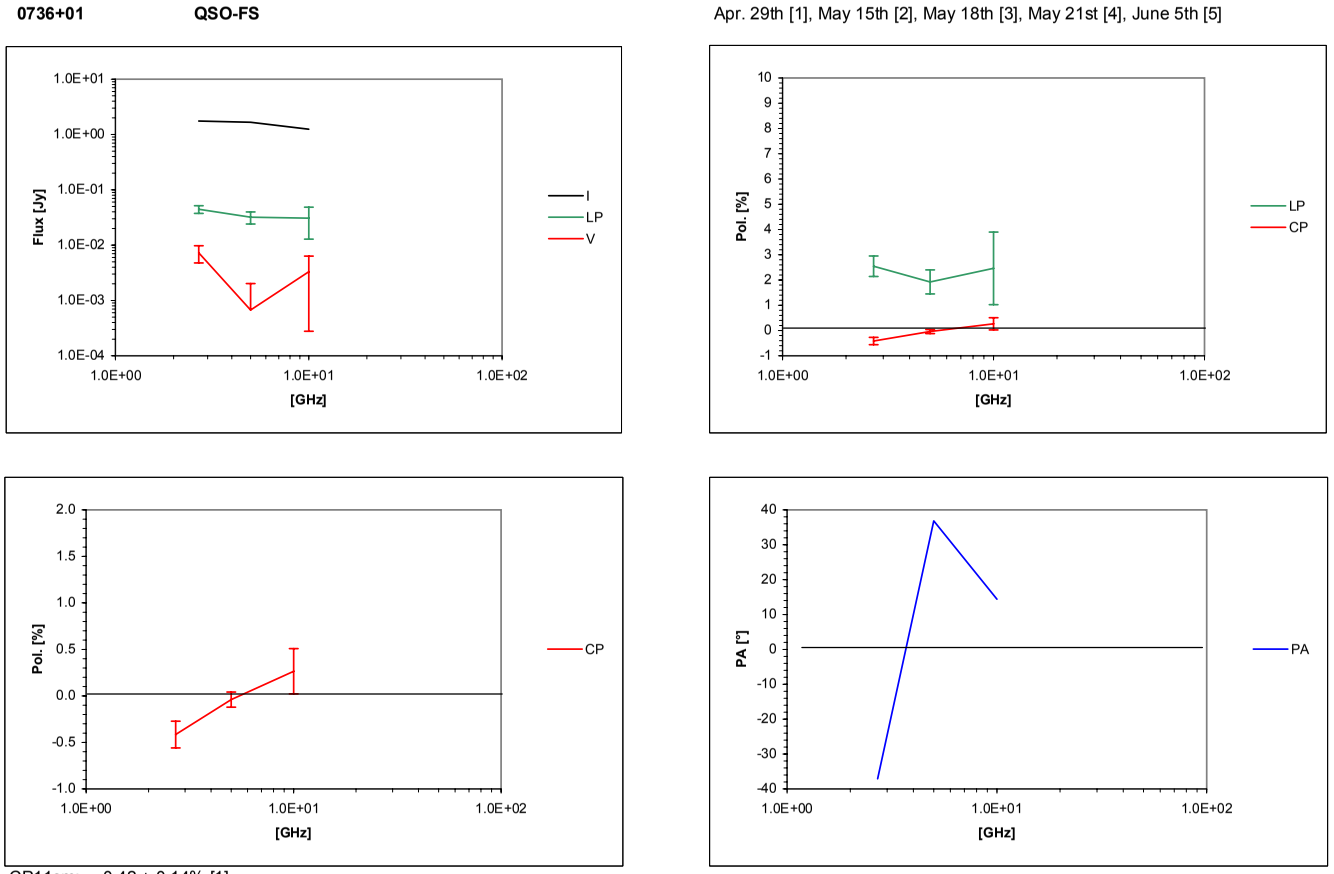

CP11cm: -0.42 ± 0.14% [1]
CP6cm: -0.04 ± 0.08% [1]
CP3.6cm:
CP2.8cm: 0.27 ± 0.24% [4]

CPSur= 0.51 ± 0.12% [Eff]

Figure B.17: Full Stokes spectra from 0743-00

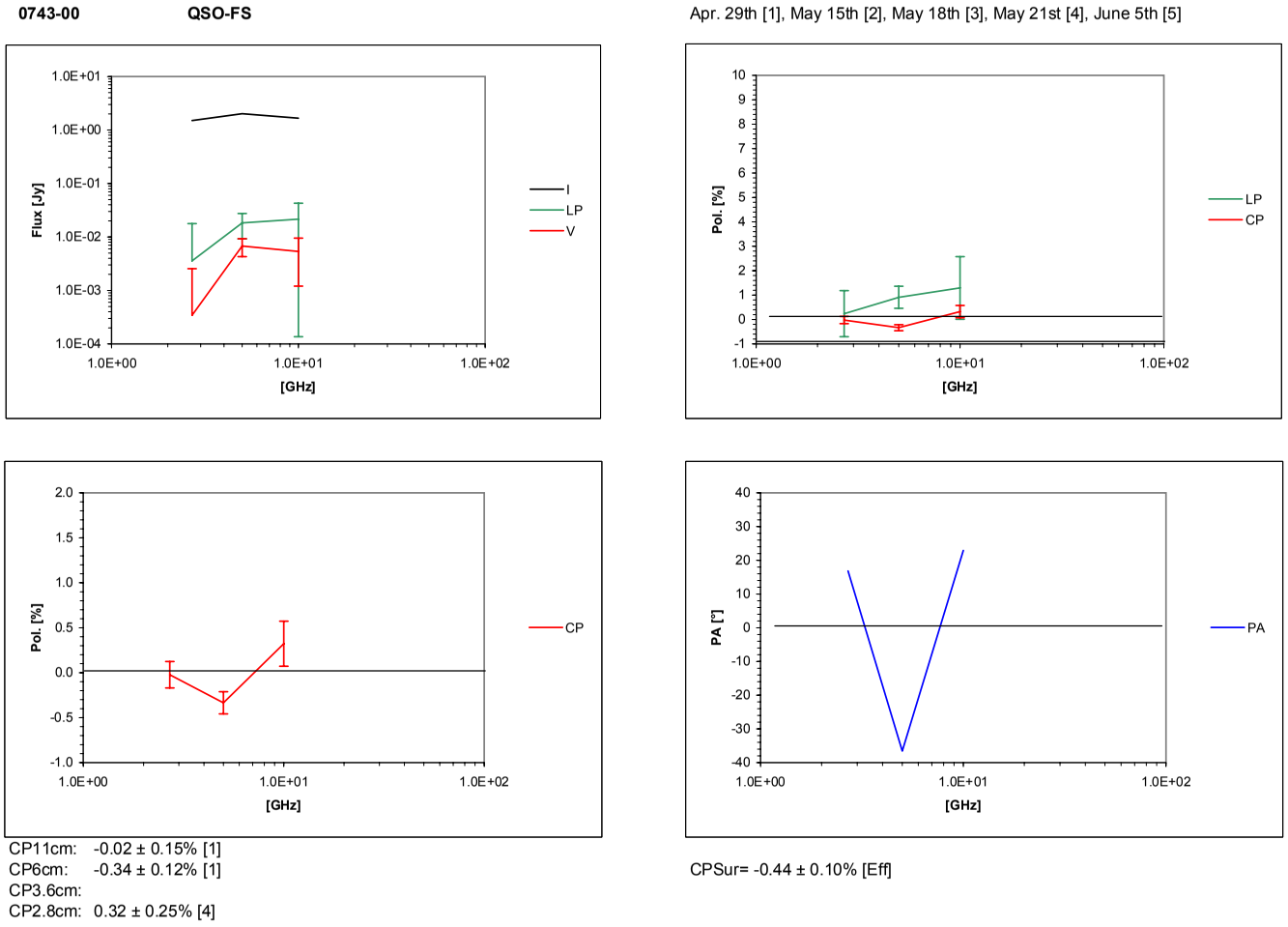

Figure B.18: Full Stokes spectra from 0809+48

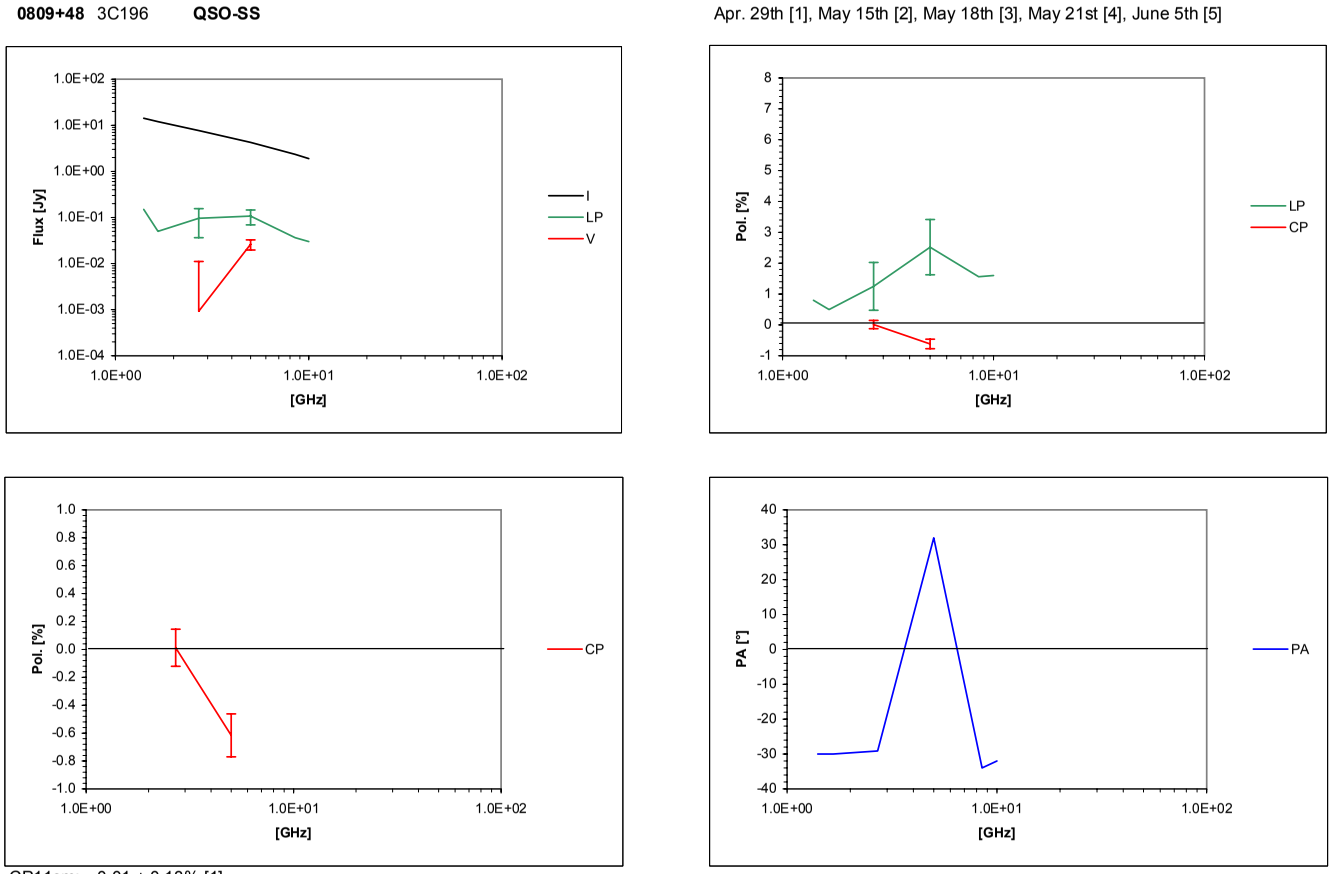

CP11cm: 0.01 ± 0.13% [1]
CP6cm: -0.62 ± 0.15% [1]
CP3.6cm:
CP2.8cm:

CPSur= -0.32 ± 0.10% [Eff]

Figure B.19: Full Stokes spectra from 0812+36

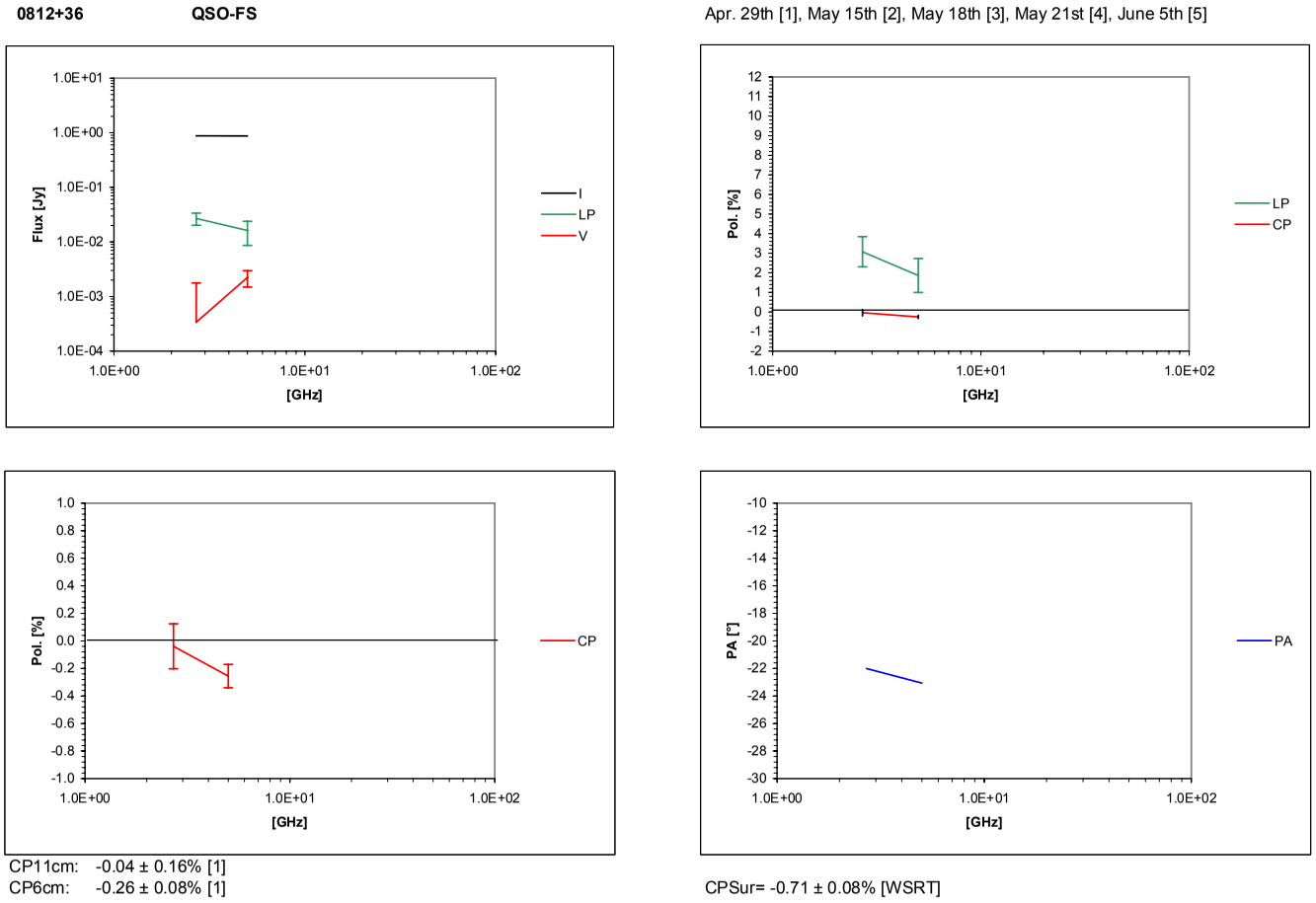

Figure B.20: Full Stokes spectra from 0831+55

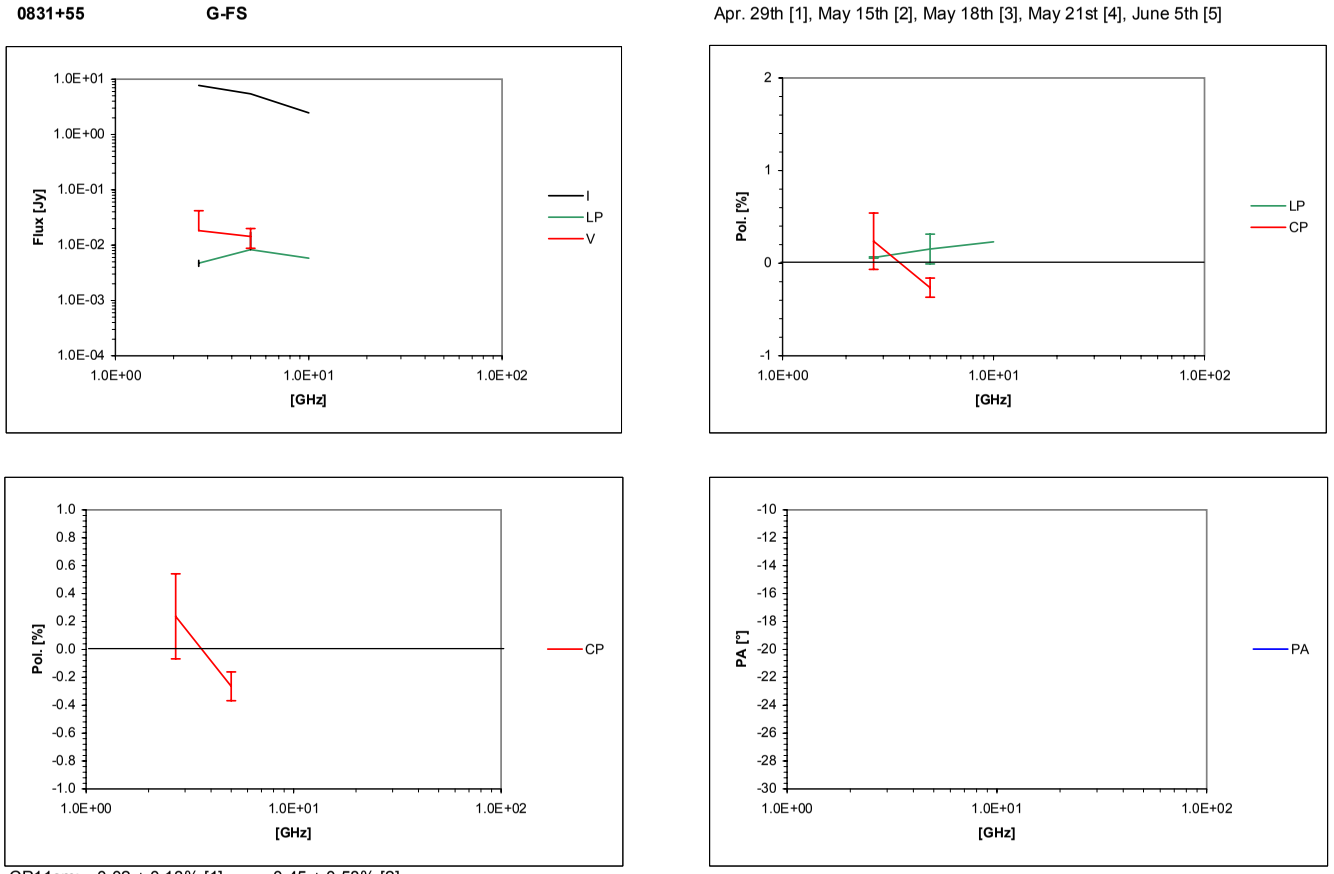

CP11cm: 0.02 ± 0.13% [1] 0.45 ± 0.58% [2]
CP6cm: -0.19 ± 0.14% [1] -0.33 ± 0.14% [2]
CP3.6cm:
CP2.8cm:

CPSur= 0.09 ± 0.15% [Eff]

Figure B.21: Full Stokes spectra from 1147+24

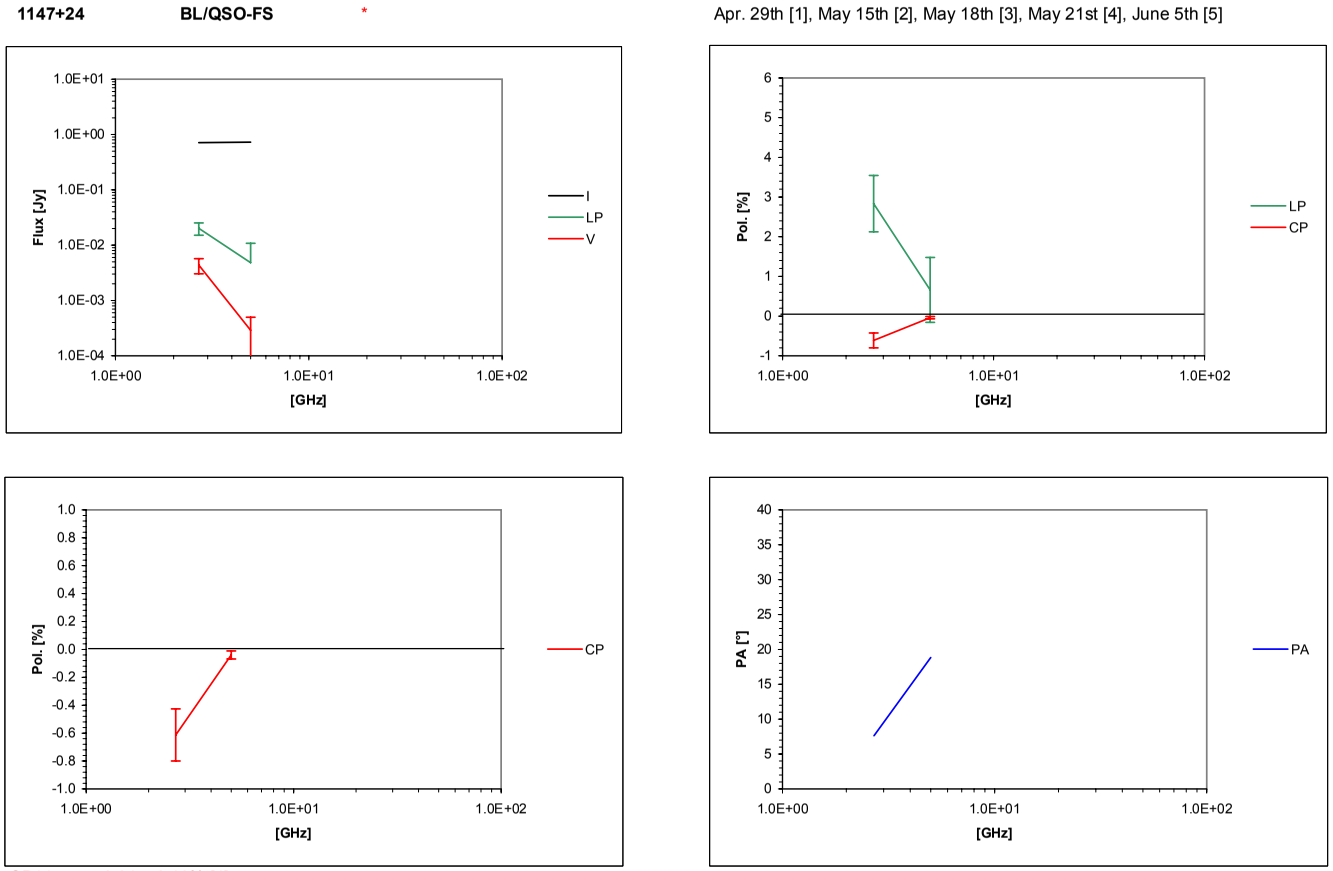

Figure B.22: Full Stokes spectra from 1749+09

1749+09 **BL/QSO-FS** **

Apr. 29th [1], May 15th [2], May 18th [3], May 21st [4], June 5th [5]

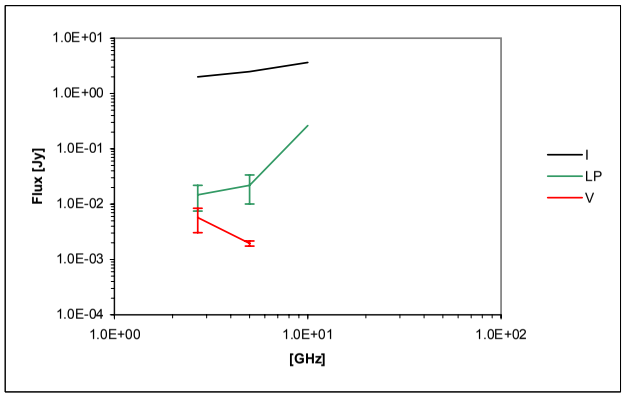

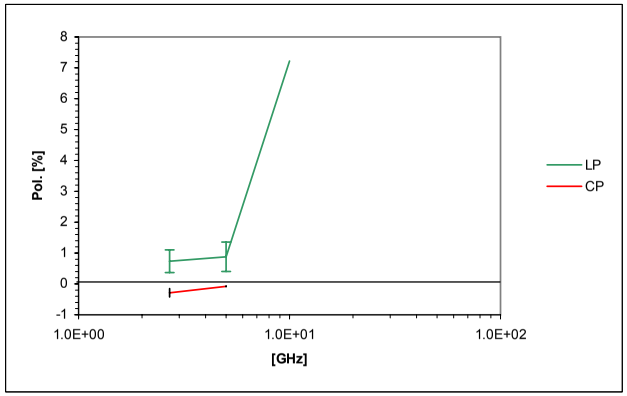

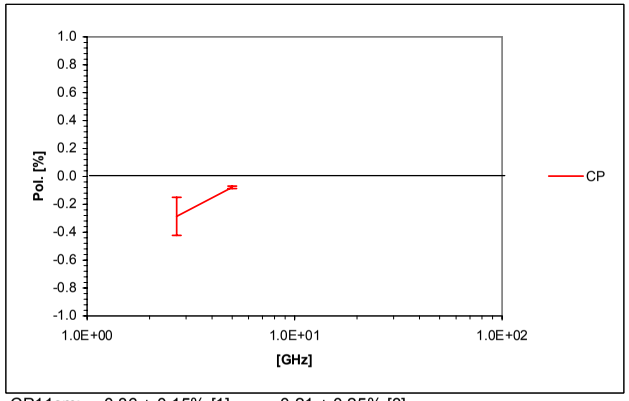

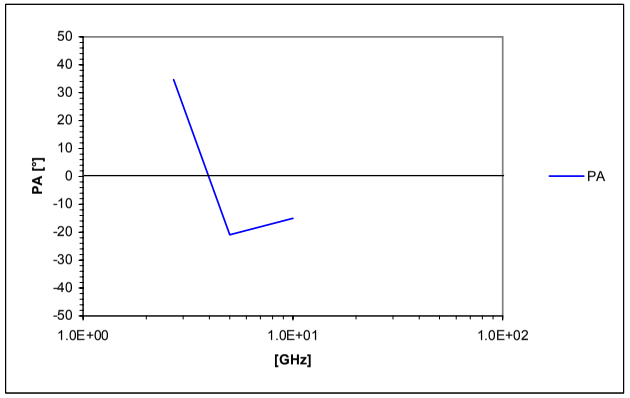

CP11cm: -0.36 ± 0.15% [1] -0.21 ± 0.25% [3]
CP6cm: -0.08 ± 0.08% [1] -0.07 ± 0.03% [3]
CP3.6cm:
CP2.8cm:

CPSur=0.56 ± 0.11% [Eff]

Figure B.23: Full Stokes spectra from 1823+56

1823+56 3C380 **BL/QSO-FS** **

Apr. 29th [1], May 15th [2], May 18th [3], May 21st [4], June 5th [5]

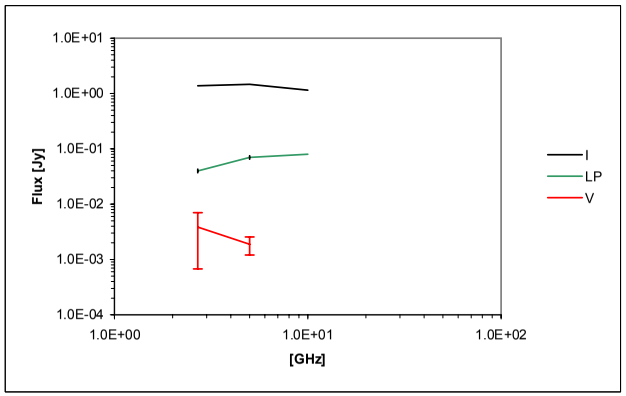

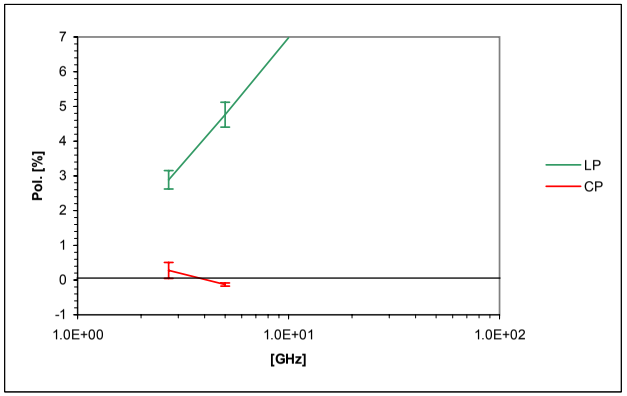

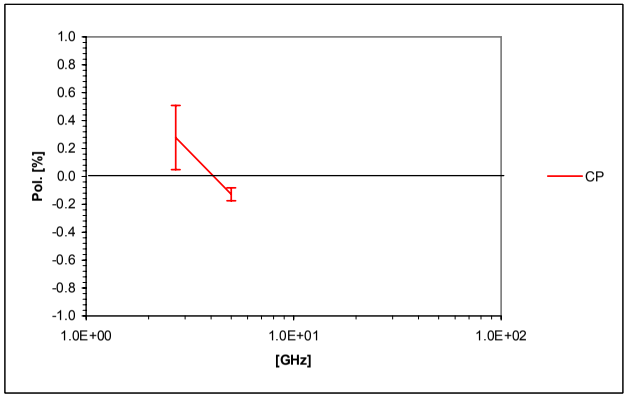

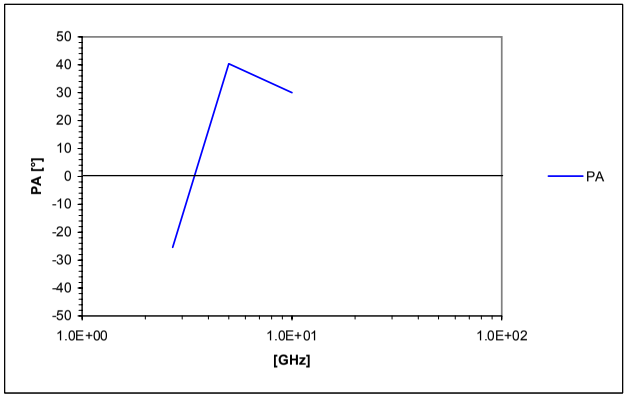

CP11cm: 0.12 ± 0.16% [1] 0.43 ± 0.24% [3]
CP6cm: -0.16 ± 0.09% [1] -0.09 ± 0.05% [3]
CP3.6cm:
CP2.8cm:

CPSur=0.48 ± 0.09% [WSRT]

Figure B.24: Full Stokes spectra from 2216-03

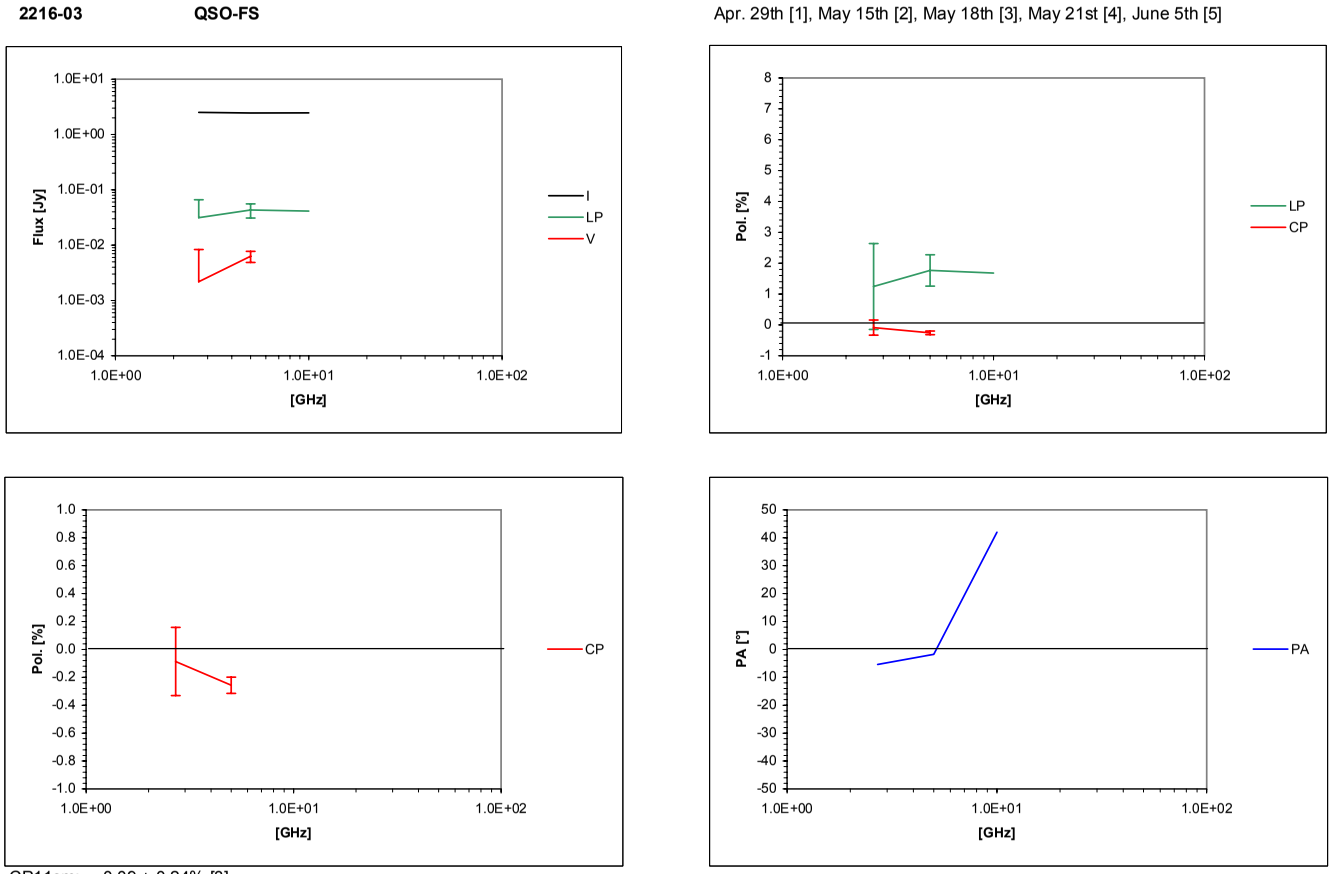

CP11cm: -0.09 ± 0.24% [3]
CP6cm: -0.26 ± 0.06% [3]
CP3.6cm:
CP2.8cm:

CPSur=-0.40± 0.10% [Eff]

Bibliography

H. D. Aller, M. F. Aller, and R. M. Plotkin. Circular Polarization Variability in Extragalactic Sources on Time Scales of Months to Decades. *Astrophysics and Space Science*, 288:17–28, March 2003.

T. Beckert. Circular Polarization and Magnetic Fields in Jet Models. *Astrophysics and Space Science*, 288:123–132, March 2003.

T. Beckert and H. Falcke. Circular polarization of radio emission from relativistic jets. *Astronomy and Astrophysics*, 388:1106–1119, June 2002.

M. Born and E. Wolf. *Principles of optics. Electromagnetic theory of propagation, interference and diffraction of light*. Oxford: Pergamon Press, 1980, 6th corrected ed., 1980.

E. Cenacchi, A. Kraus, A. Orfei, and K.-H. Mack. Full Stokes polarimetric observations with a single-dish radio telescope. *Astronomy and Astrophysics*, 498:591–599, May 2009.

J. J. Condon, W. D. Cotton, E. W. Greisen, Q. F. Yin, R. A. Perley, G. B. Taylor, and J. J. Broderick. The NRAO VLA Sky Survey. *Astronomical Journal*, 115: 1693–1716, May 1998.

W. J. Conover. *Practical nonparametric statistics*. Wiley; 3rd edition, 1998, 1998.

R. G. Conway and P. P. Kronberg. Interferometric measurement of polarization distribution in radio sources. *Monthly Notices of the RAS*, 142:11–+, 1969.

D. Fiebig, R. Wohlleben, A. Prata, and W. V. T. Rusch. Beam squint in axially symmetric reflector antennas with laterally displaced feeds. *IEEE Transactions on Antennas and Propagation*, 39:774–779, June 1991.

D. Gabuzda. The compact polarised emission of AGN. In *Proceedings of the 8th European VLBI Network Symposium*, 2006.

D. C. Gabuzda, V. M. Vitrishchak, M. Mahmud, and S. P. O'Sullivan. Radio circular polarization produced in helical magnetic fields in eight active galactic nuclei. *Monthly Notices of the RAS*, 384:1003–1014, March 2008.

J. P. Hamaker and J. D. Bregman. Understanding radio polarimetry. III. Interpreting the IAU/IEEE definitions of the Stokes parameters. *Astronomy and Astrophysics, Supplement*, 117:161–165, May 1996.

J. P. Hamaker, J. D. Bregman, and R. J. Sault. Understanding radio polarimetry. I. Mathematical foundations. *Astronomy and Astrophysics, Supplement*, 117: 137–147, May 1996.

C. Heiles. A Heuristic Introduction to Radioastronomical Polarization. In S. Stanimirovic, D. Altschuler, P. Goldsmith, and C. Salter, editors, *Single-Dish Radio Astronomy: Techniques and Applications*, volume 278 of *Astronomical Society of the Pacific Conference Series*, pages 131–152, December 2002.

D. C. Homan and M. L. Lister. MOJAVE: Monitoring of Jets in Active Galactic Nuclei with VLBA Experiments. II. First-Epoch 15 GHz Circular Polarization Results. *Astronomical Journal*, 131:1262–1279, March 2006.

D. C. Homan, J. M. Attridge, and J. F. C. Wardle. Parsec-Scale Circular Polarization Observations of 40 Blazars. *Astrophysical Journal*, 556:113–120, July 2001.

D. C. Homan, M. L. Lister, H. D. Aller, M. F. Aller, and J. F. C. Wardle. Full Polarization Spectra of 3C279. *Astrophysical Journal*, 696:328–347, May 2009.

D. L. Jauncey, E. A. King, H. E. Bignall, J. E. J. Lovell, L. Kedziora-Chudczer, A. K. Tzioumis, S. J. Tingay, J.-P. Macquart, and P. M. McCulloch. Variability in GPS Sources. *Publications of the Astronomical Society of Australia*, 20:151–155, 2003.

S. Johnston. Single Dish Polarisation Calibration. *Publications of the Astronomical Society of Australia*, 19:277–281, 2002.

T. W. Jones and S. L. O'Dell. Transfer of polarized radiation in self-absorbed synchrotron sources. I. Results for a homogeneous source. *Astrophysical Journal*, 214:522–539, June 1977.

J. G. Kirk and O. Tsang. High brightness temperatures and circular polarisation in extra-galactic radio sources. *Astronomy and Astrophysics*, 447:L13–L16, February 2006.

M. M. Komesaroff, J. A. Roberts, D. K. Milne, P. T. Rayner, and D. J. Cooke. Circular and linear polarization variations of compact radio sources. *Monthly Notices of the RAS*, 208:409–425, May 1984.

J. D. Kraus. *Radioastronomy*. Powell, Ohio: Cygnus-Quasar Books, 1986, 1986.

H. Kühr, A. Witzel, I. I. K. Pauliny-Toth, and U. Nauber. A catalogue of extragalactic radio sources having flux densities greater than 1 Jy at 5 GHz. *Astronomy and Astrophysics, Supplement*, 45:367–430, September 1981.

J.-P. Macquart and D. B. Melrose. Scintillation-induced Circular Polarization in Pulsars and Quasars. *Astrophysical Journal*, 545:798–806, December 2000.

J. P. McGuire, Jr. and R. A. Chipman. Polarization aberrations. 1. Rotationally symmetric optical systems. *Applied Optics*, 33:5080–5100, August 1994.

M. M. McKinnon. Point source polarization calibration of a phased array. *Astronomy and Astrophysics*, 260:533–542, July 1992.

R. A. Perley and B. J. Butler. An Accurate Flux Density Scale for Radio Astronomy. In *Bulletin of the American Astronomical Society*, volume 38 of *Bulletin of the American Astronomical Society*, page 146, June 2006.

D. P. Rayner, R. P. Norris, and R. J. Sault. Radio circular polarization of active galaxies. *Monthly Notices of the RAS*, 319:484–496, December 2000.

M. Ruszkowski. Linear and Circular Polarization Properties of Jets. *Astrophysics and Space Science*, 288:133–142, March 2003.

M. Stickel, K. Meisenheimer, and H. Kühr. The optical identification status of the 1 Jy radio source catalogue. *Astronomy and Astrophysics, Supplement*, 105: 211–234, June 1994.

J. Tinbergen. *Astronomical Polarimetry*. Astronomical Polarimetry, by Jaap Tinbergen, pp. 174. ISBN 0521475317. Cambridge, UK: Cambridge University Press, September 1996., September 1996.

Z. Turlo, T. Forkert, W. Sieber, and W. Wilson. Calibration of the instrumental polarization of radio telescopes. *Astronomy and Astrophysics*, 142:181–188, January 1985.

V. M. Vitrishchak and D. C. Gabuzda. New measurements of the circular polarization of the radio emission of Active Galactic Nuclei on parsec scales. *Astronomy Reports*, 51:695–708, September 2007.

V. M. Vitrishchak, D. C. Gabuzda, J. C. Algaba, E. A. Rastorgueva, S. P. O'Sullivan, and A. O'Dowd. The 15-43 GHz parsec-scale circular polarization of 41 active galactic nuclei. *Monthly Notices of the RAS*, 391:124–135, November 2008.

S. J. Wagner and A. Witzel. Intraday Variability In Quasars and BL Lac Objects. *Annual Review of Astron. and Astrophys.*, 33:163–198, 1995.

J. F. C. Wardle and D. C. Homan. Theoretical Models for Producing Circularly Polarized Radiation in Extragalactic Radio Sources. *Astrophysics and Space Science*, 288:143–153, March 2003.

J. F. C. Wardle, D. C. Homan, R. Ojha, and D. H. Roberts. Electron-positron jets associated with the quasar 3C279. *Nature*, 395:457–461, October 1998.

K. W. Weiler and I. de Pater. A catalog of high accuracy circular polarization measurements. *Astrophysical Journal, Supplement*, 52:293–327, July 1983.

K. W. Weiler and A. S. Wilson. High accuracy measurements of linear and circular polarization at 49 CM. *Astronomy and Astrophysics*, 58:17–26, June 1977.

Acknowledgements

Thanks to Anton Zensus and Neal Jackson, as representative of the EU ESTRELA Programme, who gave me the opportunity of coming in Bonn to carry out this project, while conceding me an high flexibility in its organization. Thanks to Andreas Eckart for refereeing this thesis.

I sincerely thank my first supervisor Alex Kraus, who has introduced me to one of the best radio telescopes in the world. Thanks for the freedom that you always left me and the constant confidence that something good would have come out. The feeling that this project was mine, and that it was my responsibility to find good ideas to have it working, is at the basis of the success that we obtained.

Thanks a lot to Karl-Heinz Mack, my second supervisor, for the huge amount of hours (often belonging to week-ends and evenings) spent talking with me on Skype, about such a variety of topics that it's hard to put them in a logical order (science, but also how to live in Germany being Italian and in Italy being German, my future, my house, any kind of depressions and complaints)...among all I think I will never forget the Sunday afternoon that we spent preparing that complicated WSRT schedule while I was at home in Bonn, with two ill children and a barking dog, and you were in Bologna...it's amazing how perfectly that schedule worked :-D

Thanks to Alessandro Orfei, who carefully followed the work behind the first part of this thesis. When we started working together years ago I have stolen your method of facing a problem, finding a solution and presenting the results respecting the initial deadlines. Even some Germans, the masters of this art, have been impressed by this efficiency :-)

Thanks to the Istituto di Radioastronomia-INAF, that has given me hospitality for 6 months in this last year. I'd like to thank Roberto Fanti for all the discussions about the nature of CP (*spero che avremo modo di portarle avanti in futuro*), and Daniele Dallacasa for the support with AIPS (*credimi, ti prego, gli interferometri non sono gli unici telescopi al mondo che hanno diritto di esistere* :-D). Thanks also to Franco Mantovani for the support he gave from the very beginning (*anche a me é entrato dentro qualcosa, di questa Germania, che credo non mi abbandonerá mai*).

This work owes a lot to the computer staff of Bologna and Bonn: thanks to Guido Kölsch for the constant support with Linux and the brilliant idea of using the Virtual Machine. Thanks to Franco Tinarelli and Mauro Nanni for the time they spent installing on my laptop the RadtransS code and for the assistance during the AIPS usage (*e il savoir-faire con cui avete reagito quando, dopo due giorni che ero all'IRA, avevo giá intasato le macchine con Tbyte di dati...*).

During these 3 years I experienced many useful scientific interactions, I'd like to thank in particular Thomas Krichbaum, Axel Jessner, Alan Roy, Hugh and Margo Aller (thanks also for the beautiful hospitality in Ann Arbor), Dan Homan, Wouter Vlemmings, Tim Cawthorne and Thomas Beckert.

I come from a country where the current president is one of the richest men in the world (Forbes list, 2009).

Coming from an already rich family he started the escalation in his success when he bought the only three private tv channels existing in Italy and the most important publishing houses of the country. Thanks to his undoubted ability of engaging and handling powerful connections he reached his actual political position. It's hard to say how long this condition will last: perceiving correctly the best way of impressing those who are around us is a precious gift, but, nevertheless, mistakes can always occur and the success is never fully guaranteed.

Many of my colleagues (e.g. Rashmi Verna and Rupal Mittal but also many others) come from a country that 80 years ago was led by the most powerful man in the world.

Coming from an already rich family he was banished from his caste when he left his country to study law. He came back dressed with a sort of white cotton mantel only (a *dhoti*, woven by himself) and, thanks to the courage of his convictions, he realized the most impressive political changes ever seen in history. He's been stopped when he's been killed.

I think that by small-scaling these examples to our everyday life a legitimate question arises in each of us: how do I want to reach my personal success? Which strategy should I choose?

I found my answer to these questions during the last three years. Note that I am aware that knowing the answer is not linked in any way to the realization of the success that I am personally looking for. But, perceiving that passion, truth and honesty must set the course of all of our actions is also a gift, and mistakes can never occur.

I acknowledge Emmanouil Angelakis for inspiring me the thread of these thoughts, and I would like to thank Laura, John, Eduardo, Matteo and many others for all the discussions about it.

Since I came to Bonn, a lot of people helped me feeling at home, and I'd like to thank Laura and Andrea for the nice friendship (*e le pizze al "Va Piano", la vacanza in montagna, il supporto logistico e potrei andare avanti per altre 3 pagine almeno*); Barbara for the beautiful house that she left me (without it, it wouldn't have been the same...) and all the efforts and suggestions to make Bad Godesberg my town (I swear, that even if it will take me years, I will learn the German language properly !!!); Maria and all the Italian literature club (*Milena, per me sarai sempre un esempio da seguire*); Walter for the precious help when I had my car accident during the Carnival period (!); Katja for your friendship (if my girls grew so nicely in Bonn it is also thanks to the friendship with Carlotta).

And from my Bologna: thanks to Laura, Lorenzo, Simona, Stefano, Mattia (*oddio... se penso a tutto quello che ho scritto in LaTeX... non mi sembra vero ...grazie 1000! E le partite di Skypeinmente?*), Matteo (*lo apriamo o no questo centro di ricerca ?!*) and all the friends from Astronomy, thanks also to all the "women" at the Medicina Radiotelescopes (Emma, Simona, Lorenza, Rashmi, Stefania) for all the "Welcome Home" dinners.

Besides, I will always thank all my beautiful children, and their beloved father, who shared with me this experience always filling my life with enthusiasm and positive energy.

Erklärung

Ich versichere, daß ich die von mir vorgelegte Dissertation selbständig angefertigt, die benutzten Quellen und Hilfsmittel vollständig angegeben und die Stellen der Arbeit - einschließlich Tabellen, Karten und Abbildungen -, die anderen Werken im Wortlaut oder dem Sinn nach entnommen sind, in jedem Einzelfall als Entlehnung kenntlich gemacht habe; daß diese Dissertation noch keiner anderen Fakultät oder Universität zur Prüfung vorgelegen hat; daß sie - abgesehen von unten angegebenen Teilpublikationen - noch nicht veröffentlicht worden ist sowie, daß ich eine solche Veröffentlichung vor Abschluß des Promotionsverfahrens nicht vornehmen werde.

Die Bestimmungen dieser Promotionsordnung sind mir bekannt. Die von mir vorgelegte Dissertation ist von Prof. Andreas Eckart betreut worden.

CURRICULUM VITAE

PERSONAL DATA

Name	**Elena Cenacchi**
Birth Date	January 18th, 1975
Birth Place	Bologna – Italy
Nationality	Italian
E-mail	cenacchi@mpifr.de

EDUCATION AND PROFESSIONAL APPOINTMENTS

September 1988 July 1993	**Classical High School (Liceo Classico)** L. Galvani of Bologna (Italy)
July 1993 September 1997	**Employed** in the international sales department of the family firm "Cenacchi International" (production of custom-made furnishings: www.cenacchiinternational.it). Main occupations: customer service, sales administration and accounting.
September 1997 March 2000	**Study of Aerospace Engineering** Spec.: Space and Telecommunication University of Bologna (Italy)
March 2000	**Laurea (B.S. equivalent)** in Aerospace Engineering Thesis: "A LAAS landing system at the Forlì airport. Application of the GPS satellite simulator"
September 2000 December 2004	**Study of Astronomy** University of Bologna (Italy)
December 2004	**Laurea (B.S. + M.S. equivalent) in Astronomy** Thesis: "SRT The Sardinia radio telescope. Innovative characteristics, performance prediction and applications to advanced astronomy research"
December 2004 June 2006	**Research contract** Medicina radio telescope, INAF-Istituto di Radioastronomia Bologna (Italy). Design of super-heterodyne multi-beam receivers for single dish radio telescopes. Under the supervision of: Alessandro Orfei
June 2006 Present	**Marie Curie ESTRELA PhD Studentship** IMPRS (International Max Planck Research School) Max-Planck-Institut für Radioastronomie Bonn (Germany) Full Stokes polarimetric observations of extragalactic radio sources with the Effelsberg 100-m radio telescope. Under the supervision of: Alexander Kraus

COMPLETE PUBLICATION LIST

REFEREED PUBLICATIONS

Cenacchi E., Kraus A., Orfei A., Mack K.-H. "Full Stokes polarimetric observations with a sigle-dish radio telescope"
Astronomy and Astrophysics, Volume 498, Issue 2, 2009, pp.591-599

Cenacchi E., Mack K.-H., Kraus A., Krichbaum T.P. "The 5 GHz Northern 1-Jy Full Stokes Survey"
Astronomy and Astrophysics, Submitted

NON-REFEREED PROCEEDINGS

Cenacchi E., Kraus A., Beckert T., Mack K.-H. "Circular Polarimetry of Extragalactic Radio Sources"
Workshop: "Astronomical Polarimetry 2008: Science from Small to Large Telescopes"
*ASP Conference Series, Vol. 4**, 2009, In Press*
P. Bastien & N. Manset eds.
arXiv:0901.4678

Cenacchi E., Kraus A., Mack K.-H. "Deriving AGN properties from circular and linear radio polarimetry"
Proceeding of IAU Symposium, Volume 259, 04/2009, p. 561-562
K. G. Strassmeier, A. G. Kosovichev & J. Beckmann eds.

Cenacchi E., Dallacasa D., Orfei A. "OQ208: a possibile multi-wavelength polarimetric study with the SRT"
Workshop: "Science with the Sardinia Radio Telescope"
Memorie della Società Astronomica Italiana Supplementi, Vol. 10
J. Brandt, K.-H. Mack & I. Prandoni, eds.

INTERNAL REPORTS AND MANUALS

Cenacchi E. "The Sardinia Radio Telescope Project Book"
Available at the website of Cagliari Observatory:
http://www.ca.astro.it/srt/project-book/index.htm

Cenacchi E., Orfei A., Mack K.-H., Maccaferri G. "The 32-m Medicina Radiotelescope User's Manual"
IRA Internal Report 401/07 and 402/07
Available at the website of the Istituto di Radioastronomia:
http://www.med.ira.inaf.it/ManualeMedicina/index.htm

Cenacchi E., Orfei A., Schilllirò F., Mack K.-H. "The 32-m Noto Radiotelescope User's Manual"
Available at the website of the Istituto di Radioastronomia:
http://www.med.ira.inaf.it/ManualeNoto/index.htm

Cenacchi E., Orfei A. "Multifeed receivers systems for SRT"
IRA Internal Report 384/06
Available at the website of Cagliari Observatory:
http://www.ca.astro.it/srt/project-book/4.%20Front%20End.htm